2019

# Tension and compression behavior of corroded steel beams rehabilitated with BFRP

Soham Mitra
*University of Windsor*

# Tension and compression behavior of corroded steel beams rehabilitated with BFRP

By

Soham Mitra

A Thesis

Submitted to the Faculty of Graduate Studies

through the Department of Civil and Environmental Engineering

in Partial Fulfillment of the Requirements for

the Degree of Master of Applied Science

at the University of Windsor

Windsor, Ontario, Canada

2019

# Tension and compression behavior of corroded steel beams rehabilitated with BFRP

By

Soham Mitra

APPROVED BY:

K. Tepe
Department of Electrical and Computer Engineering


N. Van Engelen
Department of Civil and Environmental Engineering


S. Das, Advisor
Department of Civil and Environmental Engineering

May 17, 2019

# Declaration of Co-Authorship and Previous Publication

### I. Co-Authorship Declaration

I hereby declare that this thesis incorporates material that is a result of joint research, as follows:

This thesis incorporates the outcome of a joint research undertaken in collaboration with MEDA Limited under the supervision of Dr. Das. The collaboration is covered in Chapters 1 - 4 of the thesis. Testing of three specimens was completed jointly by the author and Mr. Amirreza Bastani. The collaboration is covered in Chapter 2 of the thesis. In all cases, the key ideas, primary contributions, experimental designs, data analysis and interpretation, were performed by the author and the contribution of co-authors was primarily through advice and assistance with experimental testing.

I am aware of the University of Windsor Senate Policy on Authorship and I certify that I have properly acknowledged the contribution of other researchers to my thesis and have obtained written permission from each of the co-author(s) to include the above material(s) in my thesis.

I certify that, with the above qualification, this thesis, and the research to which it refers, is the product of my own work.

## II. Declaration of Previous Publication

This thesis includes two original papers that are planned to be submitted for publication in peer reviewed journals, as follows:

| Dissertation Chapter | Publication title | Publication status |
|---|---|---|
| Chapter 2 | Flexural Rehabilitation of Steel Beams with Various Corrosion Aspect Ratios with BFRP Fabric | To be submitted |
| Chapter 3 | Use of Basalt Fiber Reinforced Polymer for Flexural Rehabilitation of Steel Beams with Corrosion Defect in Compression Flange | To be submitted |

I certify that the above material describes work completed during my registration as graduate student at the University of Windsor.

I declare that, to the best of my knowledge, my thesis does not infringe upon anyone's copyright nor violate any proprietary rights and that any ideas, techniques, quotations, or any other material from the work of other people included in my thesis, published or otherwise, are fully acknowledged in accordance with the standard referencing practices. Furthermore, to the extent that I have included copyrighted material that surpasses the bounds of fair dealing within the meaning of the Canada Copyright Act, I certify that I have obtained a written permission from the copyright owner(s) to include such material(s) in my thesis.

I declare that this is a true copy of my thesis, including any final revisions, as approved by my thesis committee and the Graduate Studies office, and that this thesis has not been submitted for a higher degree to any other University or Institution.

# Abstract

The deterioration in structural integrity of North America's aging infrastructure, and the global initiative towards the use of sustainable materials in construction necessitates the use of cost-effective and eco-friendly methods for infrastructure rehabilitation. Previous studies have concluded that carbon fibre reinforced polymer (CFRP) and glass fibre reinforced polymer (GFRP) are effective in rehabilitating steel and concrete structures. However, there are limited reports on the use of eco-friendly basalt fibre reinforced polymer (BFRP). This research presents the feasibility of BFRP composites in rehabilitating steel I-beams with corrosion defects on the bottom flange as well as on the top flange through experimental and finite element methods. It was observed that BFRP composite fabric was effective in increasing the yield and ultimate load capacities of corroded steel beams. The structural behavior of rehabilitated steel beams including the complex behavior of rupture in the BFRP composite fabric was successfully modelled using Abaqus software. A good correlation between the finite element models and the experimental results was obtained, and equations for determining the optimal number of BFRP layers was developed. The results of the numerical analysis suggest that the ultimate load capacity of steel beams with corrosion defect in the bottom flange of depth 40% of flange thickness and aspect ratio of four can be restored using 12 layers of BFRP. For steel beams with corrosion defect in the top flange of depth 40% of flange thickness, 15 layers of BFRP fabrics was required for restoring the ultimate strength.

## Acknowledgement

I would like to express my sincere gratitude towards my advisor Dr. S. Das for his guidance, support, and motivation throughout this project. I consider myself extremely fortunate to have an advisor who is so much passionate about his research. I am also grateful to my committee members Dr. N. Van Engelen and Dr. K. Tepe for their help and guidance.

I would also like to thank MEDA Limited for providing technical assistance necessary for this research. I am also thankful to MEDA Limited located in Windsor, ON and NSERC located in Ottawa, ON, Canada for providing partial financial assistance for this research.

I am extremely grateful towards our lab technicians Matt St. Louis and Jerome Finnerty for their time and efforts in helping to conduct the testing and specimen preparation required to complete this thesis.

I am also very much thankful to my friends and colleagues Amirreza Bastani, Behrouz Chegeni, Emad Booya, Eric Hughes, Hossein Ghaednia, Jamshid Zohreh Heydariha, Jothiarun Dhanapal, Jeeric Penales, Karla Gorospe, Navjot Singh, Sachith Jayasuriya, and Sahan Jayasuriya for their help with the laborious tasks of specimen preparation and data acquisition.

Lastly, I would also like to thank my parents and sister for their constant support and motivation.

This thesis would not have been completed without the help and support of these people.

# Table of Contents

# List of Figures

# List of Tables

## Chapter 1: General Introduction

Many structures around the world have began to show structural damages. These damages are mainly caused due to their exposure to external factors such as freeze-thaw cycles, cyclic loads, de-icing salt spray. These structural damages are more prevalent in developed countries such as USA and Canada. According to the Infrastructure Report Card published by American Society of Civil Engineers in 2017, almost 40% of the existing bridges in the USA have already exceeded their service life of 50 years and about 9.1% of the existing bridges are structurally deficient. It is also estimated that the backlog for rehabilitation needs in USA is about 123 billion USD [1]. According to another report published by Transportation for America in 2013, it is estimated that about 66,405 bridges in North America are structurally deficient and about 260 million trips are taken daily over these deficient structures [2]. Canadian Infrastructure Report Card published in 2016 by Federation of Canadian Municipalities reports that about 5% of Canadian bridges are in very poor condition and these structures have a replacement value of about 50 billion CAD [3].

Corrosion defect in steel structures is one of the major causes of structural deterioration. The use of de-icing salt in colder countries accelerates the corrosion process and worsens the condition. These structural deficiencies and damages if unaddressed can cause catastrophic failures. One such example is the collapse of the roof of the Algo Centre Mall located in Elliot Lake, Ontario in June 2012 which killed two people and injured more than 20 people. It was reported that the cause of the collapse was due to extensive corrosion of the steel beams.[4]

Hence, there is an urgent need to develop an efficient, fast, and cost-effective solution for rehabilitation of deficient or damaged structures and structural components to meet the demand for rehabilitation. The cost-effective and convenient techniques would reduce the burden of taxpayers as well as make the bridges and highways a safer mode of transport.

### 1.1 Summary of Literature Review

This chapter provides a summary of the literature review. The focus of this literature review was to determine the previous research works completed on various repair and rehabilitation techniques available for rehabilitation of corroded steel beams and other structures.

### 1.1.1   Various Repair Methods for Steel Structures

Traditional methods used for rehabilitation of corroded steel beams are welding or bolting of steel plates to the corroded area. The standard practice starts with cleaning the corroded area followed by attaching steel plates of required dimensions by welding or bolting. These techniques are effective, in increasing the load capacity of the structures but these methods have several disadvantages. The disadvantage with these techniques includes a substantial increase in dead load of the structure and interruption of service while the repair work is in progress. These repair works are also labour intensive making them very expensive. For welding method there are chances of having weld cracking failure at the area of weld application and at the plate ends [5]. For bolting method, there is a potential of developing high-stress concentration regions around the area where the bolts are attached [6]. Moreover, bolting and welding method also increases the possibility of developing crevice corrosion and galvanic corrosion.

Use of Fibre Reinforced Polymers (FRP) for the rehabilitation and strengthening of structures has been gaining popularity due to their many advantages over the traditional methods. These materials have a very high strength-to-weight ratio. FRPs are also resistant to corrosion, fire, and chemical attacks. Moreover, the rehabilitation with FRP is not labour intensive and such rehabilitation method requires less time to complete. These make the process much cheaper and more advantageous than the traditional methods. The most common forms of FRP materials available commercially are Carbon Fibre Reinforced Polymer (CFRP), Glass Fibre Reinforced Polymer (GFRP), and Aramid Fibre Reinforced Polymer (AFRP). Basalt Fibre Reinforced Polymer (BFRP) is a relatively newer material and is gaining popularity among researchers due to its advantages which is discussed in later sections.

The FRP consists of two component and these are fabrics and  matrix. The fabrics consist of uniaxial or biaxial orientation of fibres. Fabrics are available in either thin sheet consisting of single layers of fibres or prefabricated FRP plates which consist of multiple layers of fabrics with various thicknesses. Figure 1.1 shows the different types of fabrics discussed.The matrix or epoxy is the material through which stresses are transferred between the fibres in the FRP composite. The matrix is also used to bond the fibres sheet to the structure. Matrix or epoxy can be either thermosetting or thermoplastic materials. Thermosetting matrix can be polyester, vinyl ester, and epoxy resin. Thermoplastic materials include polypropylene and polyethylene. Thermosetting materials are cost-effective and

can withstand higher temperature than the thermoplastic materials hence this type of matrix material is more commonly used in civil engineering applications.
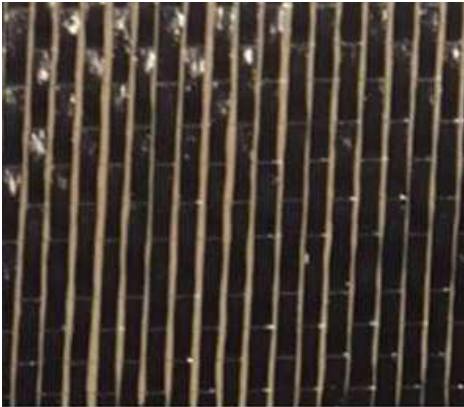

1.1a. Carbon fabrics
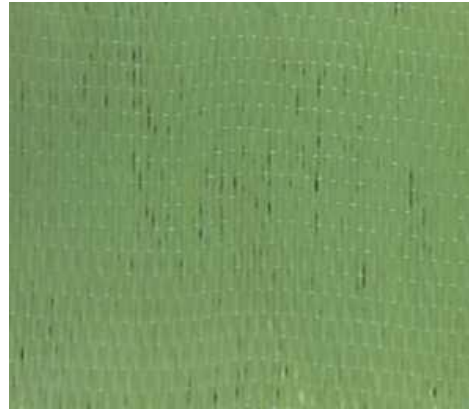

1.1b. Aramid fabrics


1.1c. E-glass fabrics
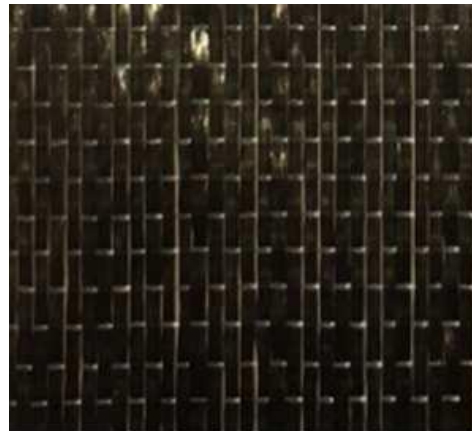

1.1d. Basalt fabrics

Figure 1.1: Different types of fabrics

Carbon fibre fabrics contains at least 92% by weight of carbon [7]. Carbon fibre fabrics are characterized by high tensile properties, low densities, high thermal and chemical stabilities, and excellent creep resistance. The carbon fibre fabric industry has been growing steadily in the past decade to meet the market demand. Manufacturing of carbon fibre fabric is a very expensive process, known as controlled pyrolysis, which involves complex methods. The first step of the process is stabilizing fibres by oxidation process at a temperature of about 200 – 400 °C. The fibres are then removed of hydrogen, oxygen, nitrogen, and other non-carbon elements by a process called

carbonization which subjects them to a high-temperature treatment of around 1,000 °C in an inert atmosphere. The carbonized fibres are further graphitized at a higher temperature of about 3,000 °C to achieve higher carbon content and higher Young's modulus. The final step of the process is post-treating the relatively inert surfaces of the carbon fibres to improve their adhesion to composite matrices [8]. The carbon fibre fabrics can be categorized in terms of their mechanical properties into ultra high modulus (>500 GPa), high modulus (>300 GPa), intermediate modulus (>200 GPa), low modulus (>100 GPa), and high strength (>4 GPa) carbon fibres [9]. The disadvantages of carbon fibre fabrics are its high cost and chances of galvanic corrosion when used with other metals like steel.

Glass fibre fabrics is made by mixing silica sand, limestone, boric acid, and other minor ingredients. The mixture is heated to about 1260 °C until it melts. The molten material is then passed through fine holes forming fine strands. The strands are then cooled, gathered, and wound. The fibres are then drawn to increase the unidirectional strength. The fibres are finally woven into various form for use in composites. Some additives are also used during the fabrication process to improve different properties of the fabrics as required. Glass fibre fabrics are ideal for use in the construction market because of their dimensional stability, high strength at low densities, good impact and corrosion resistance and good insulating properties. However, glass fibres are sensitive to moisture especially in presence of salt and alkalinity. Most common Glass fiber fabrics used are E-glass (Electrical type) and S-glass (High-performance type) [10].

Aramid fiber fabrics are manufactured fibre in which the fibre forming substance is a long chain synthetic polyamide, in which at least 85% is of amide linkages (-CO-NH-) attached directly to two aromatic rings. The aramid fibre fabrics have high strength, excellent resistance to heat and cut, good chemical resistance and low flammability. However, aramid fabrics are sensitive to acids and ultraviolet radiations. The mechanical properties of aramid products vary between carbon fibres and glass fibres [11].

Basalt fibre fabrics are manufactured by melting of quarried basalt rock. The molten rock is then passed through a fine nozzle to produce fine filaments. The process does not use any other additive and the production is in a single step process. Basalt is also the most common rock on earth. Hence, it is much cheaper than other fabrics. It is reported that the cost of basalt fiber fabric is about one-fifth of that of carbon fiber fabric [12]. It is also a greener product as compared to carbon fiber fabrics. In a study by Sim and Moon [13], it was found that that basalt fibre fabrics have a higher tensile

strength than E-glass fibre fabrics. It also has a greater failure strain than carbon fibre fabrics. However, basalt fiber fabrics has a lower modulus of elasticity than carbon fiber fabrics. It also has good resistance to chemical attack, impact load, and fire. Another big advantage of using basalt fibre fabric is its non-corrosive behavior. Hence, basalt fiber fabric can be used for the shoreline structures and can prevent corrosion during winters in colder regions where de-icing salts are used. Basalt fiber fabric has a very high thermal stability which is better than both carbon and glass fiber fabrics. Basalt fiber fabrics also has a high weathering resistance and is better than glass fiber fabrics, but it is weaker than carbon fiber fabrics [14]. Due to these advantages of basalt fiber fabrics and lower cost, it is gaining popularity among the researchers in the past decades.

### 1.1.2 Repair of beams in tension using Fibre Reinforced Polymers (FRP)

Many research studies have been conducted on the use of FRP for rehabilitation of Reinforced Concrete (RC) structures. Masoud et al. [15] used CFRP composites to rehabilitate RC beams with corrosion defects. Eight RC beams were used for the study out of which seven beams were corroded. The beams were rehabilitated using repair schemes which involved U-shaped CFRP wraps attached in the transverse direction of the beam and longitudinal strip of CFRP was used as anchorage with another longitudinal strip attached to the bottom of the beam as a flexural reinforcement. Using this technique, the ultimate load capacity of the beam improved by 38% when subjected to monotonic loading. The fatigue life also improved by 138%. Other studies by Green et al. (2003) [16] and Attari et al. [17], also found that using FRP materials like CFRP and GFRP can increase the flexural capacity of RC beams. Hence, it was concluded that FRP materials are effective in rehabilitating and strengthening of RC beams.

Fewer studies have been conducted on the use of CFRP and other fabrics for the rehabilitation of steel beam. Saidy et al. [18] simulated corrosion on steel beams by removing 50% and 75% of the bottom flange area. This study used six beams and rehabilitated five beams with CFRP plates by attaching plates underneath the bottom flange as well as on the web. One beam was left untouched for comparison. It was observed that the elastic stiffness of the beams could be partially restored up to 50% percent for the test conducted. The ultimate strength of the beams was fully restored with the rehabilitation conducted. However, the ductility of the rehabilitated beams was lower than that of the original beams. This is due to the lower failure strain of the CFRP fabrics.

Mertz and Gillespie [19] conducted rehabilitation of corroded steel beams using CFRP plates. The study tested both small and large-scale specimens under monotonic and fatigue loads. The study observed an increase in elastic stiffness for the small-scale specimens and the increase was about 20%. The increase in the ultimate strength of the rehabilitated beams was 50%. Rehabilitation of the large-scale specimens with a corrosion loss of about 40% in the tension flange resulted in an increase in the elastic stiffness of about 25% and a substantial increase in the ultimate strength. The study also observed a significant improvement in fatigue life of the specimens. It was also recommended in the study to use a layer of E-Glass fibres between the steel and CFRP to avoid direct contact of steel and CFRP to reduce the galvanic corrosion. Since carbon fibres are electrically conductive and electrochemically noble, when it is connected to steel the chances of galvanic corrosion increases.

Manalo et al. [20] rehabilitated 3 m long steel I-beams with CFRP fabrics. Damage was introduced in the steel beams in the form of a 1 mm rectangular notch through the span width at the mid-span to simulate crack and 80% of the flange thickness removed to simulate corrosion as shown in Figure 1.2. For rehabilitation firstly, the surface was prepared by introducing surface roughness by grit blasting. This is to ensure good bonding between the steel and CFRP fabrics. The ends were tapered to prevent stress concentration. A layer of glass tissue was inserted between the CFRP and steel layer to prevent galvanic corrosion. Fifteen layers of CFRP fabrics were used for rehabilitating the crack and 11 layers of CFRP fabrics were used for rehabilitation of corrosion defect. Each layer of CFRP fabric measured about 1 mm. The maximum load carrying capacity of the crack beam when rehabilitated increased by 3% as compare to the original (undamaged) beam and the maximum load carrying capacity of the beam with 80% corrosion increased to 8%. There was also a marginal increase in the yield load. The repaired beam also exhibited a 16% increase in the elastic stiffness. It was also suggested to maintain an adequate thickness of the epoxy layer as thicker epoxy layer could increase the chances of debonding failure.
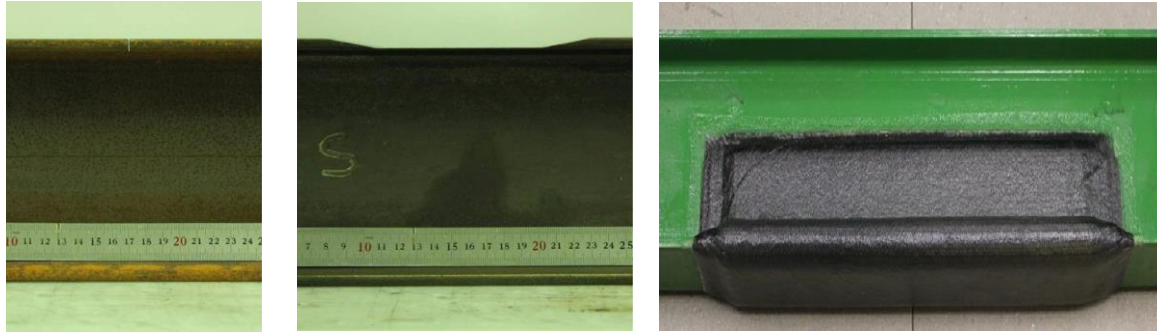
1.2a. Crack defect    1.2b. 80% Corrosion defect      1.2c. Repair pattern
(Malano et al.)       (Malano et al.)         (Malano et al.)

Figure 1.2: Different types of corrosion defects (Malano et al.)

Galal et al. (2012) [21] conducted testing with thirteen 1.6 m long steel beams of section W150 X 30 [22] to observe the behavior of damages steel beams rehabilitated with CFRP fabrics and CFRP plates. Corrosion defect was simulated in the beam by removing a percentage of thickness from the bottom flange. The percentages of corrosion used in this study are 33% and 50%. Local corrosion defect is also introduced in the form of holes in the tension flange at the mid-span. Uniform or spread corrosion defect was simulated in the beams with 450 mm notch in the mid-span. A layer of GFRP fabric was used in-between the CFRP and steel layers as a dielectric barrier to prevent galvanic corrosion. The study also used two types of epoxy as a resin and adhesive, saturating epoxy and viscous epoxy to compare the effect of epoxy types. The retrofitted beams which used viscous epoxy showed higher ultimate flexural capacity as compared to the beams that used saturating epoxy for bonding CFRP sheets to the steel beam however there was no significant influence in the yield load. It was also found that the retrofitted beams showed an increase in the ultimate load capacity. But there was a reduction in ductility for the rehabilitated beams.

El Damatty et al. [23] strengthened steel I-beams of section W150x37 [22] using 19 mm thick GFRP plates. The GFRP plates were formed by pultrusion process using unidirectional layers of GFRP sheets to provide strength and stiffness in the longitudinal direction. The plates were attached to the steel beams using a methacrylate adhesive system which is a heavy-duty adhesive system. The beams were sandblasted initially to prepare the surface for rehabilitation and ensure good bonding between the plates and the steel. The strengthened beam was cured for 15 days before it was tested in four-point bending as shown in Figure 1.3. It was observed that there was an increase in stiffness of about

15%, the yield load of the strengthened beams showed an increase of about 23% and the ultimate load of the strengthened beam increased to about 78% as compared to the reference (undamaged) steel beam. There was no failure observed at the interface of steel and GFRP indicating very good performance of the adhesive used. The mode of failure observed was a sudden drop in load value due to the tensile failure of the GFRP fabrics. Hence, it can be concluded from the studies that both CFRP and GFRP fabrics as well as plates can be effectively used for rehabilitation or strengthening of steel beams. The advantages of FRP fabrics over plates is fabrics can be applied to a structure of any shape making it possible for rehabilitation. However, FRP plates can only be applied to flat surfaces.



Figure 1.3: Failure mode observed in the rehabilitated beams (El Damatty et al.)

BFRP is a relatively newer material used in rehabilitation of structures. Sim and Moon [12] and Huang et al. [24] effectively used BFRP in the in the rehabilitation and strengthening of concrete structures. However, only a very limited number of researches have been conducted on rehabilitation of steel structures using BFRP fabrics.

Jayasuriya et al. [25] conducted rehabilitation of steel beams using BFRP fabric. In this study, seven steel I-beams of section W150 X 24 [22] were tested in four-point bending. Out of which fours beams were rehabilitated with varying number of layers of BFRP fabric. The depth of corrosion was varied at 20% and 40%. With the rehabilitation process the yield load, ultimate load, and the elastic stiffness could be fully restored for the 20% corroded beams. For the 40% corroded beam, the ultimate load and the elastic stiffness could be fully restored, however, it was not possible to restore the yield load fully. There was a significant improvement in the neutral axis depth for the rehabilitated beams. A reduction in ductility of the rehabilitated beams was observed with respect to the other beams. Nonetheless, with an increase in the number of layers of BFRP fabrics, there was an increase in

ductility. No debonding was observed. An equation for finding the optimum number of layers of BFRP fabrics required with different corrosion depth was also developed and presented. Hence, in this study, it was possible to fully rehabilitate steel I-beam with different depths of corrosion and predict the number of layers of BFRP required.

It can be found from the literature review that FRP materials have been used to rehabilitate both steel and concrete structures. One of the most researched FRP is CFRP which can be effectively used to rehabilitate and strengthen both steel and concrete structure. However, the biggest disadvantages of CFRP are it is very expensive and chances of galvanic corrosion when used in the steel structures. BFRP is a newer material and it is the suggested as an alternative FRP material. There are only a few researches available for rehabilitation using BFRP fabrics in steel structures and, to the best of authors knowledge, there are no past studies where the effect of various corrosion aspect ratio (length to width ratio of a corrosion patch) in a steel beam and rehabilitation of these steel beams using BFRP were considered. Hence, the first part of the current study focuses on rehabilitation of steel beams with different shapes of corrosion and developing an equation to predict the optimum number of layers of BFRP required for rehabilitating corrosion of various aspect ratios.

### 1.1.3   Repair of beams in compression using Fibre Reinforced Polymers (FRP)

Several studies have also been conducted for the rehabilitation of structures subject to compressive load. Abdelrahman and El-Hacha [26] tested six large-scale concrete columns of 300 mm diameter and height 1200 mm. Two different FRPs were used to rehabilitate the column in compression, CFRP and Steel Fibre Reinforced Polymer (SFRP) fabrics. The rehabilitation mechanism included the application of FRP sheet (fabric) by impregnating it with epoxy, to the concrete column in the hoop direction using wet lay-up method. A layer of epoxy was added to the outer layer of repair for complete saturation. Overlap length of 250 mm was used in each layer to prevent premature failure or debonding. For the rehabilitated beams the failure mode was reached when the FRP ruptured causing the column to fail. The repair technique was effective in increasing the axial strength of the concrete columns. The performance of columns rehabilitated with SFRP sheet (fabric) was found to be better than the columns rehabilitated with CFRP fabrics. Other similar researches were also successfully conducted for rehabilitation of reinforced concrete columns using CFRP and GFRP fabrics [27, 28, 29].

Only a handful number of researches were found which focusses on rehabilitation of steel members in compression. Liu et al. [30] conducted testing on seven steel I-section columns with cross section of S4x9.5 [22] (depth of 101.6 mm and width of 71 mm) and 3.05 m length were tested. Damage was simulated in the columns by removing 15.9 mm from the width of both the flanges for a length of 300 mm along the center of the beam as shown in Figure 1.4. Six specimens were tested. Five of them had the damage and one had no defect. Damaged specimens were rehabilitated with GFRP pipe of different length to compare the effect of GFRP repair on the damaged beams as well as check the effect of development length. The columns were tested in axial loads with four lateral supports to ensure load applied to the center of the section. GFRP pipe or jacket was used for the rehabilitation and expansive concrete was placed in between steel and concrete for better confinement of the GFRP jacket to the steel section. The repair methodology was successful in increasing the axial strength of the members. The failure mode observed in the original (undamaged) specimens were buckling of the specimen at the mid-span. However, the rehabilitated column specimens failed at the jacket termination point as shown in Figure 1.5. With the rehabilitation, the ultimate load capacity of the specimen increased to a maximum 2.33 times to that of the damaged column and about 0.97 times to that of the original (undamaged) column specimen. It was observed that with the increase in the length of the repair the axial strength of the specimen also increased.



Figure 1.4: Damage pattern in the section
(Liu et al)

Figure 1.5: Failure type of Specimens
(Liu et al)

Feng et al. [31] strengthened steel angle section of section L25X25X3 [22] with pultruded GFRP tube. Axial compressive forces were applied to the specimens. The GFRP tube consisted of E-Glass

fibre and vinyl resin with a petal shaped section of length 250 mm and inner diameter of 35 mm. The strengthened specimens were made with and without filling materials in between the FRP and steel as shown in Figure 1.6. The filling materials used in this study were high strength non-shrinkage grouts and bamboo splits after stewing and drying. It was found that due to use of filling materials the load increased much more than that when no filling materials were used. Fourteen specimens were strengthened and tested with both rigid and pinned boundary conditions. It was concluded that the technique used for strengthening was effective in increasing the axial compressive capacity of the specimens. The failure mode of the strengthened specimens changed from global buckling failure to localized failure which occurred at the end where the GFRP pipe terminates. The maximum load-bearing capacity of the strengthened specimens increased to 2.86 times that of the unstrengthened specimen. There was also an improvement in ductility of the strengthened specimens.



Figure 1.6: Control specimen along with two types of repair (Feng et al.)

From the literature review, it can be concluded that some previous researches were completed in rehabilitating or strengthening concrete structures using FRP materials under compression load. However, only a limited number of research work have been undertaken in rehabilitation or strengthening of steel members in compression. In these researches, steel columns under axial load was studied. The past researches used mostly CFRP or GFRP materials for the rehabilitation of steel structures. However compressive failure can also occur in beams with the deterioration or corrosion of the top flange. To the best of author's knowledge, no past research on the rehabilitation of the compressive zone in beams has been completed. Hence, the third chapter of the current study focusses

on the feasibility of using BFRP for rehabilitation of corroded steel beams in the compression zone using both experimental and numerical methods.

## 1.2 Objectives

This research study was conducted to develop an effective rehabilitating technique for rehabilitation of corroded steel beams in tension flange and as well as in compression flange. The rehabilitation was undertaken using unidirectional BFRP fabric. The objectives of this research study are the following:

a) To determine the improvement in load and moment carrying capacities of steel beams with corrosion defect in tension flange. Aspect ratio of the corrosion patch was varied.

b) To determine the improvement in load and moment carrying capacities of steel beams with corrosion defect in the compression flange when rehabilitated with BFRP fabrics.

c) To determine the change in ductility of the rehabilitated beams.

d) To develop a finite element models for the corroded, uncorroded, and rehabilitated beams.

e) To determine the optimum thickness of BFRP fabrics needed for rehabilitation of beams with corrosion defect in in the tension and compression flanges.

## 1.3 Methodology

Nine full-scale tests were conducted to compare the effects of rehabilitation using BFRP fabrics for steel beams with different aspect ratios of corrosion in the bottom flange (tension zone). Five beams had a corrosion aspect ratio of 4, three beams had a corrosion aspect ratio of 1 and one beams had no corrosion defect and it was used as the reference specimen for comparing the effect of corrosion and the rehabilitation.

For developing a repair technique for rehabilitation of steel beams with BFRP fabrics in the top flange (compression zone) with various corrosion depths, seven full-scale tests were conducted. Four beams had a maximum depth of corrosion of 40% of the flange thickness, two beams had a maximum depth

of corrosion of 20% of the flange thickness and one beam had no defect and was used for comparing the effects of rehabilitation with BFRP fabric.

The methodology used for preparing the rehabilitated beams and the test setup used for the conducting the full-scale tests are discussed in the following section.

### 1.3.1 Rehabilitation technique for steel beams with corrosion in the bottom flange

For preparing specimens for rehabilitation, wide flange steel beams (I-shaped) of section W150 X 24 (CSA 2017) [22] were cut to a length of 2000 mm. Corrosion defect was simulated in the beams by removing a maximum of 40% of the flange thickness using a Computer Numerical Control (CNC) machine. Two different aspect ratios of corrosion patch were simulated in the beams, aspect ratio of 1 and aspect ratio of 4 as shown in Figure 1.7.



Figure 1.7a: Corrosion of aspect ratio of 4          Figure 1.7b: Corrosion of aspect ratio of 1
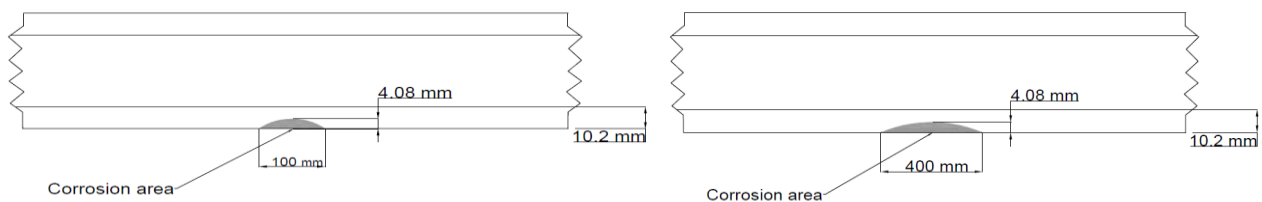
Figure 1.7: Corrosion profile of different shapes

The surface of the beams was first cleaned to a white metal finish to remove grease or dirt and ensure proper bonding with FRP. This is done by sandblasting of the beams. The surface was further cleaned with compressed air and acetone before application of BFRP fabrics. The first step in the application of BFRP fabrics was the application of primer to the areas where BFRP would be applied. MasterBrace P3500 was used as a primer in this study. The use of primer was to ensure adequate bonding between steel and the BFRP. The primer was allowed to become tack free and epoxy was applied within 24 hours of the primer application. The epoxy used for this case is MasterBrace SAT 4500 which consists of two parts: part a which is the resin and part b which is the hardener. The BFRP fabrics were applied by impregnating them with epoxy and attaching them to the beam using the wet lay-up method. The corroded area was first filled up with narrow strips of BFRP fabrics. This was done to avoid stress concentration in that zone. The dry BFRP fabrics layers were then cut

to the required length of 1200 mm X 100 mm and was attached in layers. The beams were cured for seven days before testing. This was done to ensure that the matrix attained its full strength and each layer of BFRP had a good bonding with itself as well as with the steel. After seven days of curing the beams were ready for testing.

The beams were tested with a four-point bending loading as shown in Figure 1.8. This setup was used to have a constant moment along the mid-span of the beam section in which corrosion was simulated and rehabilitation was done. The beam specimen as well as the spreader beams had a pin and roller boundary conditions. The spreader beam is a steel beam of length 800 mm with a very high stiffness value. The span length of the beam specimen was 1500 mm. The load was applied through a loading actuator to the spreader beam. The load was then transferred from the spreader beam to the specimen through loading plates which were at a spacing of 500 mm. Five Linear Variable Differential Transformers (LVDTs) were used to obtain the deflections at various locations of the beams. Four of the LVDT's had a maximum stroke of 150 mm, which means the maximum deflection that could be recorded in the LVDT was 150 mm. The out of plane LVDT had a stroke of 75 mm. One LVDT was placed at the center of the beam, two other LVDTs were placed at 375 mm from the mid-span of the beam, one LVDT was used to monitor and record the out-of-plane deflection. One LVDT was part of the loading actuator and also measured the displacement at the mid-span of the specimen as shown in Figure 1.8. These data from the LVDT's were used to obtain and plot the load-deflection as well as moment-curvature relationships of the beams.
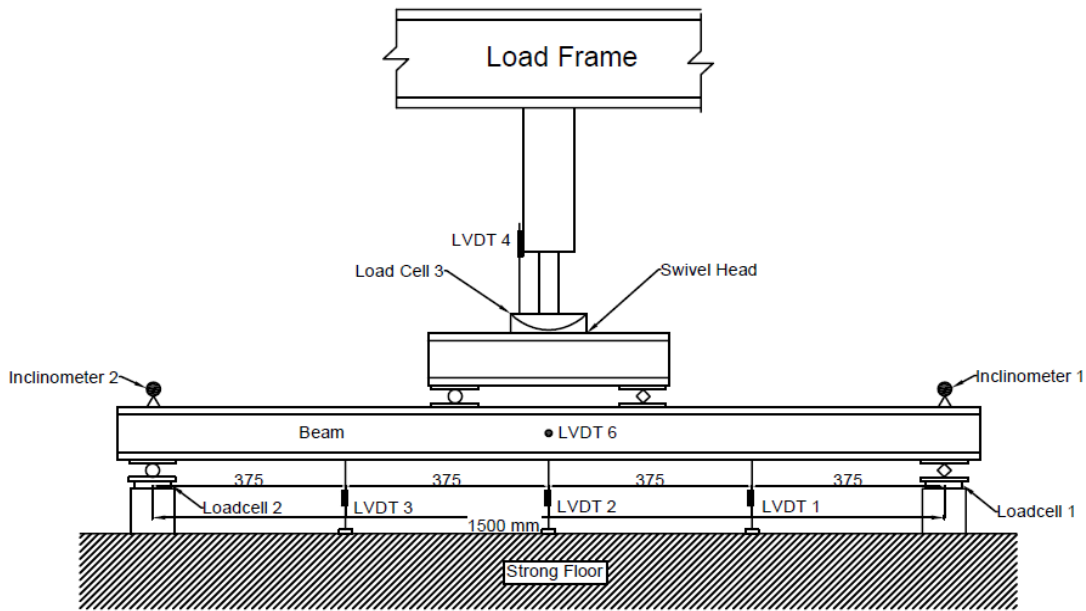
Figure 1.8: Schematic view of the test setup

Strain gauges were also attached to the beams. Kyowa strain gages of type KFRP-5-120-C1-1, having a gauge length of 5 mm and resistance of 120 ohms were used for all the experiments. For applying the strain gauge, the area was cleaned by fine grinding and further cleaned with acetone. This was to remove any grease, oil or dirt which might affect the strain reading and ensure good bonding with the steel. Loctite 401 was used as a glue to attach the strain gauges. The leads of the strain gauge were soldered with a wire which was connected to the data acquisition system. Electrical tape was used to cover the leads to avoid any contact with the steel and hence, to prevent electrical conduction. Seven strain gauges were attached to the mid-span of the beam for capturing the neutral axis depth during loading as shown in Figure 1.9a. Four strain gauges were attached at 250 and 450 mm away from the mid-span of the beam, one strain gauge was attached to the steel surface and one strain gauge was attached to the surface of BFRP at each location as shown in Figure 1.9b to check any debonding between BFRP and steel substrate.
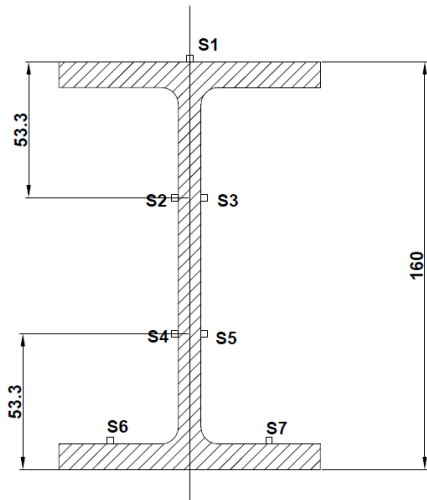
Figure:1.9a. Position of strain gauges at the mid-span of the beam
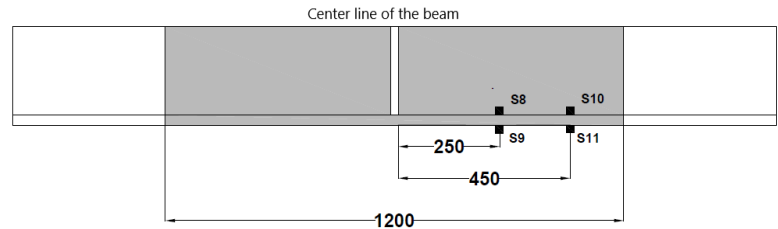
Figure: 1.9b. Position of strain gauges along the fabric

Figure 1.9: Position of strain gauges

All the data were captured using a computerised data acquisition system which had a capacity of recording two data points per second. Labview software developed by National Instruments was used to capture the data points.

### 1.3.2 Rehabilitation technique for steel beams with corrosion in the top flange

Specimens having the same dimension as shown in section 1.3.1 were also used for this case. The corrosion for this case was also simulated using CNC machine. The corrosion was simulated by removing maximum 20% and 40% of the top flange thickness as shown in Figure 1.10.
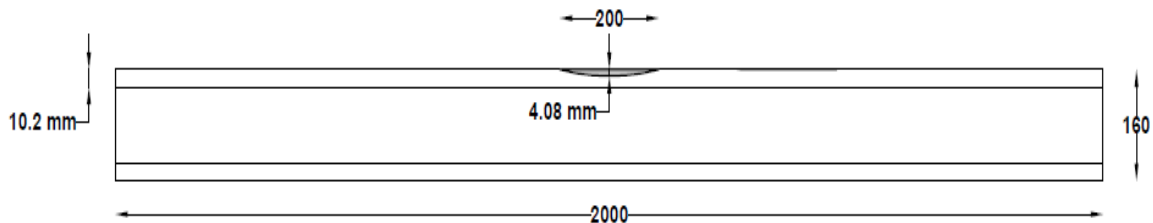


Figure 1.10: Corrosion profile of beam with 40% corrosion

To rehabilitate the beams the surface preparation of the beam, application of primer, application of BFRP layers using epoxy to the beams and curing of the beams, were done in the same process as discussed in section 1.3.1. However, in this case, the dry BFRP fabrics layers cut to the length of 500 mm X 100 mm and applied to the top flange of the beam where the corrosion was simulated. Depending on the percentage of corrosion the number of layers to be applied was decided.

The beams were tested with a four-point loading setup as shown in Figure 1.11. This setup is similar to the setup showed in section 1.3.1. The difference, in this case, was to use a longer spreader beam of length 1200 mm and the spacing between the point of application of the load to the specimen was 750 mm. The position of LVDT's was similar to that discussed in section 1.3.1.
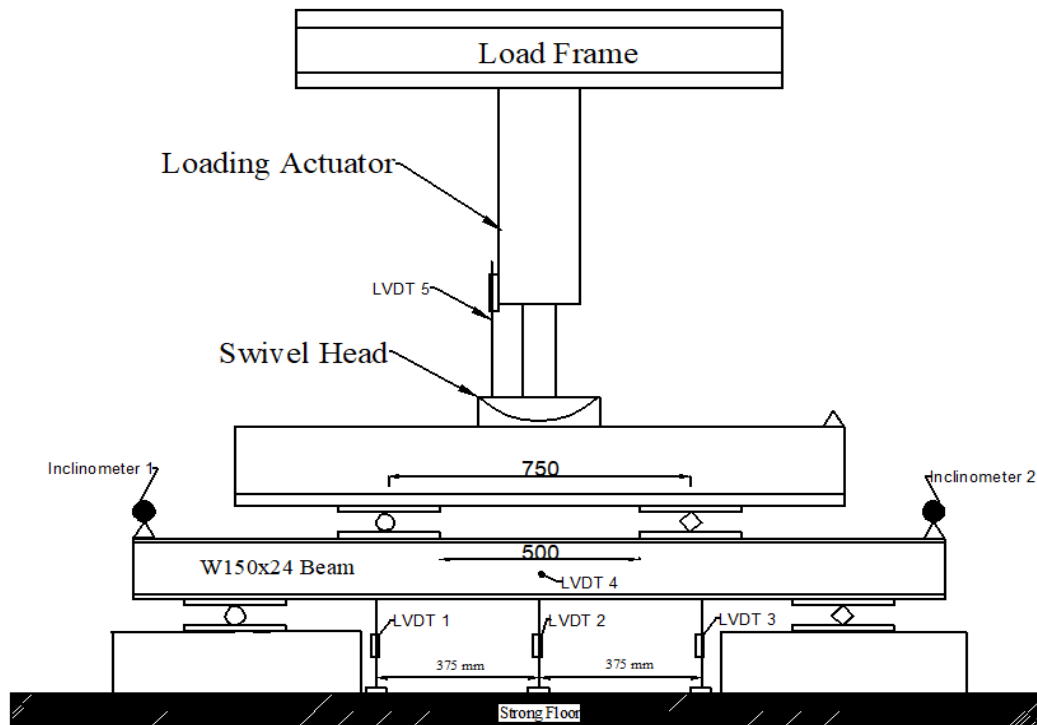


Figure 1.11: Schematic view of the test setup.

Strain gauges were also used in this setup. The same type of strain gauge was used as described in Section 1.3.1 and attached using the same procedure. However, the point of application of strain gauges is different. Seven strain gauges were attached to the mid-span of the beam for capturing the neutral axis depth during the application of load as shown in Figure 1.12. Two strain gauges were attached at 200 mm from the center of the beam, one strain gauge was attached to the steel substrate and one strain gauge was attached to the BFRP as shown in Figure 1.13. to check any debonding between BFRP and steel.

All the data were captured using a data acquisition system which had a capacity of recording two data points per second. Labview software developed by National Instruments was used to capture the data points.
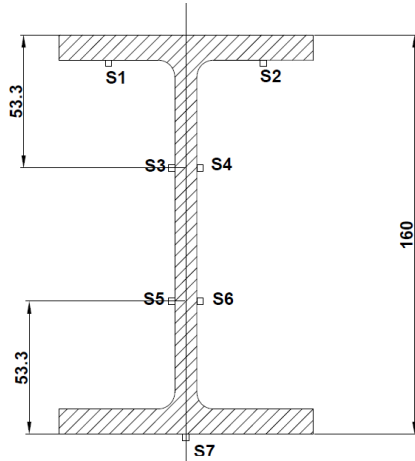
Figure 1.12: Position of strain gauge at the mid-span of the beam
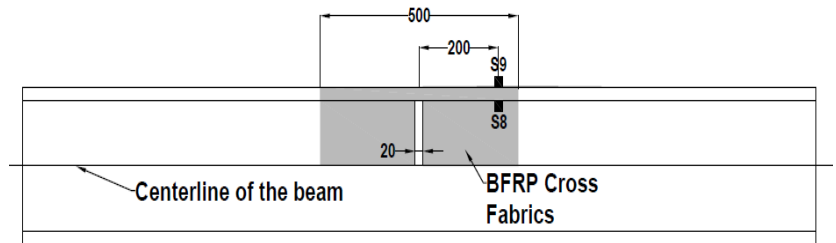
Figure 1.13: Position of Strain gauges along the length of the BFRP fabric

### 1.3.3 Standard tensile test for BFRP fabric

The tensile properties of BFRP fabric were determined by conducting tests as per ASTM D3039/D3039M–14 standard (ASTM 2014) [32]. Using the standard specification, the coupons were made to a length of 250 mm, a width of 15 mm, and a gauge length of 138 mm. The thickness of the specimen was dependent on the thickness of BFRP. The BFRP fabrics used in this study had a thickness of 0.45 mm. Tabs were used to tap the ends of the coupon to the grips of the testing machine. Four tabs made of GFRP circuit boards were used for tapping one coupon specimen. The tabs were epoxied to the specimen for smooth transfer of load as per the standard. The fibres were aligned to 0 degrees and 90 degrees with the load application direction, to obtain the tensile properties both along and across the fabric direction. The test setup of the tensile test is shown in Figure 1.14. Digital Image Correlation (DIC) technique was used for the analysis of the data.

Figure 1.14: Test setup for tension test

### 1.3.4 Standard compressive test for BFRP fabric

The compressive properties of BFRP were determined by conducting tests as per ASTM D3410/D3410M–16 standard (ASTM 2018) [33]. Using the standard specification, the coupons were made to a length of 150 mm, width of 10 mm, and a gauge length of 20 mm for the 0-degree specimens. A width of 25 mm was used for the 90-degree specimens gauge length and total length was same a that of 0-degree specimens. The thickness of the specimen was dependent on the thickness of BFRP. The minimum thickness required for BFRP fabrics was 3.77 mm. Hence, 8 layers of fabrics were used in this study. Tabs were used to tap the ends of the coupon to the grips of the testing machine. Four tabs made of GFRP circuit boards of length 65 mm were used for tapping one coupon specimen. The tabs were epoxied to the specimen for smooth transfer of load as per the standard. The fibres were aligned to 0 degrees and 90 degrees with the load application direction to obtain the compressive properties both along and across the fabric direction. The test setup of the compressive test is shown in Figure 1.15. Digital Image Correlation (DIC) technique was used for the analysis of the data.
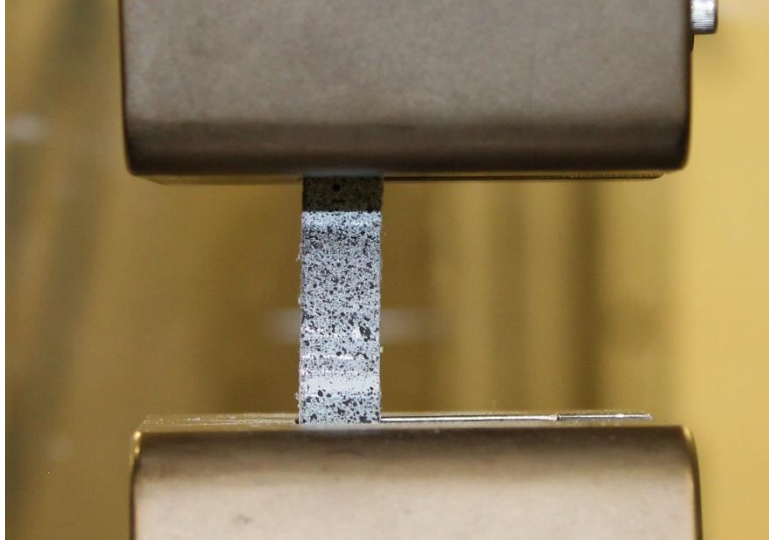
Figure 1.15: Test setup for compression test

### 1.3.5 Standard tensile test for steel

The tensile properties of steel specimens were found by conducting tests as per ASTM E8/E8M-15a standard (ASTM 2015) [34]. Using this ASTM standard, the modulus of elasticity, the yield strength, the yield point of elongation, and the tensile strength were determined. The test specimens were machined to a standard shape as per the specification and is shown in Figure 1.16. The rate of loading at the crossheads was set for a strain rate of 0.1 mm/mm/min. Extensometers were used to measure the strain of the specimen.



Figure 1.16: Steel specimens before and after testing

**1.4 Organization of Thesis**

This thesis consists of four chapters. The current chapter (first chapter) provides a general introduction, a summary of the literature reviews, and the methodology used.

The second chapter discusses the feasibility of rehabilitation of steel beams with different aspect ratios of corrosion patch in the tension flange using BFRP fabric. A parametric study using finite element method is also presented in this chapter. The finite element method was used to determine the optimum thickness of BFRP fabric required for successful rehabilitation of corroded beams with various aspect ratios of the corrosion patch.

The third chapter discusses the feasibility of rehabilitation of steel beams when the corrosion patch has been developed in compression flange. The load-deflection and moment-curvature were analyzed for all the repaired beams. Ductility and strain behavior of the repaired cases was also analysed. Finally, finite element models were developed for conducting a parametric study to determine the optimum thickness of BFRP fabrics required for different depth of corrosion.

The last chapter, Chapter 4 discusses a general discussions and conclusions.

## 1.5 References

[1] ASCE: American Society of Civil Engineers, "ASCE Infrastructure Report Card," 2017, ASCE, Virginia, USA, 1-6.

&lt;www.infrastructurereportcard.org/a/#p/bridges/overview&gt;

[2] Davis, S.L. and Goldberg, D., "The fix we're in for the state of our nation's bridge", Transportation for America, Washington, D.C, 2013.

[3] FCM: "Informing the Future: The Canadian Infrastructure Report Card (CIRC-2016)", Federation of Canadian Municipalities, Ottawa, Ontario , Canada, 2016, 1-164.

&lt;http://canadianinfrastructure.ca/en/index.html&gt;

[4] Saffarini, H., De Raff, M., Hughes, C., Pal, C., "Forensic Engineering Investigation -- Algo Mall Centre Collapse", The Elliot Lake Inquiry, Elliot Lake, ON: NORR, 2013.

[5] Bhattacharya, D.K., "Failures of welded joints", Proceedings of COFA 1997, National Metallurgical Laboratory, Jamshedpur , India, 1997, 212–220.

[6] Venkatesan, S. and Kinzel, G., "Reduction of Stress Concentration in Bolt-Nut Connectors", Journal of Mechanical Design, 128(6), 2006,1337-1342, DOI: 10.1115/1.2336254

[7] Fitzer, E., Edie, D.D., Johnson, D.J., "Carbon fibres-present state and future expectation", Carbon Fibres Filaments and Composites, 1st ed., Springer, New York, NY, USA, 1989, 3–41.

[8] Huang, X., "Fabrication and Properties of Carbon Fibres", Materials, 2 (4), 2009, 2369-2403. DOI: 10.3390/ma2042369

[9] Chung, D.L., "Carbon Fibre Composites", Butterworth-Heinemann, Boston, MA, USA, 1994.

[10] Textile learner BlogSpot, " Glass Fibre Composites | Properties of Glass Fibre | Manufacturing of Glass Fibre | Applications of Composite Glass Fibre", http://textilelearner.blogspot.com/2012/09/glass-fibre-composites-properties-of.html, viewed on October 14, 2018.

[11] Aramid fibre (presented by Fibremax Ltd), "Aramid fiber – Stronger and safer with aramid fiber", http://www.aramid.eu/, viewed on October 14, 2018.

[12] Swentek I, Thompson J, Meirson G, Ugresic V and Henning F, "Comparison of basalt, glass, and carbon fiber composites using the high-pressure resin transfer molding process", Technical Report, Western University, London, ON, Canada, 2016, 1–25.

[13] Sim, J., Park, C. and Moon, D.Y., "Characteristics of basalt fiber as a strengthening material for concrete structures". Composites Part B: Engineering, 36 (6-7), 2005, 504–512. DOI: https://doi.org/10.1016/j.compositesb.2005.02.002

[14] Ólafsson, H. and Þórhallsson, E. R., "Basalt fibre bar reinforcement of concrete structures", Basalt fibre Seminar, Reykjavik University, Iceland, January 2009, 1-11.

[15] Masoud, S., Soudki, K. and Topper, T., "CFRP-strengthened and corroded RC beams under monotonic and fatigue loads", Journal of Composites for Construction, 5 (4), 2001, 228–236. DOI: https://doi.org/10.1061/(ASCE)1090-0268 (2001) 5:4(228)

[16] Green, M.F., Dent, A.J.S., and Bisby, L.A., "Effect of freeze-thaw cycling on the behavior of reinforced concrete beams strengthened in flexure with fibre reinforced polymer sheets", Canadian Journal of Civil Engineering, 30(6), 2003, 1081-1088. DOI: 10.1139/L03-059

[17] Attari, N., Amziane, S., and Chemrouk, M., "Flexural strengthening of concrete beams using CFRP, GFRP and hybrid FRP sheets", Journal of Construction and Building Materials, 37, 2012, 746-757. DOI: https://doi.org/10.1016/j.conbuildmat.2012.07.052

[18] Al-Saidy A.H., Klaiber F.W. and Wipf T.J., "Repair of steel composite beams with carbon fibre-reinforced polymer plates", Journal of Composites for Construction, 2004, 8 (2), 163–72. DOI: https://doi.org/10.1061/(ASCE)1090-0268(2004)8:2(163)

[19] Mertz, D. R., and Gillespie, J. W., ''Rehabilitation of steel bridge girders through the application of advanced composites materials'' Final Rep., NCHRP-93-ID011, Transportation Research Board, Washington, DC., 1996, 1-34.

[20] Manalo, A., Sirimanna, C., Karunasena, W., McGarva, L., and Falzon P., "Pre-impregnated carbon fibre reinforced composite system for patch repair of steel I-beams", Journal of Construction and Building Materials, 105, 2016, 365–76. DOI: https://doi.org/10.1016/j.conbuildmat.2015.12.172

[21] Galal, K., Seif ElDin, H.M., and Tirca, L., "Flexural performance of steel girders retrofitted using CFRP materials," Journal of Composites for Construction, 16(3), 2012, 265-276. DOI: https://doi.org/10.1061/(ASCE)CC.1943-5614.0000264

[22] CISC: Canadian Institute of Steel Construction, "Handbook of Steel Construction", Markham, ON, Canada, 2017.

[23] El Damatty AA, Abushagur M and Youssef MA. "Experimental and analytical investigation of steel beams rehabilitated using GFRP sheets",    Steel and Composite Structures, 3 (6), 2003, 421–438. DOI: http://dx.doi.org/10.12989/scs.2003.3.6.421

[24] Huang L, Li Y and Wang Y. "Strengthening effects of BFRP on reinforced concrete beams", Journal of Southeast University National, 29 (2), 2013, 182–186. DOI: 10.3969/j.issn.1003-7985.2013.02.013

[25] S. Jayasuriya, A. Bastani, S. Kenno, T. Bolisetti and S. Das, "Rehabilitation of corroded steel beams using BFRP fabric", Structures, 15, 2018, 152–161. DOI: https://doi.org/10.1016/j.istruc.2018.06.006

[26] Abdelrahman, K. and El-Hacha, R., "Behavior of large-scale concrete columns wrapped with CFRP and SFRP sheets", Journal of Composites for Construction. 16(4), 2012, 430-439. DOI: 10.1061/(ASCE)CC.1943-5614.0000278.

[27] Bisby, L. A., Kodur, V. K-R., and Green, M. F. ,"Numerical parametric studies on the fire endurance of fibre-reinforced-polymer confined concrete columns ", Canadian Journal of Civil Engineering, 31(6), 2004, 1090–1100. DOI: https://doi.org/10.1139/L04-071

[28] Ilki, A., Peker, O., Karamuk, E., Demir, C., and Kumbasar, N., "FRP retrofit of low and medium strength circular and rectangular reinforced concrete columns", Journal of Materials in Civil Engineering, 20(2), 2008, 169–188. DOI: 10.1061/(ASCE)0899-1561(2008)20:2(169)

[29] Issa, M. A., Alrousan, R. Z., and Issa, M. A., "Experimental and parametric study of circular short columns confined with CFRP composites", Journal of Composites for Construction, 13 (2), 2009 ,135–147. DOI: https://doi.org/10.1061/(ASCE)1090-0268(2009)13:2(135)

[30] X. Liu, A. Nanni, and P. F. Silva, "Rehabilitation of compression steel members using FRP pipes filled with non-expansive and expansive lightweight concrete", Advances in Structural Engineering, 8(2), 2005, 129-142. DOI: https://doi.org/10.1260/1369433054038029

[31] P. Feng, S. Bekey, Y. Zhang, L. Ye and Y. Bai, "Experimental study on buckling resistance technique of steel members strengthened using FRP", International Journal of Structural Stability and Dynamics, 12(1), 2012, 153-178. DOI: https://doi.org/10.1142/S0219455412004604

[32] ASTM. Standard Test Method for Compressive Properties of Polymer Matrix Composite Materials with Unsupported Gage Section by Shear Loading D3410/D3410M-16. PA: ASTM International, West Conshohocken, Pennsylvania, USA, 2018.

[33] ASTM. Standard Test Method for Tensile Properties of Polymer Matrix Composite Materials. D3039/D3039M-14. PA: ASTM International, West Conshohocken, Pennsylvania, USA, 2014.

[34] ASTM. Standard Test Methods for Tension Testing of Metallic Materials. E8/E8M-15a. PA: ASTM International, West Conshohocken, Pennsylvania, USA, 2015.

**Chapter 2: Flexural Rehabilitation of Steel Beams with Various Corrosion Aspect Ratios with BFRP Fabric**

## 2.1 Introduction

In recent years, increasing number of structural steel members with long service lives have begun to show corrosion damage that has been accumulated over time. These deficient structures will further age, crack, and weaken over time. Corrosion is one of the major causes of structural deterioration. Moreover, the prevalent use of de-icing salts in the colder countries further worsens the condition of these steel structures. According to the Infrastructure Report Card published by American Society of Civil Engineers in 2017, almost 40% of the existing bridges in the USA have already exceeded their design life of 50 years and 9.1% of existing bridges are structurally deficient [1]. In a report published by Transportation for America in 2013, about 66,405 bridges in North America are structurally deficient and about 260 million trips are taken over these deficient bridges every day [2]. According to the Canadian Infrastructure Report Card published in 2016 by Federation of Canadian Municipalities, about 5% of Canadian bridges are in very poor condition and has an estimated replacement value of about 50 billion CAD [3]. Many of these structures needs immediate rehabilitation or strengthening to meet their structural demands. Traditional repair methods in steel structures which includes welding or bolting of additional steel plates have many drawbacks. Some of the major drawbacks are an increase in dead load, fatigue failure due to stress concentration resulting from welding or drilling, reduction in the durability due to the corrosion, and lesser adaptability of attached plates to fit the complex profiles. In addition, the regular services may have to be interrupted while rehabilitation work is progress. There is also a potential risk of weld cracking failure.

There is a need for better and cost-effective solutions with the use of new, environmentally friendly, weather resistant, and lighter materials to mitigate the disadvantages of structural rehabilitation using traditional bolting and welding methods. One possible alternative is the use of fibre reinforced polymer (FRP) composites. The main advantages of FRPs are their high strength-to-weight ratio and resistance to corrosion and chemical attacks. These composites could be found in various forms such as carbon fibre reinforced polymer (CFRP), glass fibre reinforced polymer (GFRP), and aramid fibre reinforced polymer (AFRP).

26

## 2.2 Literature Review

Few studies have been conducted on rehabilitation of steel beams using CFRP and GFRP fabrics as well as plates. In this paper, fabric refers to a single layer of the FRP fabric and is applied to the structures in layers using an adhesive system. Plate refers to a specific thickness of the FRP which have already been bonded and cured by the manufacturer and can be applied directly to the deficient structures for rehabilitation. In a study carried out by Mertz and Gillespie in 1996 [4], CFRP plates were used for rehabilitation of corroded steel beams. The study tested both small-scale and large-scale specimens. The study found increases in elastic stiffness and ultimate strength of rehabilitated steel beams by about 20% and 50%, respectively for the small-scale specimens. For large-scale specimens, the elastic stiffness increased by about 25% and ultimate strength increased by about 30%. Sen et al. [5] in 2001 strengthened W200X165X35.9 steel beams with 5 mm thick CFRP laminate and found that the ultimate strength of the beams increased up to 52 %. In 2004, Saidy et al. [6] also conducted rehabilitation of steel beams with CFRP plates and concluded that the elastic stiffness can be partially restored up to 50% using CFRP plates and the ultimate strength of the beams can be restored to that of the original beam. However, there was a reduction in the ductility of the repaired beams. In a similar research, Malano et al. [7] in 2016 rehabilitated steel I-beams with corrosion and crack defects in the flange using CFRP fabrics. The depth of corrosion was 80% of the flange thickness removed for a length of 90 mm and crack was simulated using a 1 mm wide rectangular notch through entire flange width. The study showed that the ultimate strength of the repaired beams reached that of the uncorroded beam for both defects. The repaired beams also exhibited 16% higher elastic stiffness. In 2009, Chen and Das [8] also observed similar benefits from steel beams rehabilitated by CFRP fabrics. In this study, it was concluded that the elastic stiffness of corroded beams could be improved, and ultimate strength could reach that of the original beam. Selvaraj and Madhavan [9] in 2017 strengthened 1400 mm ISMC (Indian Standard Medium Weight Channels) 125 steel beams with CFRP fabric using two types of strengthening: surface strengthening and closed strengthening. It was found that with multiple layers of CFRP, the increase in beam capacity was about 40% for closed strengthening and 17% for surface strengthening. El Damatty et al. [10] in 2003 conducted flexural rehabilitation of W150x37 I-shaped steel beams using 19 mm thick GFRP plates. The study found an increase in elastic stiffness of 15%, increase in yield moment of 23%, in addition to a significant increase in ultimate moment capacity of 78%. In this study, debonding failure was prevented by using a strong methacrylate adhesive system (A0420). Hence, it can be concluded from

the previous studies that CFRP and GFRP fabrics can be used effectively for both rehabilitation as well as the strengthening of steel beams.

Basalt Fibre Reinforced Polymer (BFRP) fabric is a relatively new material. Hence, a very limited number of studies for rehabilitation or strengthening of structures using BFRP fabric has been completed. Basalt fibre fabric is manufactured by melting quarried Basalt rock. This material does not have any additives; hence, it is an environmentally friendly material. Moreover, its cost is by far less than carbon fibre fabric. Bastani et al. [11] reported that the cost of basalt fibre fabric is about 1/5th of the cost of similar carbon fibre fabric. Basalt fibre fabric has a better tensile strength than E-glass fabric and more ductility than carbon fibre fabric. Basalt fibre fabric also has a good resistance to chemical attack, impact load, and fire [12]. The tensile strength of basalt fibre fabric is about 30% of that of carbon fibre fabric and 60% higher than that of glass fibre fabric [13].

CFRP and GFRP have commonly been used for rehabilitation and strengthening of concrete structures [14]. However, the application of BFRP for rehabilitation of reinforced concrete beams is very limited. Sim et al. [13] in 2005 used BFRP fabric as a strengthening material for reinforced concrete beams. The research also focused on the durability of basalt fabric. It was observed that under accelerated weathering conditions, the strength reduction rate of BFRP fabric is lower than that of GFRP fabric, which is an indication that BFRP fabric has more durability. The strength of the beams significantly increased with the use of multiple layers of BFRP fabric. The mode of failure was rupture of fabrics causing a sudden load drop. Huang et al. in 2013 [15] also investigated the strengthening effect of BFRP fabric on concrete beams. The study concluded that BFRP fabric can be effectively used as a strengthening material for concrete beams and the strength of concrete beams strengthened with BFRP fabric lies in between strengths of concrete beams strengthened with similar CFRP and GFRP fabrics. Hence, only two previous studies on rehabilitation of concrete beams with BFRP fabrics were found in the literature.

A limited research on use of BFRP fabrics for rehabilitation and strengthening of steel beams is available. In a study completed by Bastani et al. in 2019 [11] five steel beams with corrosion defect in the web region were rehabilitated using BFRP fabrics. Using BFRP fabrics the yield load capacity, ultimate load capacity, and the stiffness of the beam were restored to that of an uncorroded beam. In

another study, Jayasuriya et al. [16] in 2018 conducted rehabilitation of structural steel beams with various corrosion depths with BFRP fabric. The study concluded that the ultimate strength of the corroded beams could be restored to the strength of the virgin or control beam with application of adequate thickness of BFRP fabrics. In this study the shape and area of corrosion defect was kept unchanged.

The severity of corrosion damage in a steel structure or steel structural component can be measured by the depth of corrosion, as well as the shape and area of the corrosion defect. However, literature review did not find any previous research where behavior of rehabilitated steel beams with various shapes of corrosion was studied. Hence, the current research was carefully designed and executed to determine the structural performance of steel beams with rectangular corrosion shape with various aspect ratios rehabilitated with BFRP fabric. The study was completed using both experimental and numerical methods.

## 2.3 Experimental Program

In this study, a wide flange steel beam (I-shaped) with the designation of W150X24 (CSA 2017) [17] was selected for making all the beam specimens. Table 2.1 shows the test matrix used in the experimental program. A total of 10 steel I-beams were tested in this study. Three of these beams were control beams and seven were rehabilitated with BFRP fabric. The control beam that did not have any corrosion defect is called control uncorroded beam specimen or virgin beam specimen and it is identified as "UB" in Table 2.1. The remaining nine beams had corrosion defects. The width of the flange was 100 mm. The beam specimens were corroded through the width of the flange, but two corrosion length were considered. Four beams had a square corrosion shape, measuring 100 mm long x 100 mm wide or aspect ratio (corrosion aspect ratio of 1) and five beams had a rectangular corrosion shape, measuring 400 mm long x 100 mm wide (corrosion aspect ratio of 4). Two of these nine beams had corrosion defect, however, they were not rehabilitated and hence, they are called control corroded specimens (CC). These two beams are identified as "CC100" and "CC400". In the specimen ID of these beams "CC" indicates control corrosion specimens; and "100" and "400" are the length of the corrosion defect with AR of 1 and 4, respectively. The flange thickness of steel beams was locally reduced to simulate loss of wall thickness due to corrosion as shown in Figure 2.1. The depth of corrosion was kept unchanged at 40% of the flange thickness for all the test specimens.

The specimen IDs of the beams rehabilitated with BFRP fabrics are "R100_7L", "R100_10L", "R400_7L", "R400_10L", "R400_15L" and "R400_20L". The specimen ID of the rehabilitated specimens reflects  the length of corrosion and the number of BFRP fabric layers used. For example, the specimen "R100_7L" indicates that this specimen had a corrosion patch of 100 mm x 100 mm (aspect ratio or AR of 1) and the specimen was rehabilitated with seven layers of BFRP fabrics. One beam was rehabilitated with narrow strips of cross BFRP fabrics before the final rehabilitation pattern was determined and this specimen is identified as R100_7L_PC. Where, "PC" represents partial cross fabrics. The Specimen R400_20L was tested to check the effects of applying very thick repair which will be discussed in detail in later sections.



(a) Beam with Corrosion Defect (AR = 1)    (b) Beam with Corrosion Defect (AR = 4)
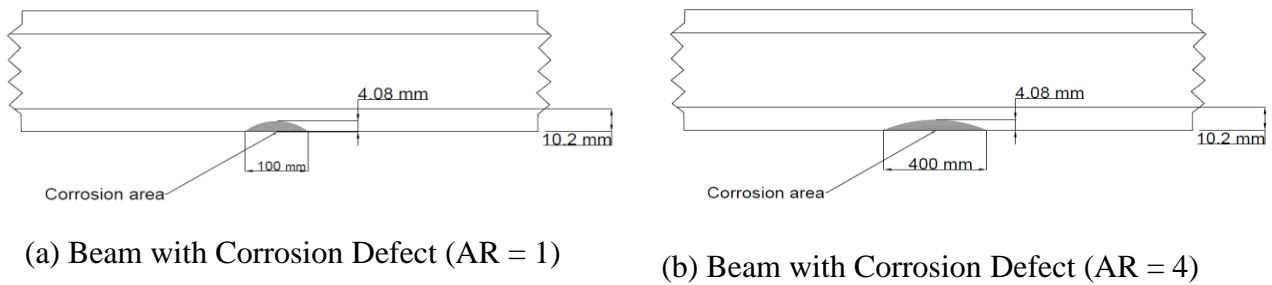
Figure 2.1: Corrosion profile of different shapes

Table 2.1: Test Matrix

| Specimen ID | AR | Type of Beam | Length of Corrosion | No. of Basalt layers | Total Thickness of the repair (mm) |
|---|---|---|---|---|---|
| UB | - | Control Uncorroded (Virgin) | - | - | - |
| CC100 | 1 | Control Corroded | 100 | - | - |
| CC400 | 4 | | 400 | - | - |
| R100_7L | 1 | Rehabilitated Specimens (AR 1) | 100 | 7 | 3.15 |
| R100_10L | 1 | | 100 | 10 | 4.5 |
| R400_7L | 4 | | 400 | 7 | 3.15 |
| R400_10L | 4 | Rehabilitated Specimens (AR 4) | 400 | 10 | 4.5 |
| R400_15L | 4 | | 400 | 15 | 6.75 |
| R400_20L | 4 | | 400 | 20 | 9 |

Tension testing of coupon specimens made from these beam specimens was conducted in accordance with ASTM E8/E8M-15a (ASTM 2015) [18] to obtain the material properties of the steel beams. The results are presented in Figure 2.2. BFRP unidirectional fabric was used to rehabilitate the beams with corrosion defect. Tension tests were also conducted on coupons made from BFRP fabric as per ASTM D3039/D3039M-14 (ASTM 2014) [19]. The result obtained is shown in Figure 2.3.
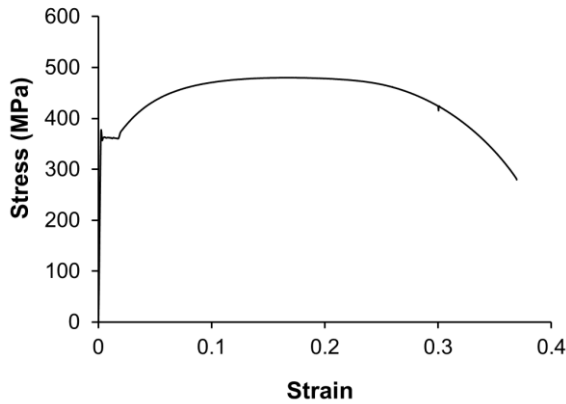


Figure 2.2: Stress-strain behavior of steel
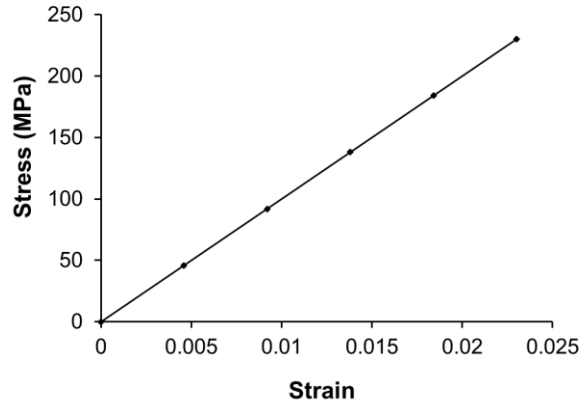
Figure 2.3: Stress-strain behavior of BFRP

The unidirectional dry basalt fibre fabric was attached to the steel beams using two-part epoxy resin. In order to ensure a good bond between the epoxy and the steel substrate, the repair area of the steel beam was first sandblasted, as suggested by McKnight et al. [20] and then covered with a primer layer. Within 24 hours of applying the primer, the BFRP fabric layers were impregnated with epoxy resin and then attached to the specimen using the wet lay-up method. In this method, small pieces of epoxy-saturated basalt fabric were first placed on the corrosion area to fill the gap of the corrosion area and avoid any stress concentration. Then precut fabric layers of 1200 mm length were attached in layers by impregnating with epoxy resin and then by applying uniform pressure on each layer. The first beam was rehabilitated with seven layers of BFRP fabric. Cross straps (BFRP fabrics wrapped in the perpendicular direction) were also attached to reduce the risk of de-bonding of the longitudinal fabrics.

The four-point bending load was applied to all beam specimens (Figure 2.4). The test setup involved the use of a loading actuator to apply the bending load on the test specimen through a spreader beam. Each beam was 2000 mm long and the span length of each beam was 1500 mm. A total of five Linear Variable Differential Transformer (LVDTs) were used in the setup. LVDTs were used to capture the

31

deflection values at the mid-span (LVDT 2 in Figure 2.4); at one-third distance from both supports (LVDT 1 and LVDT 3), at the top of loadcell 3 to verify the deflection values at the mid-span (LVDT 4), and to measure the out-of-plane deflection (LVDT 5). The data from LVDTs 1, 2, and 3 were used to obtain the deflection and curvature profile of the beam. Inclinometers were attached at both ends of the beam to check the symmetry of the setup during the application of load using the slope values. The beam specimens were loaded monotonically using the displacement control method. The photo of the experimental setup is shown in Figure 2.5.
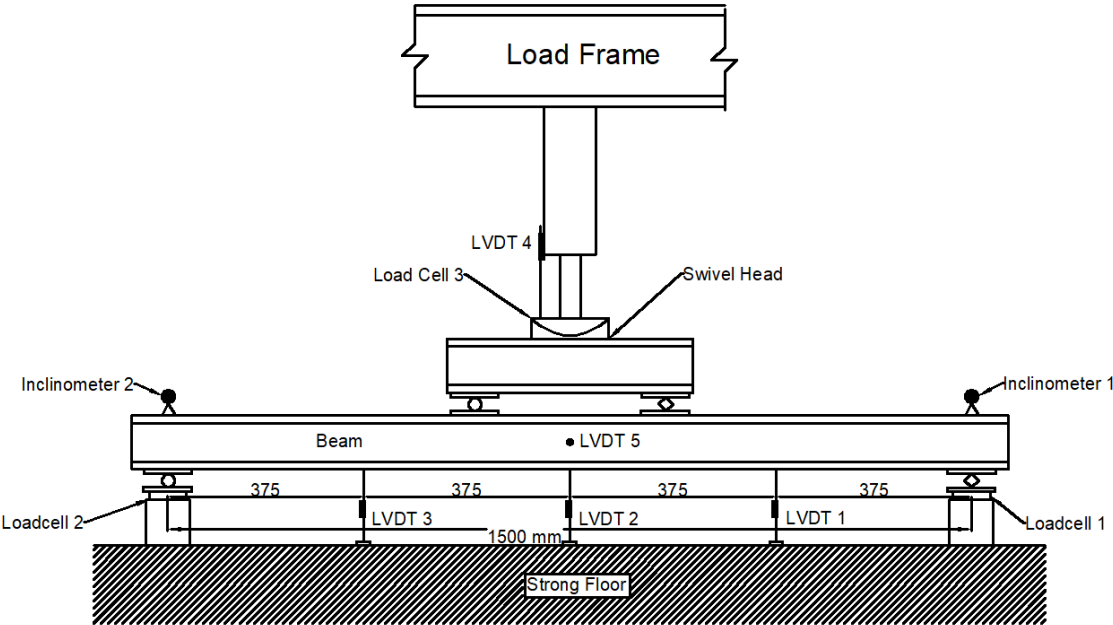


Figure 2.4: Schematic view of the test setup
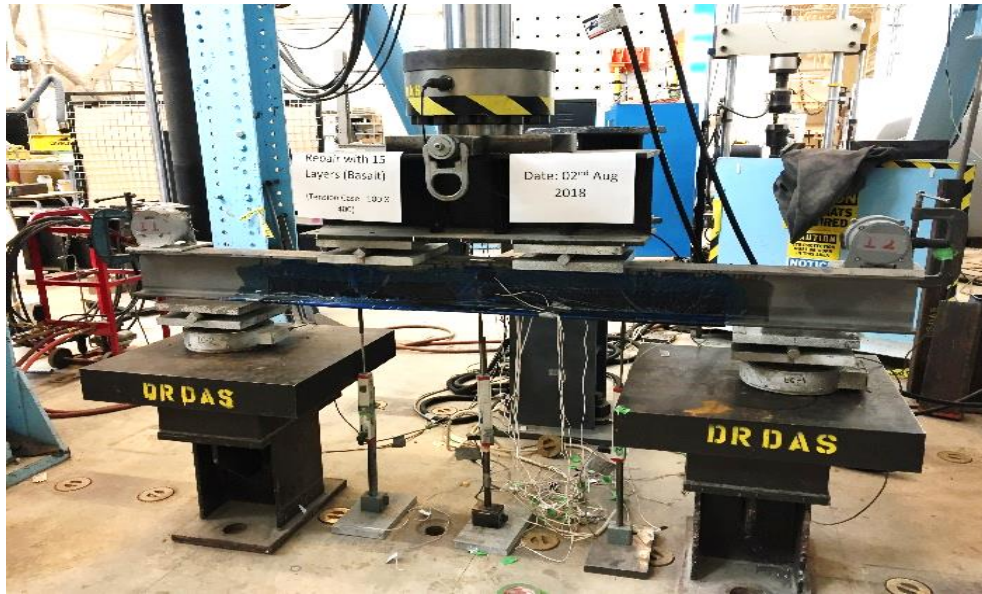
Figure 2.5: Experimental setup

The first objective of the test program was to develop a repair technique for the beams such that de-bonding or slippage of the fabric can be avoided. Hence, the first corroded beam specimen (R100_7L_PC) was repaired with seven longitudinal layers of BFRP and 100 mm wide BFRP cross straps were attached at three regions of the beam: at the mid-span and at two ends as shown in Figure 2.6. However, it was observed that debonding of the fabrics occurred in between two cross straps as shown in Figure 2.7.
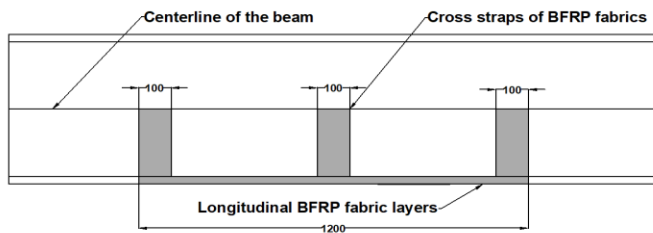


Figure 2.6: Repair pattern



Figure 2.7: Debonding of BFRP fabric

The load-deflection curve of the R100_7L_PC and its comparison with the uncorroded control beam (UB) and the beam with control corrosion (CC100) is shown in Figure 2.8. The load value was obtained from the loadcell attached to the loading actuator and the deflection was measured from LVDT 2. It was observed that the load capacity of the repaired beam R100_7L_PC improved initially. However, at a deflection of about 20 mm, that is soon after yielding of the beam, debonding occurred and the load dropped to that of the control corroded beam specimen, CC100 beam. Hence, this repair scheme was not able to improve the load capacity of the corroded beam at higher deflection values since debonding occurred at an early stage of loading. Consequently, for rehabilitation of subsequent beams, it was decided to apply cross straps for the entire length of the repair to prevent the debonding. In a study conducted by Narmashiri et al [21] in 2012 it was also found that with a longer bond length, the chances of debonding of CFRP fabric failure reduced.
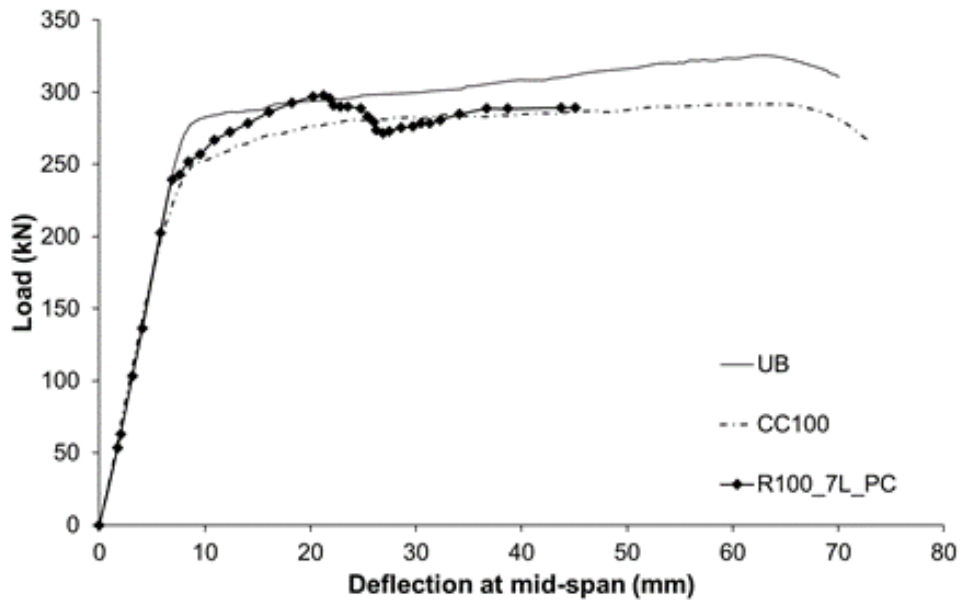


Figure 2.8: Comparison of Load-deflection curve of 40R100_7L_PC compare to control beams

A schematic view and a photo of the repair scheme adopted for remaining specimens is shown in Figures 2.9 and 2.10. A 20 mm gap was provided at the mid-span of the beam to facilitate the attachment of strain gauges.
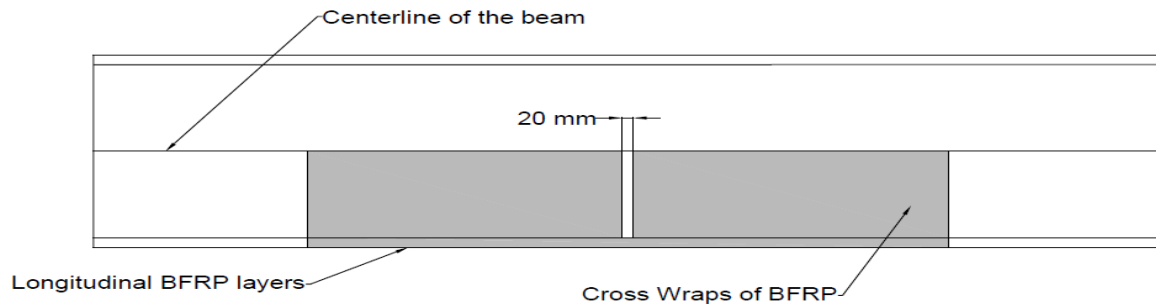
Figure 2.9: Schematic layout of the rehabilitation scheme



Figure 2.10: Photo of the final rehabilitation scheme with strain gauge

Strain gauges were also installed to acquire strain values at various locations of the beam during testing. A total of 11 strain gauges were installed. Seven strain gauges (S1 to S7 in Figure 2.11a) were installed at the mid-span of the steel beam to study the change in neutral axis depth at different deflection values. Remaining four strain gauges (S8 to S11 in Figure 2.11b) were used to monitor any possible debonding or slippage between the BFRP fabrics and the steel substrate. Strain gauges S9 and S11 were installed on the BFRP fabric and strain gauges S8 and S10 were installed on steel substrate. The strain gauges S8 and S9 were located at 250 mm away from the mid-span of the beam whereas, strain gauges S10 and S11 were placed at 450 mm away. All the experiment data was collected using a data acquisition system connected to a computer.

(a) Position of strain gauges at the mid-span of the beam

(b) Position of strain gauges along the fabric
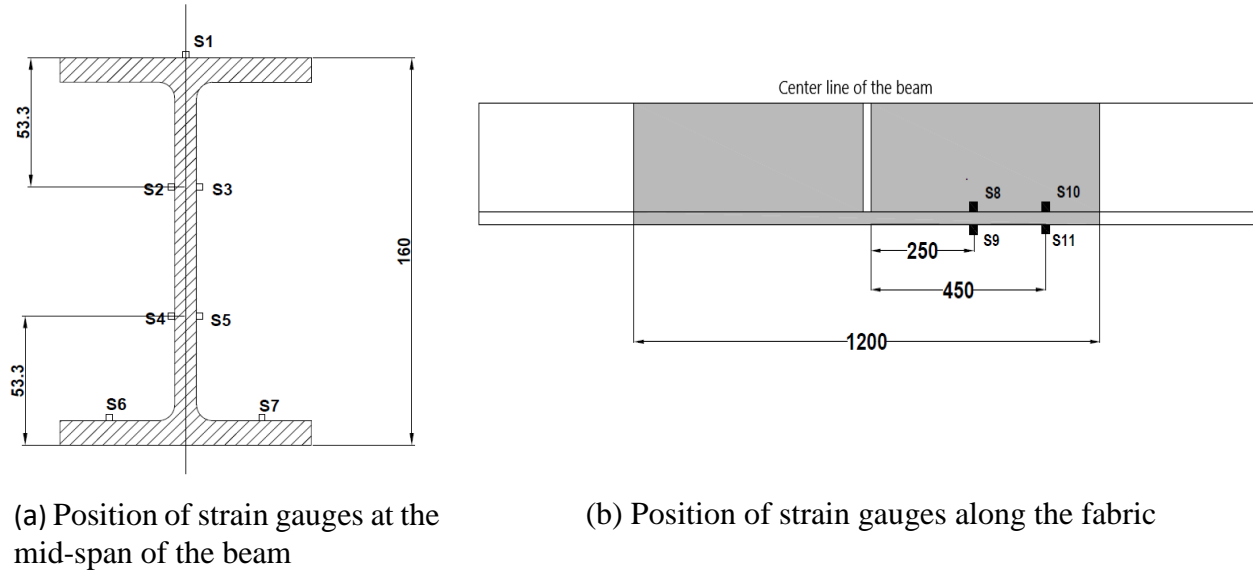
Figure 2.11: Position of strain gauges

## 2.4 Results and Discussion

One objective of the research was to develop a relationship between the increase in bending load or moment capacity of the rehabilitated beam with the number of layers of BFRP applied for different corrosion AR. The load-deflection and moment-curvature curves obtained from the tests were plotted for each specimen. These curves were used to determine the effect of the aspect ratio (AR) of corrosion patch on the load carrying capacity of the specimen and its relationship with the number of BFRP layers. To further generalize the effects of different aspect ratios and the number of layers, finite element method was used, and this will be discussed in later sections.

### 2.4.1 Load-Deflection Behavior

The load-deflection behaviors for each test are plotted. The deflection data was obtained from the LVDT located at the mid-span of the beam (LVDT 2). The load values were obtained from the loadcell attached to the loading actuator. Figures 2.12 and 2.13 show the load-deflection behaviors of the steel beams with 100 mm x 100 mm corrosion shape (AR of 1) and 100 mm x 400 mm corrosion shape (AR of 4), respectively. It was observed that for both corrosion aspect ratios, the load-deformation behaviors were similar. The rehabilitated beam first showed an elastic behavior until yielding occurred, then the non-linear portion started, and the load increased to its ultimate load, followed by a sudden drop in the load due to the rupture of the BFRP fabrics. This was followed by a slight increase in load because of the stress redistribution and the load value beyond the drop was slightly higher than the beams with control corrosion (specimens CC100 in Figure 2.12 and CC400

36

in Figure 2.13), indicating that the fabrics did not have any significant beneficial strengthening effect once the BFRP fabric ruptured. Similar behavior was also observed by Jayasuriya et al. [16]. Jayasuriya et al. studied the effect of depth of corrosion while rehabilitating the steel beam with BFRP fabric. Figure 2.14 shows the rupture of BFRP fabrics in the beam and Figure 2.15 shows the final deflected shape of the rehabilitated beam as observed in the experimental study.
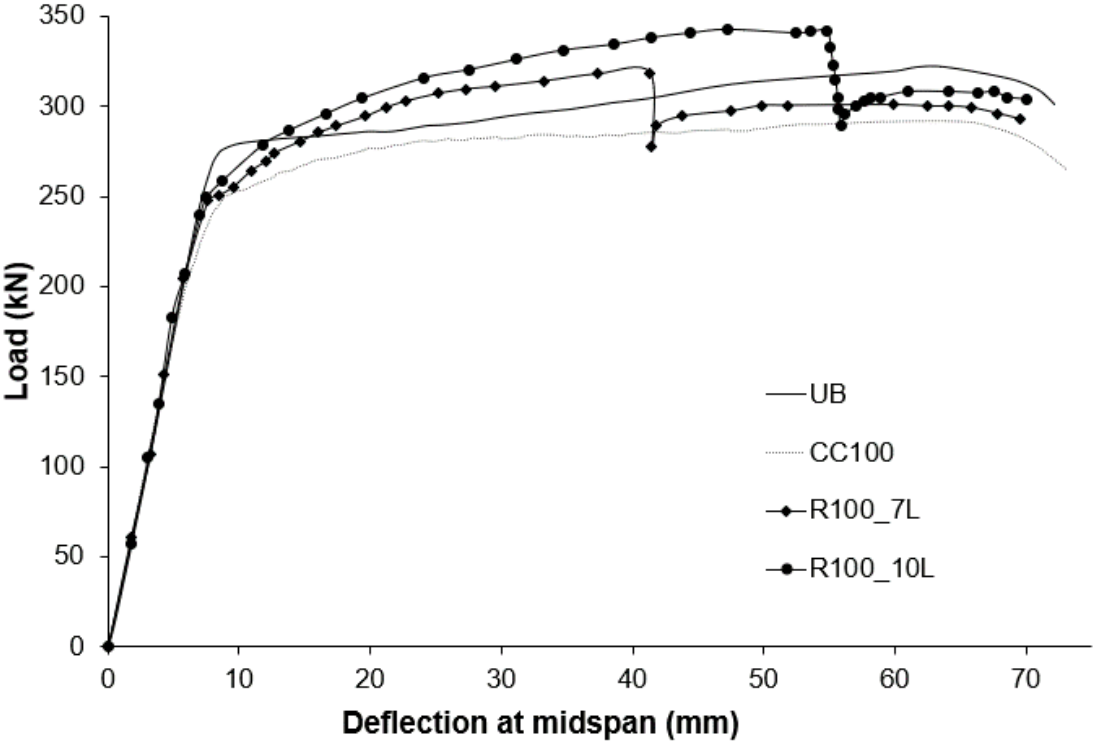


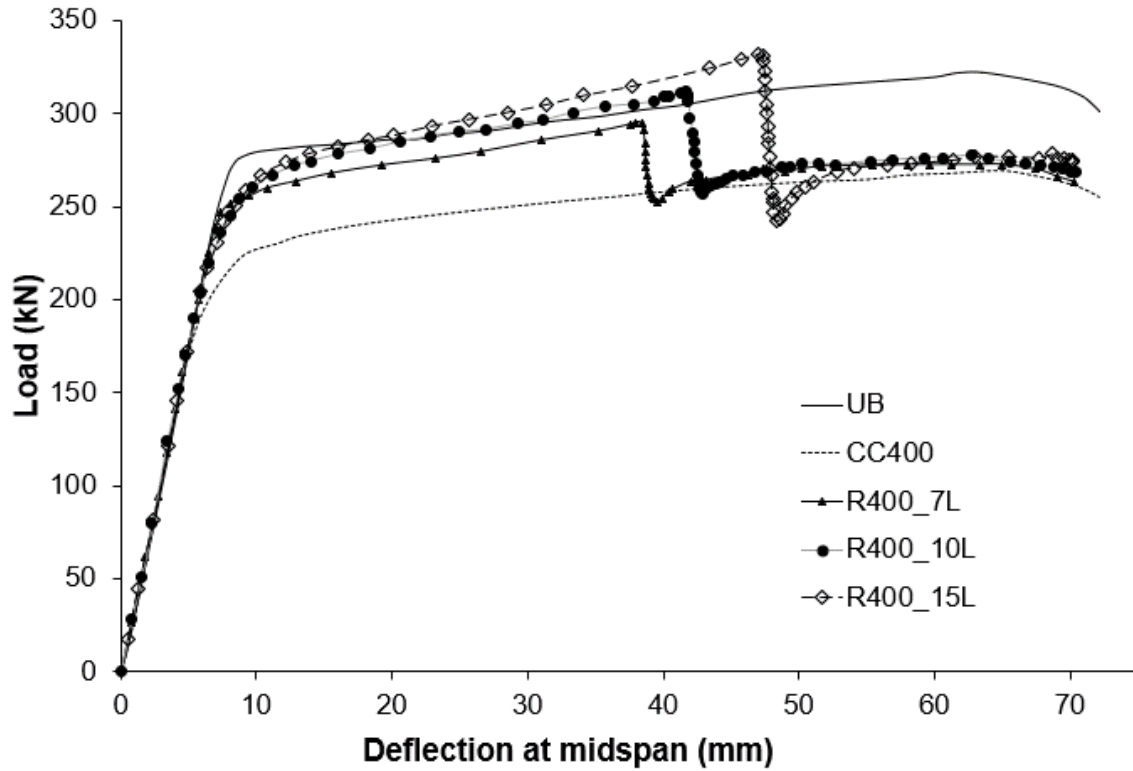Figure 2.12: Load-deflection curves of beams with corrosion AR of 1

Figure 2.13: Load-deflection curves of beams with corrosion AR of 4



Figure 2.14: Failure mode showing rupture of BFRP
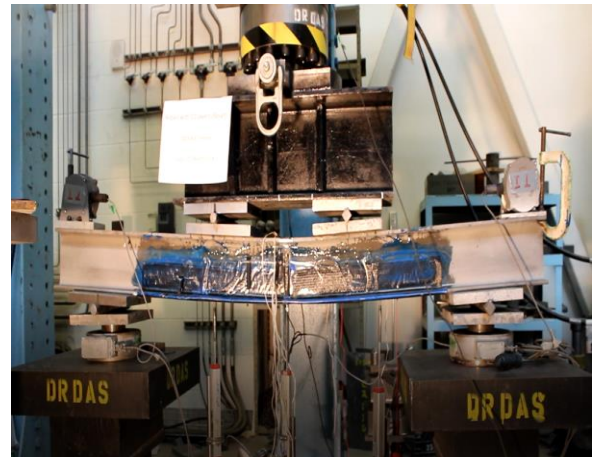


Figure 2.15: Final deflected profile of the steel beam

Table 2.2 summarises the yield and ultimate load values of all specimens. With the use of BFRP fabric, there was a moderate increase in yield load and a substantial increase in ultimate load for each specimen when compared to the uncorroded control (virgin) specimen, UB. Similar behavior was observed by other researchers in rehabilitating steel beams using GFRP and CFRP fabrics [8,10]. As shown in Table 2.2, for beams with corrosion aspect ratio (AR) of 1, the yield load increased from 229.8 kN in control corrosion beam (specimen CC100) to 247.4 kN when rehabilitated when seven layers of BFRP fabrics were used (specimen R100_7L). The ultimate load increased from 286.4 kN to 318.6 kN, which is an increase of 11.3%. However, neither the yield nor the ultimate load for specimen R100_7L reached the yield or ultimate loads of the uncorroded (virgin) beam, UB. When 10 layers of BFRP fabrics were applied, the yield load did not reach the value of the uncorroded (virgin) beam, UB, but the ultimate load exceeded that of the UB specimen. Therefore, it can be concluded that the optimum number of layers needed to completely restore the ultimate load of a beam with corrosion aspect ratio of 1 will be in between 7 and 10. For beams with corrosion aspect ratio of 4, it can be concluded from Table 2.2 that the optimum number of BFRP layer to fully restore the beam to the level of ultimate strength of control (virgin) beam is in between 10 and 15.

Table 2.2: Comparison of yield and ultimate loads for all beam specimens

| Specimen ID | Yield Load ($P_y$) (kN) | Ultimate Load ($P_u$) (kN) | % Change of $P_y$ compare to UB | % Change of $P_u$ compare to UB | % Change of $P_u$ compare to control corroded |
|---|---|---|---|---|---|
| UB | 273.3 | 322.2 | Reference beam | Reference beam | - |
| CC100 | 229.8 | 286.4 | -15.90% | -11.10% | Reference beam |
| R100_7L | 247.4 | 318.6 | -9.50% | -1.10% | 11.30% |
| R100_10L | 249.4 | 341.9 | -8.70% | 6.10% | 19.40% |
| CC400 | 225.4 | 267.0 | -17.50% | -17.10% | Reference beam |
| R400_7L | 246.9 | 295.1 | -9.60% | -8.40% | 10.50% |
| R400_10L | 253.7 | 311.6 | -7.20% | -3.30% | 16.70% |
| R400_15L | 258.5 | 331.7 | -5.40% | 2.90% | 24.20% |

Figures 2.16a and 2.16b compare load-deflection behaviors of corroded beams with two different aspect ratios but rehabilitated with same number of BFRP fabric layers. Table 2.3 summarises the key information for these plots. It can be found from Table 2.3 that the increase in the ultimate load of the beam with a corrosion aspect ratio of 1 and rehabilitated with seven layers of BFRP fabric (R100_7L) is 7% higher than the beam with a corrosion aspect ratio of four and rehabilitated with seven layers of BFRP fabric (R400_7L). The deflection at the ultimate load also increased by 8.7 % when compared with specimen with corrosion aspect ratio of one, indicating a higher ductility for specimen with aspect ratio of one. Similar behavior is observed with beams rehabilitated with ten layers of BFRP fabric. The increase in the ultimate load of Specimen R100_10L (AR = 1) compared to Specimen 40R400_10L (AR = 4) is about 14% higher. Deflection at ultimate load also increased by 24% for Specimen R100_10L. Hence, it can be concluded that for beams with corrosion of lower aspect ratio, the increases in the yield and the ultimate loads are greater than the beams with corrosion of higher aspect ratio if the number of BFRP fabric is kept unchanged. As well the ductility of the beams with a smaller corrosion aspect ratio is more than the ductility of the beams with a larger corrosion aspect ratio when same number of BFRP fabrics is used.

Table 2.3: Comparison of beams rehabilitated with the same number of BFRP layers but different corrosion aspect ratios

| Specimen ID | Ultimate Load ($P_u$) | Deflection at mid-span | % Increase in $P_u$ w.r.t Control | % Increase in $P_u$ w.r.t AR 4 | % Increase in failure deflection w.r.t AR 4 |
|---|---|---|---|---|---|
| CC100 | 286.3 | 46.03 | Reference Beam | - | - |
| CC400 | 267.1 | 69.1 | Reference Beam | - | - |
| R400_7L | 295.1 | 37.9 | 10.50% | Reference Beam | Reference Beam |
| R100_7L | 318.6 | 41.3 | 11.30% | 7.2% | 8.7% |
| R400_10L | 311.6 | 41.6 | 16.70% | Reference Beam | Reference Beam |
| R100_10L | 341.9 | 54.8 | 19.40% | 14.1% | 24.0% |
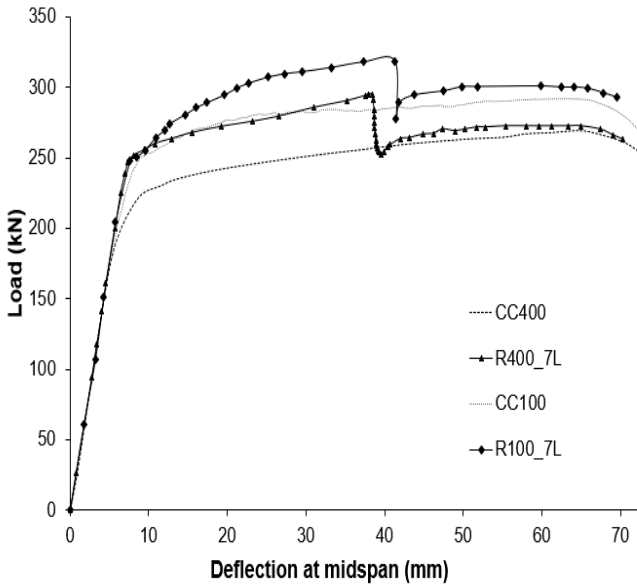
(a) Repair with 7 layers of BFRP for AR of 1 and 4
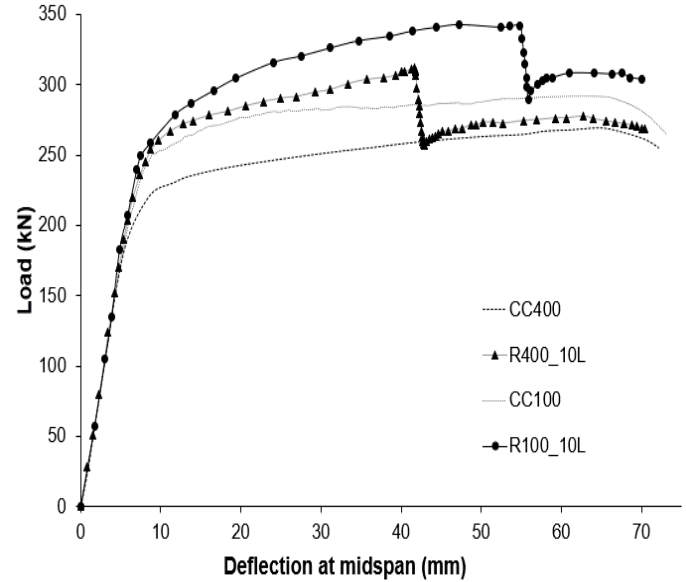
(b) Repair with 10 layers of BFRP for AR of 1 and 4

Figure 2.16: Load-deflection behavior for beams with same number of BFRP fabric layers

From Figures 2.12 and 2.13, it can be concluded that the ultimate load capacity of the repaired beams increased as the number of BFRP layers increased. However, the literature review showed that the risk of de-bonding failure increases as the number of FRP layers increases.  Sen et al. [5] found that after an optimum number of CFRP layers, the likelihood of de-bonding between CFRP composites and the steel surface begins to increase. In the current study a test was conducted on a corroded beam, with corrosion aspect ratio of four. This beam  was repaired with 20 layers of BFRP fabric (specimen R400_20L). The load-deflection behavior of this specimen is shown in Figure 2.17. This figure shows that the initial load-deflection behavior was similar to that of identical corroded specimen but repaired with 15 layers of BFRP fabric, specimen R400_15L. However, at the mid-span deflection of about 17.5 mm, de-bonding of the BFRP initiated, which is indicated by the small drop in the load. Debonding of BFRP fabric continued until about 30 mm of mid-span deflection when BFRP fabrics ruptured. At this stage, load dropped significantly, and the beam was never able to the regain a load value larger than that of control corrosion specimen, CC400. Hence, the performance of beam R400_20L was unsatisfactory if compared with the performance of the beam R400_15L. The debonding pattern of specimen R400_20L can be found in Figure 2.18. Hence, this study indicates that using a very thick BFRP fabrics for repair of corroded beam needs to be avoided to eliminate

unwanted and premature debonding failure. For this study, the maximum number of BFRP layers successfully used for rehabilitation was 15 layers.
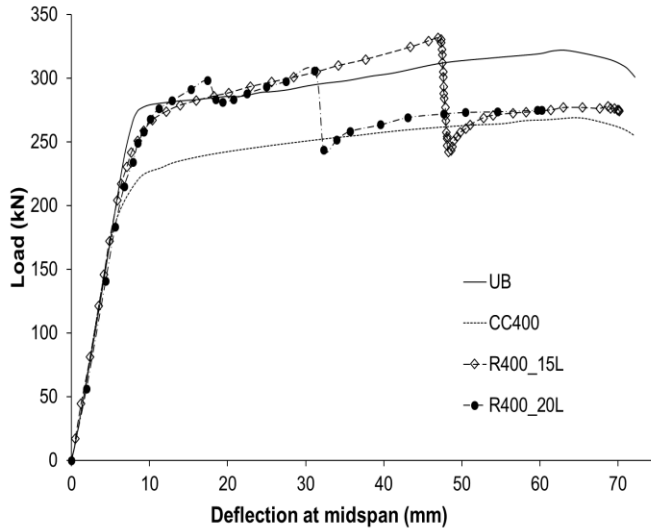


Figure 2.17: Load-deflection behavior of R400_15L and R400_20L



Figure 2.18: Photo showing the debonding for thick repairs

### 2.4.2 Moment-Curvature and Ductility

The moment-curvature relationships of the beams with corrosion aspect ratios of 1 and 4 are plotted in Figures 2.19 and 2.20, respectively. The curvature was obtained using the deflection data obtained from LVDTs 1, 2 and 3, while the moment was determined from the data obtained from the loadcell. The moment-curvature plot provides general bending behavior of W150X24 beams with two corrosion aspect ratios irrespective of the loading and boundary condition. The yield moment, ultimate moment, and curvatures are presented in Table 2.4. It can be observed that the ultimate moment carrying capacity of the uncorroded control (virgin) specimen UB is 80.9 kN-m. It reduced to 71.2 kN-m and 67.0 kN-m for control corroded specimens CC100 and CC400, respectively. However, upon rehabilitation using 10 layers of BFRP fabric for CC100 and 15 layers of BFRP fabric for CC400, the ultimate moment capacity increased and exceeded that of the uncorroded control (virgin) beam, UB. The section ductility for each beam is calculated using the curvature values. Section ductility is defined as the curvature at the ultimate moment ($\phi_u$) divided by curvature at yield moment ($\phi_y$) as shown in Equation 2.1.

$$\text{Section Ductility } (\mu) = \frac{\phi_u}{\phi_y}. \tag{2.1}$$

42

The ductility was also calculated using an energy-based approach as recommended and used by Tomlinson and Fam [22]. In this method, the ratio of total energy dissipated at ultimate load and total energy dissipated at yield load, is considered as the ductility or energy dissipation ratio ($\mu_E$) as shown in Equation 2.2. In this equation, $\Delta U$ is the deflection at the ultimate load, $\Delta Y$ is the deflection at the yield load and P is the applied load on the beam.

$$\text{Energy dissipation ratio } ( \mu_E ) = \frac{\int_0^{\Delta U} P(\Delta)d\Delta}{\int_0^{\Delta Y} P(\Delta)d\Delta} \tag{2.2}$$
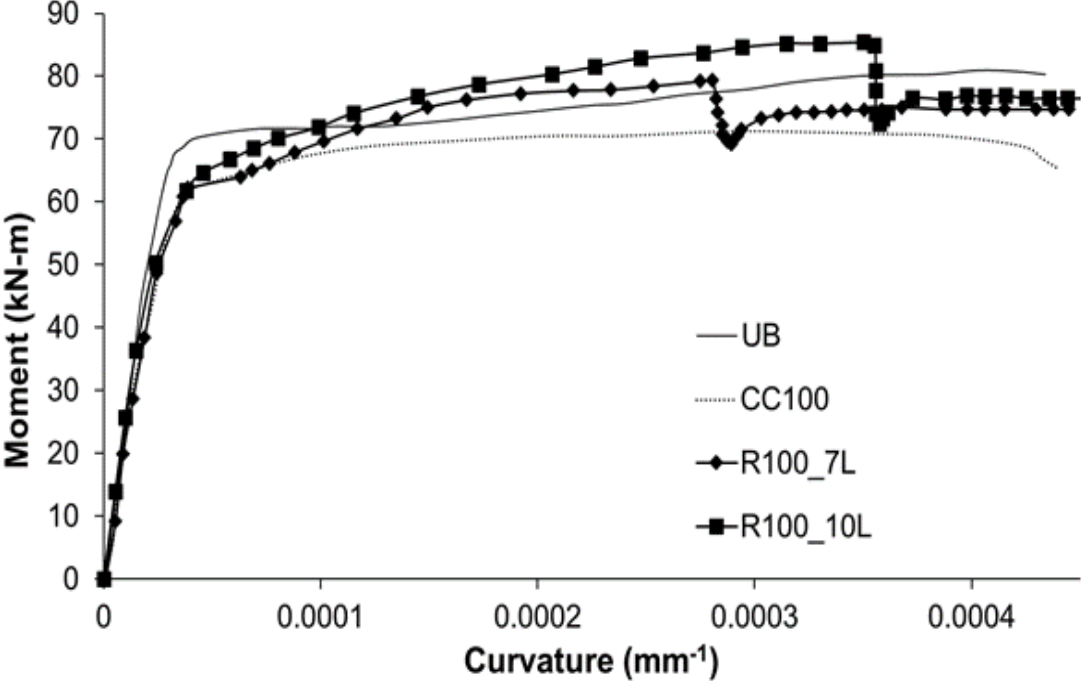


Figure 2.19: Moment-curvature diagrams for beams with corrosion AR of 1
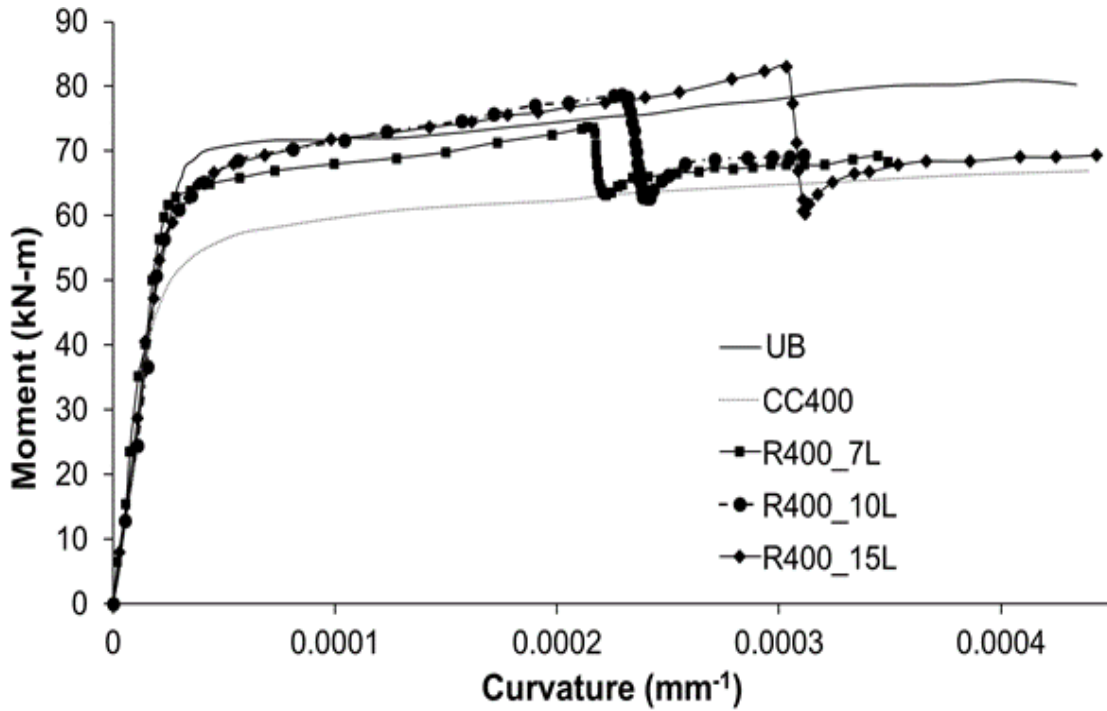
Figure 2.20: Moment-curvature diagrams for beams with corrosion AR of 4

Table 2.4: Comparison of yield moment, ultimate moment and ductility of the beams

| Specimen ID | Yield Moment (kN-m) | Yield Curvature ($ø_y$) | Ultimate Moment (kN-m) | Ultimate Curvature ($ø_u$) | Section ductility $ø_u/ø_y$ | Relative Ductility | Energy dissipation ratio ($\mu E$) | Relative Ductility |
|---|---|---|---|---|---|---|---|---|
| UB | 67.7 | $3.25 \times 10^{-5}$ | 80.9 | $4.03 \times 10^{-4}$ | 12.4 | 1.00 | 13.57 | 1.00 |
| CC100 | 60.8 | $3.40 \times 10^{-5}$ | 71.2 | $3.82 \times 10^{-4}$ | 11.3 | 0.91 | 12.7 | 0.94 |
| CC400 | 53.1 | $3.62 \times 10^{-5}$ | 67.0 | $3.82 \times 10^{-4}$ | 10.6 | 0.85 | 12.3 | 0.91 |
| R100_7L | 62.2 | $3.57 \times 10^{-5}$ | 79.3 | $2.80 \times 10^{-4}$ | 7.9 | 0.64 | 9.2 | 0.68 |
| R100_10L | 63.9 | $3.81 \times 10^{-5}$ | 85.0 | $3.55 \times 10^{-4}$ | 9.3 | 0.75 | 12.3 | 0.90 |
| R400_7L | 59.8 | $2.49 \times 10^{-5}$ | 73.8 | $2.14 \times 10^{-4}$ | 8.6 | 0.69 | 8.2 | 0.61 |
| R400_10L | 60.9 | $2.60 \times 10^{-5}$ | 78.7 | $2.29 \times 10^{-4}$ | 8.8 | 0.71 | 9.2 | 0.68 |
| R400_15L | 62.7 | $3.23 \times 10^{-5}$ | 83.1 | $3.03 \times 10^{-4}$ | 9.4 | 0.76 | 10.6 | 0.78 |

Both ductility calculations show that the ductility of the uncorroded (virgin) beam (UB) and control corroded beams (40CC100 and 40CC400) are higher than the rehabilitated beams. This is due to the fact that failure of rehabilitated beam was due to rupture of the BFRP fabrics and the rupture strain of BFRP fabric is much less than the failure strain of steel substrate. However, it was found that as the number of BFRP layers increases the ductility of the rehabilitated beams also increases. This is because the energy required to cause the rupture of fabrics becomes higher with an increase in the number of BFRP fabric layers. The curvature at which the ultimate load occurs also increases with the increase in the number of layers of BFRP fabric indicating an increase in ductility. However, it was not possible to restore the ductility of the rehabilitated beams to that of the level of uncorroded control specimen (UB). As well, the ductility of rehabilitated beams was generally less than the ductility of control corroded beam except for the rehabilitated beam R100_10L which exhibited a ductility of 0.9 and this is almost the same as the control corroded beam, CC100 with ductility ratio of 0.94.

### 2.4.3    Strain Analysis

The layout of the strain gauges is shown in Figure 2.11. All the strain values are shown in micro-strain ($\mu\varepsilon$). Strain gauges S1 to S7 were used to determine the neutral axis depth and strain gauges S8 to S11 were used for checking any debonding between steel and BFRP fabrics. The strain vs. mid-span deflection for specimen R400_7L is shown in Figure 2.21. The strain values shown in Figure 2.21 are the strain values at the mid-span of the beam. Strain gauges S1 and S3 showed negative strain values since they were located at the compression zone. Strain gauges S5 and S7 showed positive values or tension. Strain gauges S1 and S7 were located at the extreme vertical faces of the beam or 53.3 mm from the mid-height of the beam. Strain gauges S3 and S5 were located at 26.7 mm from the mid-height of the beam. Hence, the strain values at strain gauges S1 and S7 for both tension and compression were higher than strain gauges S3 and S5.
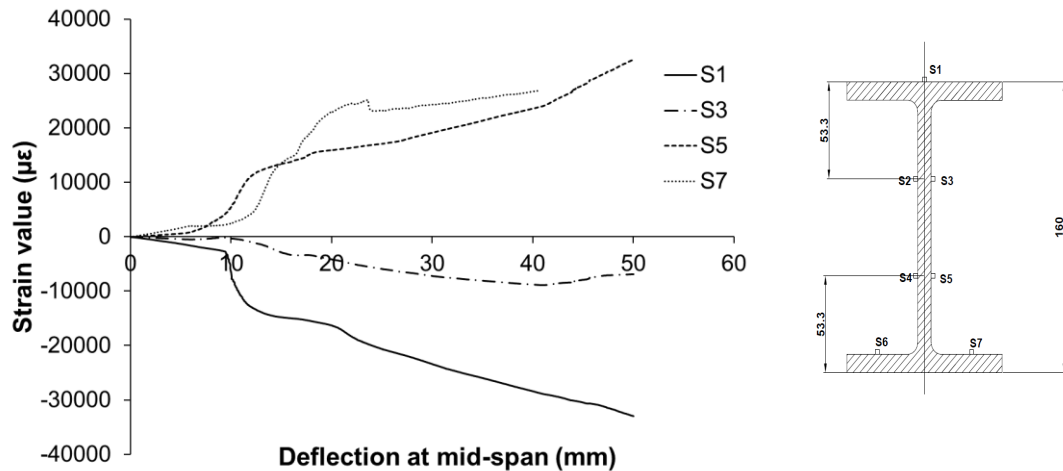
Figure 2.21: Strain vs. deflection at mid-span for specimen 40R400_7L

Figures 2.22 and 2.23 present the strain values of the steel and BFRP at 250 mm and 450 mm from the mid-span of specimen R100_7L, respectively (see Figure 2.11b for strain gauge locations). It was observed that the strain values of the BFRP (S9 and S11) were slightly higher than the strain values obtained from steel substrate (S8 and S10). This is due to the fact the distances of these strain gauges from the neutral axis were different. Distance of strain gauges S9 and S11 from the mid-height of the beam section was 83.15 mm and distance of strain gauges S8 and S10 was 69.9 mm. Nonetheless, the strain gauges showed similar strain patterns indicating that there was no debonding between the BFRP fabrics and steel substrate. It should be noted that the strain gages S9 and S11 were installed on BFRP fabrics and strain gauges S8 and S10 were installed on steel substrate (see Figure 2.11b).

46
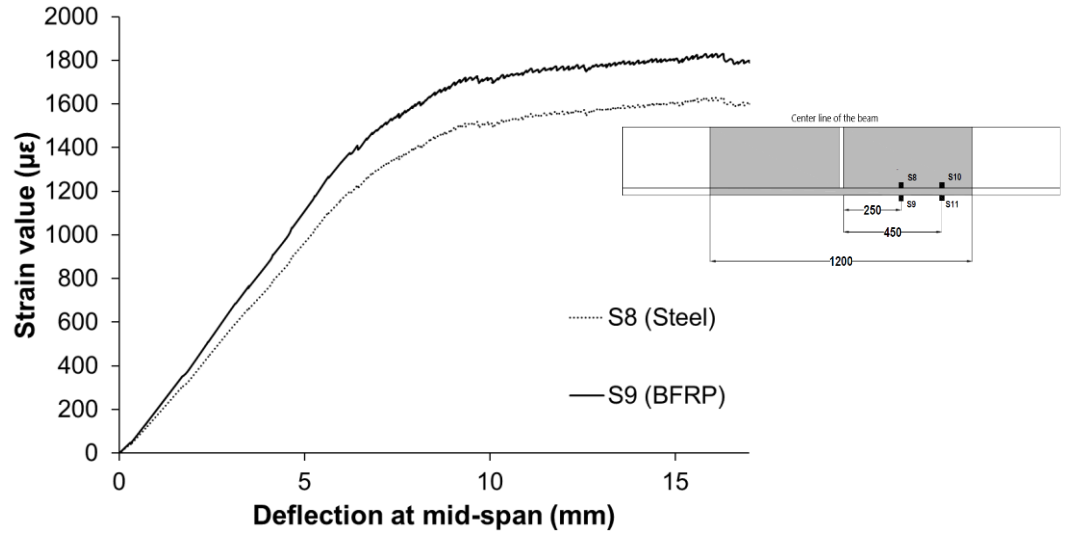
Figure 2.22: Comparison of strain value of steel vs. BFRP at 250mm from center for 40R100_7L
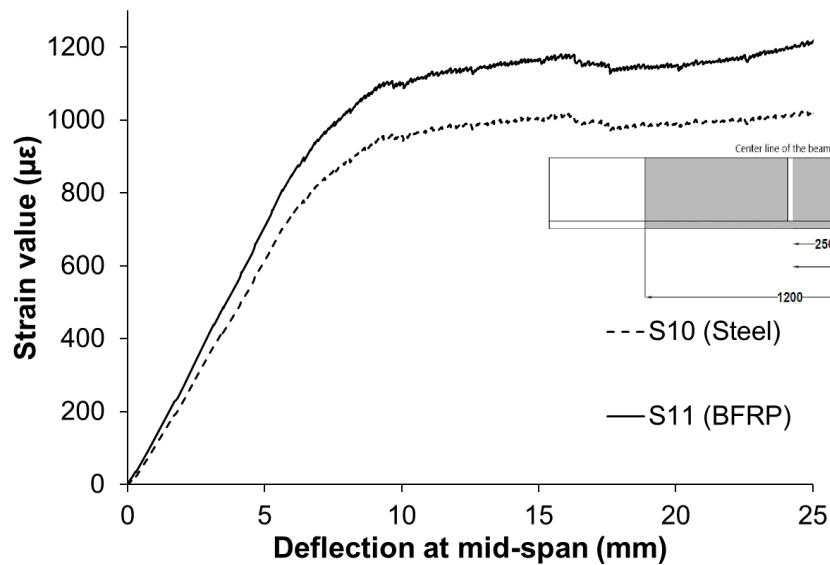


Figure 2.23: Comparison of strain value of steel vs. BFRP at 450mm from center for 40R100_7L

Another indicator for the improvement in behavior of the rehabilitated beams is the location of the neutral axis. The neutral axis of the un-corroded control (virgin) beam is expected to be located at the mid-height (~80 mm) of the beam section. At the mid-span of the beam, the location of the neutral axis moves up due to corrosion defect in the bottom flange. As the beam is rehabilitated, it is expected that the neutral axis should move downward to its original location (location of the uncorroded control or virgin beam). The neutral axis depths at 30 mm deflection and at the mid-span of the beam

specimen for all the beams are presented in Table 2.5. The deflection of 30 mm is used because at that deflection all the specimens past the yielding load, however, BFRP fabrics did not rupture. Figures 2.24a and 2.24b show the variation of neutral axis depth for specimens with corrosion aspect ratios of 1 and 4, respectively. It can be observed that the neutral axis depth moves upward for control corroded specimens (CC100 and CC400) with respect to the uncorroded beam. However, with the application of BFRP, the neutral axis depth improves (moves downward) and restores to near mid-height of the beam. Hence, it can be concluded that with the application of BFRP in corroded beams of both aspect ratios, the neutral axis depth can be successfully restored to its uncorroded control (virgin) beam level.

Table 2.5: Neutral axis depth at 30 mm deflection

| Specimen ID | NA Depth (mm) |
|---|---|
| UB | 80 |
| CC100 | 65.56 |
| R100_7L | 75.5 |
| R100_10L | 79.8 |
| CC400 | 63.73 |
| R400_7L | 69.69 |
| R400_10L | 75.11 |
| R400_15L | 81.23 |
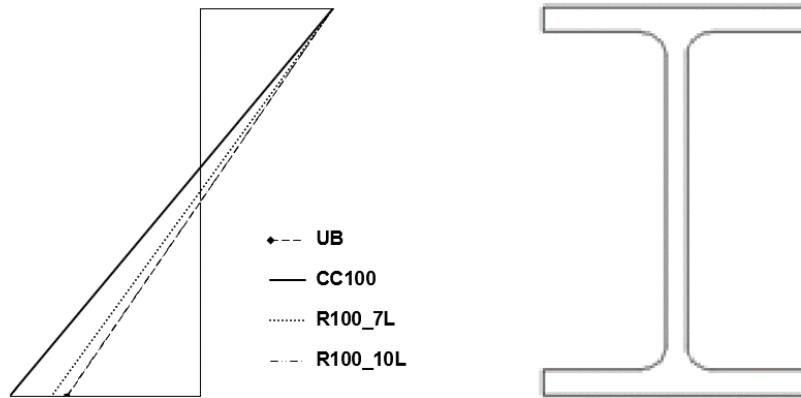
Figure 2.24a: Neutral axis depth for beams with corrosion AR of 1
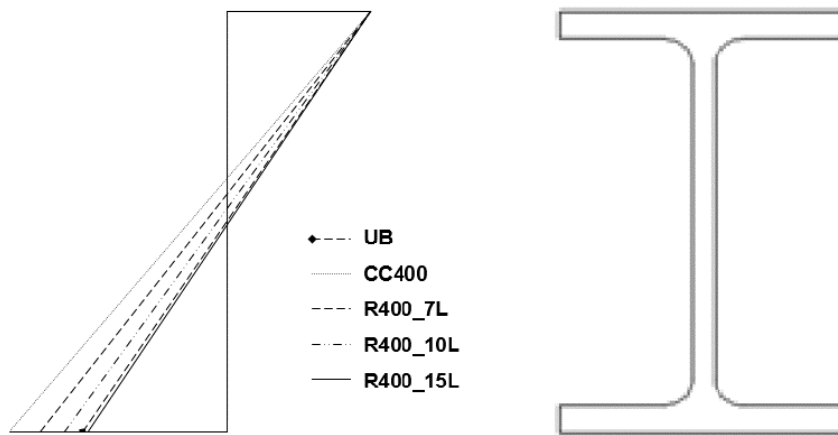


Figure 2.24b: Neutral axis depth for beams with corrosion AR of 4

## 2.5  Parametric Study Using Finite Element Method

Experimental testing is the most reliable method for determining the behavior and change in characteristics of steel beams rehabilitated with BFRP fabrics. However, it is not realistic to conduct experiments for every scenario because the experimental work is expensive and time-consuming. Hence, in this study, numerical method was also used to study the effect of rehabilitation of corroded steel beam using BFRP fabric to supplement the experimental tests. Finite element (FE) analysis method was used in the numerical study and commercially available software Abaqus/Standard [23] was used. The primary objective of the numerical study was to develop a semi-empirical equation for determining the optimum number of layers of BFRP fabrics required to repair corroded beams with various aspect ratios. Hence, a parametric study for varying corrosion aspect ratios and number of

BFRP layers, was conducted using finite element (FE) method. The FE models were validated with experimental results.

Twenty-node quadratic brick or solid element with reduced integration (C3D20R) with a mesh size of 10 mm was used to model the steel beam and 8-node quadrilateral continuum shell element with reduced integration (SC8R) of mesh size 10 mm was used to model the BFRP fabric. The optimum mesh size for the steel beam and BFRP fabric was determined through a mesh convergence study. The mesh convergence study for steel is shown in Figure 2.25. The geometry of the shell element was modeled as a solid, however, its kinematic and constitutive behaviors were assigned similar to that of a conventional shell element. The material properties of steel were obtained from tension testing of coupons made from each material as per ASTM standards, as shown in Figure 2.1.
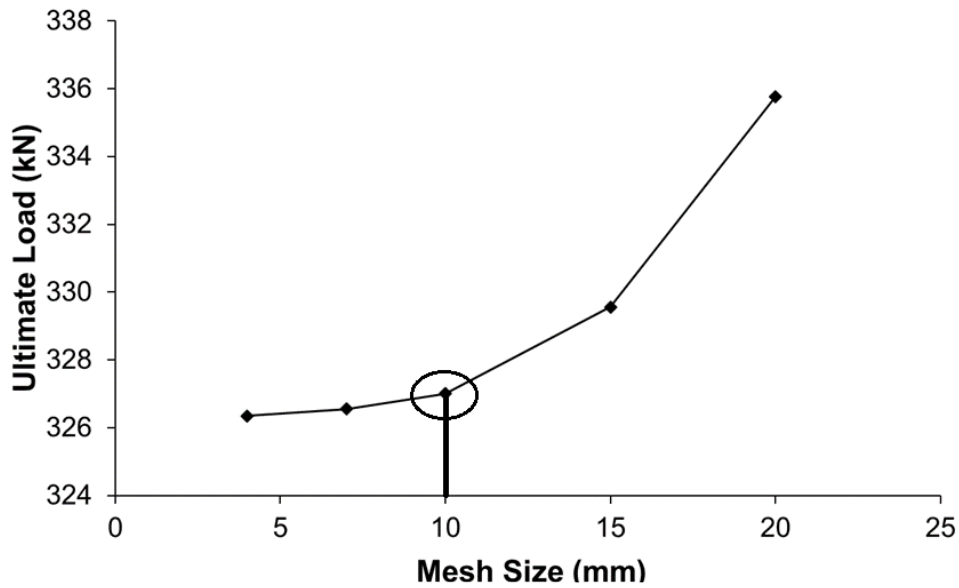


Figure 2.25: Mesh Convergence study for specimen UB

The material properties of BFRP fabrics were obtained from the coupon tests and shown in Table 2.6.

Table 2.6: Tensile properties of BFRP fabric

| E (GPa) | $X_T$ (MPa) | $\varepsilon_y$ (%) |
|---------|-------------|---------------------|
| 25      | 570         | 2.5                 |

The damage properties of the BFRP composite was simulated using Hashin criteria [24]. Hashin criteria considers four damage initiation criteria. These are tensile fibre failure, compressive fibre failure, tensile matrix failure, and compressive matrix failure. The equation for each failure criteria is shown in Equations 2.3 to 2.6. The damage initiation starts when one of these criteria is satisfied. The BFRP fabrics were attached to the bottom of the beams which is the tension zone. Hence, the fabrics were expected to fail in tension, and thus, the tensile fibre failure was expected to be the dominant failure mode for the rehabilitated beams. This was confirmed from the test data.

Tensile fibre failure $\qquad \left(\frac{\sigma_{11}}{X_T}\right)^2 + \alpha\left(\frac{\sigma_{12}}{S_1}\right)^2 = \begin{cases} \text{no failure, } x < 1 \\ \text{failure, } x \geq 1 \end{cases}$ (2.3)

Compressive fibre failure $\quad \left(\frac{\sigma_{11}}{X_C}\right)^2 = \begin{cases} \text{no failure, } x < 1 \\ \text{failure, } x \geq 1 \end{cases}$ (2.4)

Tensile matrix failure $\qquad \left(\frac{\sigma_{22}}{Y_T}\right)^2 + \left(\frac{\sigma_{12}}{S_1}\right)^2 = \begin{cases} \text{no failure, } x < 1 \\ \text{failure, } x \geq 1 \end{cases}$ (2.5)

Compressive matrix failure

$$\left(\frac{\sigma_{12}}{S_1}\right)^2 + \left(\frac{\sigma_{22}}{2S_2}\right)^2 + \left(\left(\frac{Y_C}{2S_2}\right)^2 - 1\right)\left(\frac{\sigma_{22}}{Y_C}\right) = \begin{cases} \text{no failure, } x < 1 \\ \text{failure, } x \geq 1 \end{cases} \qquad (2.6)$$

In Equations 2.3 to 2.6, $X_T$ represents longitudinal tensile strength, $X_C$ represents longitudinal compressive strength, $Y_T$ represents transverse tensile strength, $Y_C$ represents transverse compressive strength, $S_1$ represents longitudinal shear strength, $S_2$ represents transverse shear strength, $\sigma_{ij}$ represents principal stress components for the lamina and $\alpha$ is the contribution of the shear stress to the fiber tensile criteria.

Fracture energy was defined in the FE models to define the crack growth in the composite. The Fracture energy parameter (Gc) is defined as the amount of energy needed to cause complete failure or damage of the BFRP fabric. The equation for calculating $G_C$ is given in Equation 2.7

$$G_C = \frac{l^* * \sigma_u * \varepsilon_u}{2} \qquad (2.7)$$

In this equation, $\sigma_u$ and $\varepsilon_u$ are the ultimate stress and ultimate strain values of the composite (BFRP fabrics). l* is the characteristic length of the composite. l* is a function of the mesh size and thickness of the composite and was determined using method proposed by Bažant and Oh [25].

In the FE models, the BFRP fabric was modeled as a single layer of equivalent thickness which is the total thickness of BFRP fabrics applied for the rehabilitation. Surface to surface tie constraint was used to attach the BFRP fabric to the steel beam substrate. Surface to surface tie constraint was used in the model because no de-bonding or slippage was observed in any test specimens (Table 2.1). Figure 2.26 shows the comparison of load-deflection data obtained from the tests with the data obtained from FE models for beams with corrosion aspect ratio of 4, while Figure 2.27 compares the load-deflection data obtained from the experiments and finite element models for beams with a corrosion aspect ratio of 1. The comparison of the results obtained from experiments and the FE models are also presented in Table 2.7. It is observed that there is a good agreement between the load-deflection data obtained from the tests and the FE models. The maximum percentage error obtained for ultimate load is 4.41 % and it was for beam R400_15L.
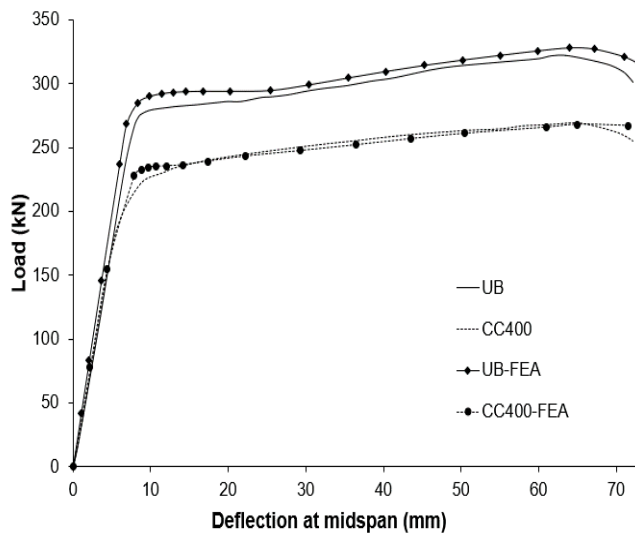


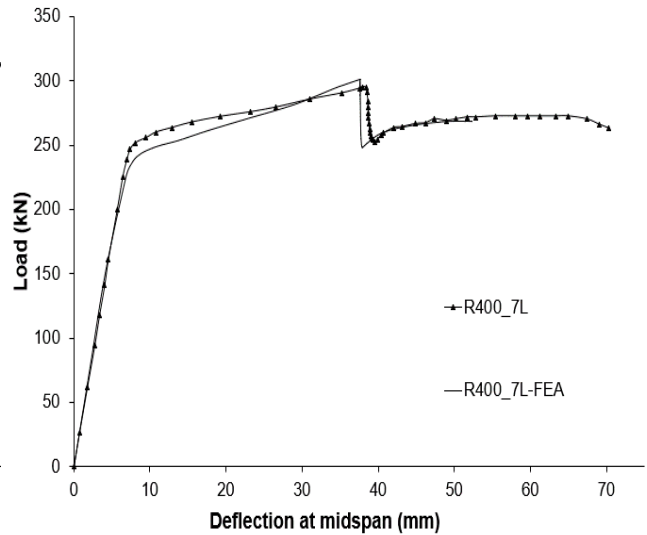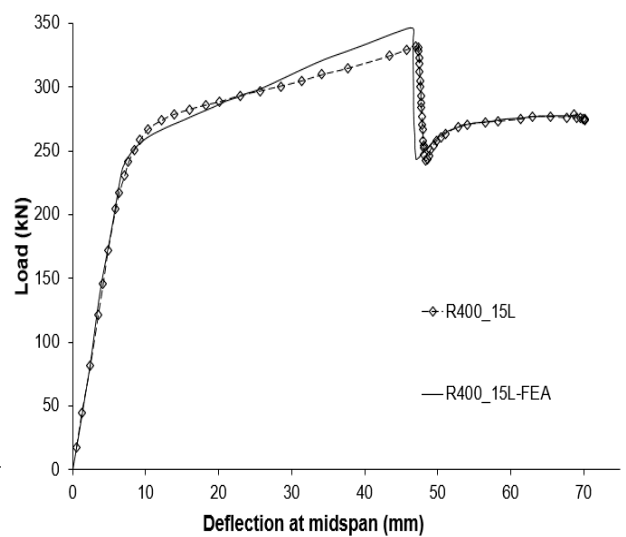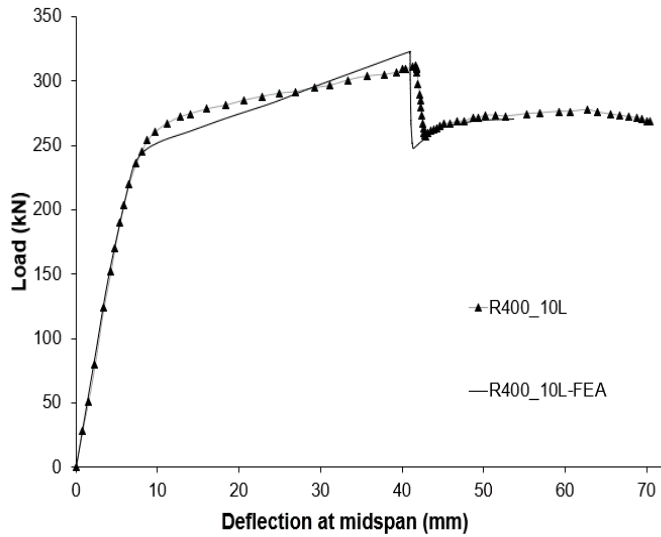Figure 2.26a: Control specimens UB and CC400    Figure 2.26b: Rehabilitated specimen R400_7L

Figure 2.26c: Rehabilitated specimen R400_10L    Figure 2.26d: Rehabilitated specimen R400_15L

Figure 2.26: Validation of FEM model data for corrosion aspect ratio of 4



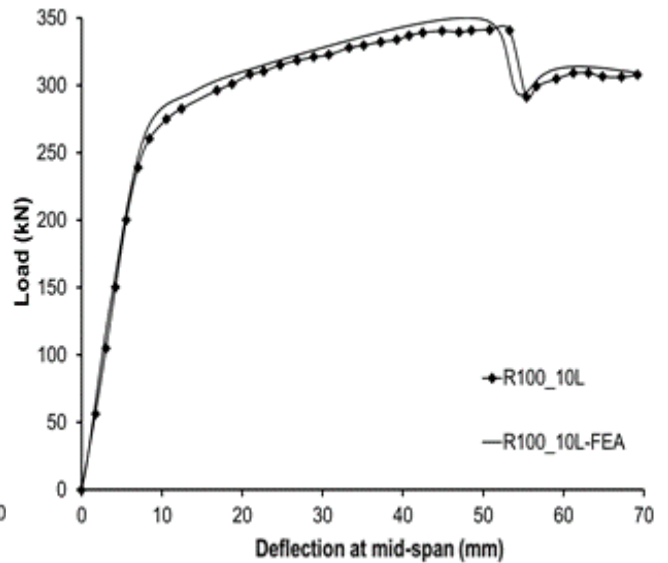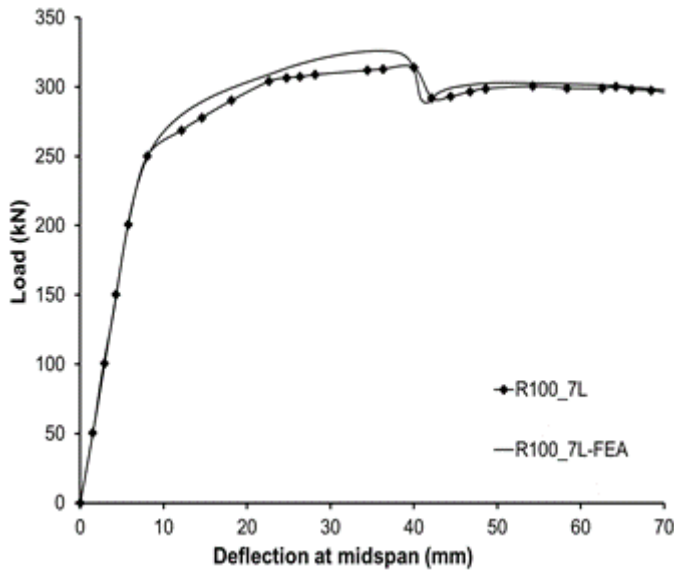Figure 2.27a: Rehabilitated specimen R100_7L    Figure 2.27b: Rehabilitated specimen R100_10L

Figure 2.27: Validation of FEM model data for corrosion AR of 1

Table 2.7: Comparison of experimental data and FEM model results

| Specimen ID | Experiment Yield Load (kN) | FE Model Yield Load (kN) | % Difference in Yield Load | Experiment Ultimate Load (kN) | FE Model Ultimate Load (kN) | % Difference in Ultimate Load |
|---|---|---|---|---|---|---|
| UB | 273.3 | 284.9 | 4.24% | 322.2 | 327.0 | 1.49% |
| CC100 | 229.8 | 232.5 | 1.17% | 286.4 | 292.3 | 2.07% |
| CC400 | 218.1 | 227.9 | 4.49% | 267.1 | 269.1 | 0.79% |
| R100_7L | 247.4 | 260.0 | 5.09% | 318.6 | 325.0 | 2.00% |
| R100_10L | 249.4 | 265.0 | 6.26% | 341.9 | 350.0 | 2.35% |
| R400_7L | 246.9 | 236.2 | 4.33% | 295.1 | 301.2 | 2.08% |
| R400_10L | 253.6 | 239.8 | 5.44% | 311.6 | 322.9 | 3.65% |
| R400_15L | 258.5 | 245.1 | 5.18% | 331.7 | 346.3 | 4.41% |

The deflected shape for specimen R100_10L obtained from the FE analysis is shown in Figure 2.28. The shape of the BFRP composite after its rupture is shown in Figure 2.29. The other rehabilitated specimens also showed similar behavior (See Appendix A Figures A.1 -A.8). The validated FE models were then used to conduct a parametric study where corrosion aspect ratio was varied from 1 to 6 while keeping the corrosion depth unchanged at 40% of flange thickness. The plot of the optimum number of layers with different corrosion depth is shown in Figure 2.30. The optimum number of layers is the minimum number of BFRP fabric layer required to be applied to the corroded beam to restore the ultimate strength of the corroded steel beams to the level of uncorroded (virgin) beam.
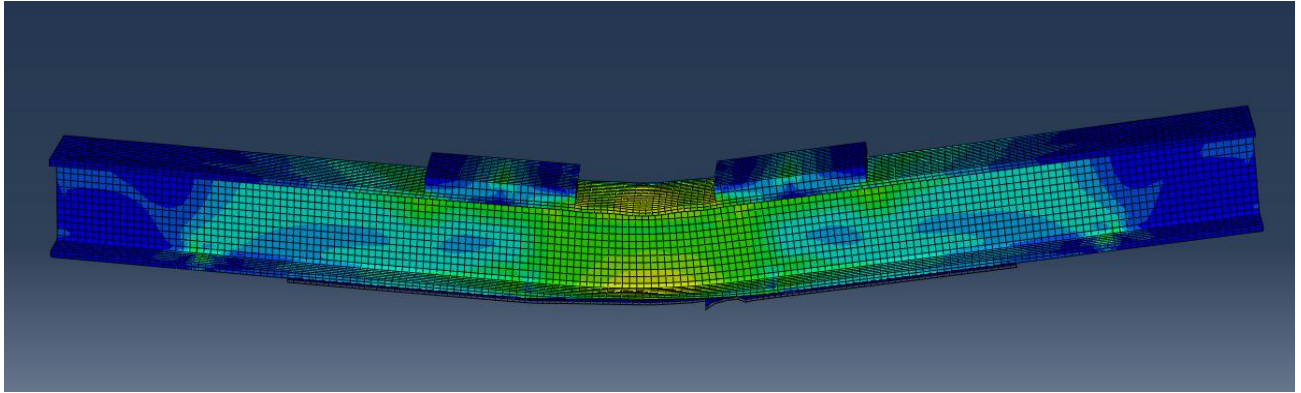
Figure 2.28: Final Deflected shape in the FEM model
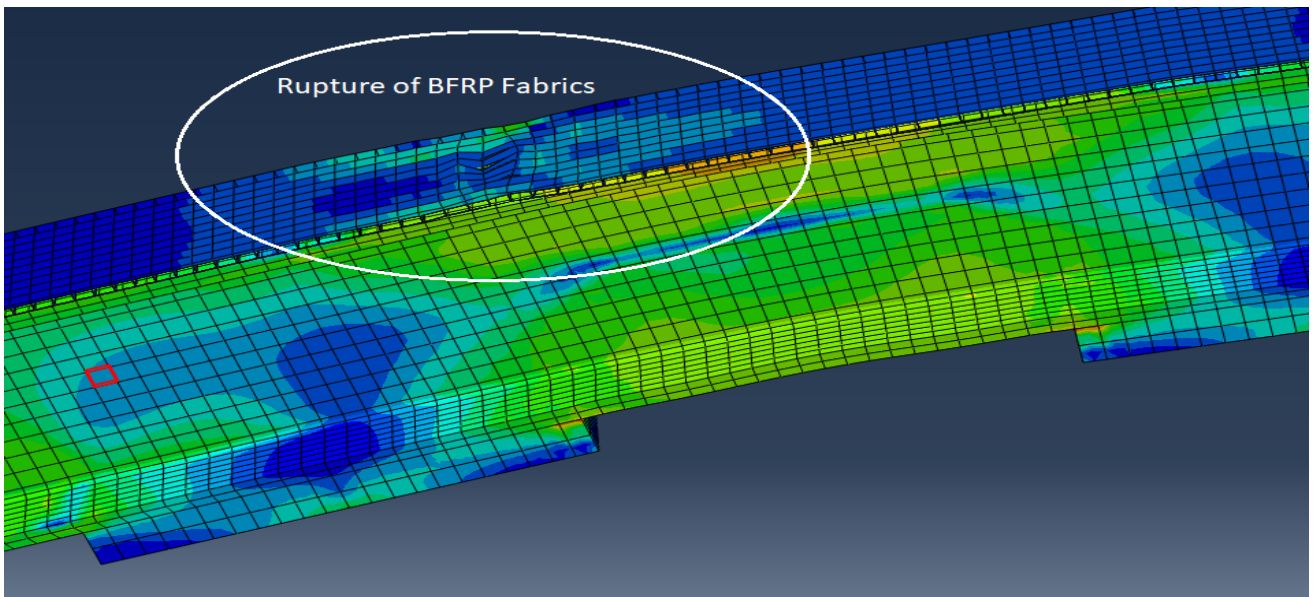


Figure 2.29: Shape of the BFRP laminate after rupture point
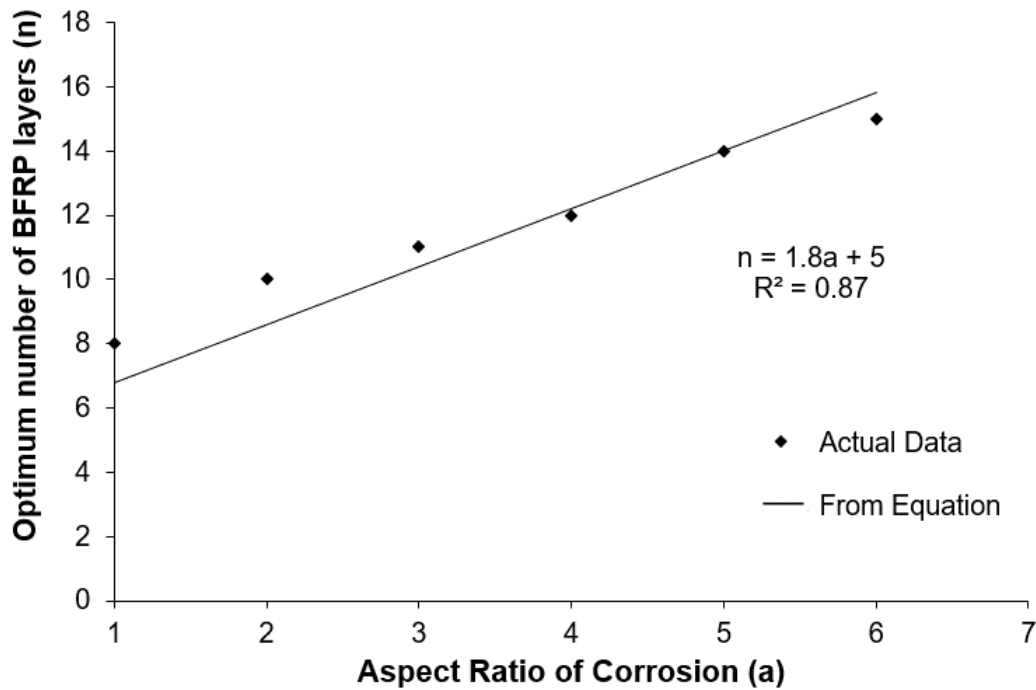
Figure 2.30: Relation between aspect ratio of corrosion and optimum BFRP layers

The following equation is also proposed for determining the optimum number of BFRP layers when aspect ratio of the corrosion is varied.

$$n = 1.8a + 5 \qquad (2.5)$$

In the above equation, n is the optimum number of BFRP layers and a is the aspect ratio of the corrosion patch. The coefficient of determination, $R^2$ value, of this equation is 0.87, which indicates that it is a good fit for the current set of data. It can be observed from Figure 2.30 that the number of layers of BFRP fabrics needed for repair increases with the increase in the aspect ratio of the corrosion patch.

Equation 2.5 has been developed based on the data obtained from the current study and is valid only for W150X24 beams with a corrosion depth of 40% of the flange thickness and for corrosion aspect ratio of one to six. Further research is required to develop a more comprehensive equation that is applicable for different types of beams and other parameters.

## 2.6 Conclusions

In this research, the feasibility of Basalt Fibre Reinforced Polymer (BFRP) composites in rehabilitating steel beams with various corrosion shapes is discussed using both experimental and finite element methods. It can be concluded that BFRP fabric can be used as an effective rehabilitation

material for corroded steel beams with various corrosion aspect ratios. Basalt fibre fabric is a new and green material that can be an attractive alternative to the other fabrics including carbon and glass fibre fabrics. The following conclusions can be made from this study and however, these conclusions may be limited to the scope of this study

1. The rehabilitation technique used in this study was successful in eliminating de-bonding of BFRP fabrics. The study showed the cross fabrics need to be continuous along the length of repair to be able to avoid debonding failure.

2. BFRP fabrics were able to fully restore the ultimate strength of corroded steel beams suffered from corrosion damage of various aspect ratios. Though the yield strength of the rehabilitated beams was improved, the improvement was not enough to reach the yield strength of the uncorroded control (virgin) beam.

3. Corroded beams with corrosion patch of lower aspect ratio experienced a higher increase in ultimate load as compared to beams with a higher corrosion aspect ratio when rehabilitated with the same number of BFRP fabrics. It was also observed that the ductility of the beams with lower corrosion aspect ratio was higher than the ductility of the beams with higher corrosion aspect ratios when rehabilitated with same number of BFRP fabrics.

4. The study showed that there is an optimum number of layers of BFRP fabrics that results in best performance in terms of strength and ductility of a rehabilitated beam. For the current study, the optimum number of BFRP fabrics was found to be 15. Use of large number of BFRP fabrics may lead to a premature debonding failure.

5. A new semi-empirical equation is proposed, which can be used to determine the optimum number of BFRP fabric layers required to repair corroded steel beams with corrosion patch of various aspect ratios.

6. Ductility of the rehabilitated beams was found to be less than that of the uncorroded beams or control corroded (virgin) beams. However, it was found that an increase in the number of layers of BFRP results in a higher ductility of the beams.

## 2.7 Acknowledgments

## 2.8 References

[1]     ASCE: American Society of Civil Engineers, "ASCE Infrastructure Report Card," 2017, ASCE, Virginia, USA, 1-6.
<www.infrastructurereportcard.org/a/#p/bridges/overview>

[2]     Davis, S.L. and Goldberg, D., "The fix we're in for the state of our nation's bridge", Transportation for America, Washington, D.C, 2013.

[3]     FCM: "Informing the Future: The Canadian Infrastructure Report Card (CIRC-2016)", Federation of Canadian Municipalities, Ottawa, Ontario , Canada, 2016, 1-164.
<http://canadianinfrastructure.ca/en/index.html>

[4]     Mertz, D. R., and Gillespie, J. W., ''Rehabilitation of steel bridge girders through the application of advanced composites materials'' Final Rep., NCHRP-93-ID011, Transportation Research Board, Washington, DC., 1996, 1-34.

[5]     Sen, R., Liby, L. and Mullins, G. "Strengthening steel bridge sections using CFRP laminates", Composites Part B: Engineering, 2001, 32 (4), 309-322. DOI: https://doi.org/10.1016/S1359-8368(01)00006-3

[6]     Al-Saidy A.H., Klaiber F.W. and Wipf T.J., "Repair of steel composite beams with carbon fibre-reinforced polymer plates", Journal of Composites for Construction, 2004, 8 (2), 163–72. DOI: https://doi.org/10.1061/(ASCE)1090-0268(2004)8:2(163)

[7]     Manalo, A., Sirimanna, C., Karunasena, W., McGarva, L., and Falzon P., "Pre-impregnated carbon fibre reinforced composite system for patch repair of steel I-beams", Journal of Construction and Building Materials, 2016, 105, 2016, 365–76. DOI: https://doi.org/10.1016/j.conbuildmat.2015.12.172

[8]     Chen, M. and Das, S., "Experimental study on repair of corroded steel beam using CFRP", Steel and Composite Structures, 2009, 9 (2), 103–18. DOI: 10.12989/scs.2009.9.2.103

[9]     Selvaraj, S. and Madhavan, M., "CFRP strengthened steel beams: improvement in failure modes and performance analysis", Structures, 2017, 12, 120–131. DOI: https://doi.org/10.1016/j.istruc.2017.08.008

[10]   El Damatty AA, Abushagur M and Youssef MA. "Experimental and analytical investigation of steel beams rehabilitated using GFRP sheets",          Steel and Composite Structures, 3 (6), 2003, 421–438. DOI: http://dx.doi.org/10.12989/scs.2003.3.6.421

[11] Bastani, A., Das, S. and Lawn, D., "Rehabilitation of shear deficient steel beams using BFRP fabric", Structures, 19, 2019, 349-361, DOI: https://doi.org/10.1016/ j. istruc.2019.01.019

[12] Sim, J., Park, C. and Moon, D.Y., "Characteristics of basalt fiber as a strengthening material for concrete structures". Composites Part B: Engineering, 36 (6-7), 2005, 504–512. DOI: https://doi.org/10.1016/j.compositesb.2005.02.002

[13] Ólafsson, H. and Þórhallsson, E. R., "Basalt fibre bar reinforcement of concrete structures", Basalt fibre Seminar, Reykjavik University, Iceland, January 2009, 1-11.

[14] Mettemeyer, M.; Serra, P.; Wuerthele, M.; Schuster, G. and Nanni, A., "Shear load testing of carbon fibre reinforced polymer strengthened double tee beams in precast parking garage", Proceedings of the 4th international symposium on fibre reinforced polymer reinforcement for concrete structures, ACI SP-188, Baltimore, MD, November 1999, 1063-1072.

[15] Huang L, Li Y and Wang Y. "Strengthening effects of BFRP on reinforced concrete beams", Journal of Southeast University National, 29 (2), 2013, 182–186. DOI: 10.3969/j.issn.1003-7985.2013.02.013

[16] S. Jayasuriya, A. Bastani, S. Kenno, T. Bolisetti and S. Das, "Rehabilitation of corroded steel beams using BFRP fabric", Structures, 15, 2018, 152–161. DOI: https://doi.org/10.1016/j.istruc.2018.06.006

[17] CISC: Canadian Institute of Steel Construction, "Handbook of Steel Construction", Markham, ON, Canada, 2017.

[18] ASTM. Standard Test Methods for Tension Testing of Metallic Materials. E8/E8M-15a. PA: ASTM International, West Conshohocken, Pennsylvania, USA, 2015.

[19] ASTM. Standard Test Method for Tensile Properties of Polymer Matrix Composite Materials. D3039/D3039M-14. PA: ASTM International, West Conshohocken, Pennsylvania, USA, 2014.

[20] McKnight S., Bourban P., Gillespie Jr. J., and Karbhari V., "Surface preparation of steel for adhesive bonding in rehabilitation applications", Third Materials Engineering Conference, Infrastructure: New Materials and Methods of Repair, San Diego, November 1994, 1148-1155.

[21] Narmashiri, K., Jumaat, M. Z., and Sulong, N. H. R., "Strengthening of steel I-beams using CFRP strips: an investigation on CFRP bond length, Advances in Structural Engineering, 15 (12) , 2012, 2191- 2204, DOI: https://doi.org/10.1260/1369-4332.15.12.2191

[22] Tomlinson, D., and Fam, A., "Performance of concrete beams reinforced with basalt FRP for flexure and shear," Journal of Composites for Construction, 9 (2) ,2014, 1-10.

[23] "SIMULIA", Analysis User's Manuals. Rising Sun Mills, Providence, RI, USA: Dassault Systèmes Simulia Corp, Rising Sun Mills, Providence, RI, USA, 2018.

[24] Hashin Z., "Failure criteria for unidirectional fibre composites". Journal of Applied Mechanics, 47(2), 1980, 329–34. DOI:10.1115/1.3153664

[25] Bažant Z.P., Oh B.H., "Crack band theory for fracture of concrete", Materials and Construction, 16(3), 1983, 155–77. DOI: https://doi.org/10.1007/BF02486267

## Chapter 3: Use of Basalt Fiber Reinforced Polymer for Flexural Rehabilitation of Steel Beams with Corrosion Defect in Compression Flange

### 3.1 Introduction

Many structures around the world suffers from structural deficiency due to their exposure to external factors such as cyclic loads, winter salt spray, freeze-thaw cycle over a prolonged period. These structural deficiencies, if unaddressed, can cause catastrophic failures. The collapse of the Hartford Civic Center in Connecticut, USA in 1978, where the roof of the structure collapsed is an example of catastrophic failure of steel structures in the recent past [1]. According to a report published in 2013 by Transportation for America, about 66,405 bridges in North America are structurally deficient and about 260 million trips are taken over these deficient bridges every day [2]. Every year the cost of rehabilitating deficient structures keeps increasing due to further aging of these structures creating a huge backlog of structures with rehabilitation needs. In the Infrastructure report card published by ASCE in 2017, the backlog for rehabilitation in USA alone is estimated at US$123 billion [3]. The 2016 Canadian infrastructure report card estimates the cost of replacement of roads and bridges in poor or very poor conditions to be about Can$50 billion [4]. Hence, there is an urgent need to develop efficient and cost-effective methods for the rehabilitation of structures.

Newer and cost-effective methods are being developed for rehabilitation of steel and as well as reinforced concrete (RC) structures. Al-Salim et al. [5] carried out a test program to rehabilitate RC beams with damage in the compression zone. Seven beams were tested in this study. Damage was introduced to these specimens by crushing and removing 3 cm deep concrete from the top of the beam. The lengths of the crushed section used in this study were 10%, 20% and 30% of the tested beam length. The damaged region was rehabilitated with polyester glue line. Shear connectors were used to prevent debonding. The results showed that the ultimate load capacity of the rehabilitated beam increased up to 32.4%. Improvement in ductility of the beam as compared to the damaged beam was also observed.

One of the major causes of deterioration in steel structural members is corrosion. Traditional methods for rehabilitating corroded steel structures are bolting or welding new steel plates over the corroded area. These methods are time consuming and expensive. Other disadvantages of these methods include significant increase in dead load and increase in the probability of stress concentrations near the welded/bolted areas causing premature fatigue failure.

61

Fibre Reinforced Polymers (FRP) have been introduced as a better alternative to the traditional rehabilitation methods. One of the advantages of FRP material is its high strength-to-weight ratio. Hence, the strength of the structures can be increased without a significant increase in the dead load if FRP is used for rehabilitation. Commercially available FRP materials include Carbon Fiber Reinforced Polymer (CFRP), Glass Fiber Reinforced Polymer (GFRP), and Aramid Fiber Reinforced Polymer (AFRP).

## 3.2 Literature Review

It was found from the literature review that these commercially available FRPs have been successfully used to rehabilitate the tension zone of steel structures, [6, 7] as well as RC structures [8, 9]. Abdelrahman and El-Hacha [10] rehabilitated large-scale concrete columns by wrapping them with two types of FRP fabrics, Steel Fiber Reinforced Polymer (SFRP) and Carbon Fiber Reinforced Polymer (CFRP) fabrics. The performance of columns rehabilitated with SFRP fabric was found to be better than the columns rehabilitated with CFRP fabric. The columns rehabilitated with CFRP fabric exhibited about 38% increase in axial strength while the columns rehabilitated with SFRP fabric exhibited an increase in axial strength of about 70% while compared with columns without any rehabilitation. Another study conducted by Ilki et. al [11] and this study consisted of 68 reinforced concrete column specimens which were tested under uniaxial compression load. The specimens had a height of 500 mm and had both circular and square cross-sections of different dimensions. These specimens were jacketed externally with unidirectional CFRF fabrics of different thickness using epoxy primer and adhesive. It was observed that there was an increase in compressive strength of up to 6.9 times due to jacketing the columns with CFRP fabrics. Hence, literature shows that the FRP fabrics can be successfully used for the improvement in the axial strength of reinforced concrete columns.

Liu et al. [12] conducted a study on rehabilitation of damaged steel columns using GFRP jackets with both expansive and non-expansive lightweight concrete. The expansive concrete was used in between the column and GFRP jacket to help the GFRP jacket be confined to the steel columns. Seven 3.05 m long I-shaped steel columns with cross section of S4X9.5 [13] were tested under axial load. The damage was simulated in the columns by removing a width of 15.9 mm from both ends of the top and bottom flanges up to a length of 300 mm along the mid-span of the column. With this retrofitting, the ultimate load capacity of the rehabilitated specimen increased up to 2.33 times than that of the

damaged column and was about 0.97 times of the undamaged specimen. With expansive concrete, the ultimate load increased by another 15% while comparing with the column rehabilitated with non-expansive concrete. Hence, the rehabilitation scheme used in this study was effective for rehabilitation of damaged steel column members.

Feng et al. [14] used pultruded GFRP tubes with lightweight bamboo splits as filler material to strengthen steel columns. Fourteen specimens were tested under axial compressive load in this study. Using this rehabilitation technique, the type of failure observed was buckling of the section outside the rehabilitated zone. The load carrying capacity of the strengthened specimens increased to a maximum of 2.86 times that of the uncorroded specimen. Hence, this technique was found to be effective in the strengthening of steel columns.

Basalt Fiber Reinforced Polymer (BFRP) is a relatively newer material which has been gaining popularity among researchers due to its advantages over other FRPs. The advantages of BFRP fabrics over other FRPs include, it is an environment-friendly material which is about one-fifth of the cost of CFRP fabrics [15]. BFRP fabrics have a higher ductility than CFRP fabrics and are also reported to have better corrosion and weathering resistance than E-Glass fabrics. BFRP fabrics also have good heat and fire resistance as well as high resistance to UV rays. [16].

In the literature, only a limited number of studies were found on the rehabilitation of steel structures when subjected to axial compression load. No previous studies considered the rehabilitation of compression zone of a steel flexural member like a steel beam. Hence, the current study focused on developing a method for rehabilitation of steel beams with corrosion defect in the top flange (compression zone under bending load). Unidirectional BFRP fabric was used for the rehabilitation. The feasibility of this method was examined by using both experimental and numerical methods. The finite element (FE) method was used for the numerical study.

## 3.3 Experimental Program

Standard hot rolled W150 X 24 (CSA 2017) steel I-section beams [13] of length 2000 mm were used as specimens for this study. Uniaxial tensile testing was conducted on coupon specimens prepared from these beam specimens as per ASTM E8/E8M-15a (ASTM 2015) [17], to obtain the material properties of the steel. The yield strength and the ultimate strength were found to be 379 MPa and

484 MPa, respectively. The modulus of elasticity (E) was found to be 205 GPa. The stress-strain curve obtained from this data is presented in Figure 3.1a.

For the rehabilitation process, unidirectional BFRP fabric sheets were used. The fabrics were attached to the steel substrate using two-part epoxy resin. Unidirectional compression tests were conducted from the coupons made from these fabrics as per ASTM D3410/D3410M − 16 standard (ASTM 2018) [18]. The stress-strain curve of the BFRP fabrics, obtained from this test, is shown in Figure 3.1b.
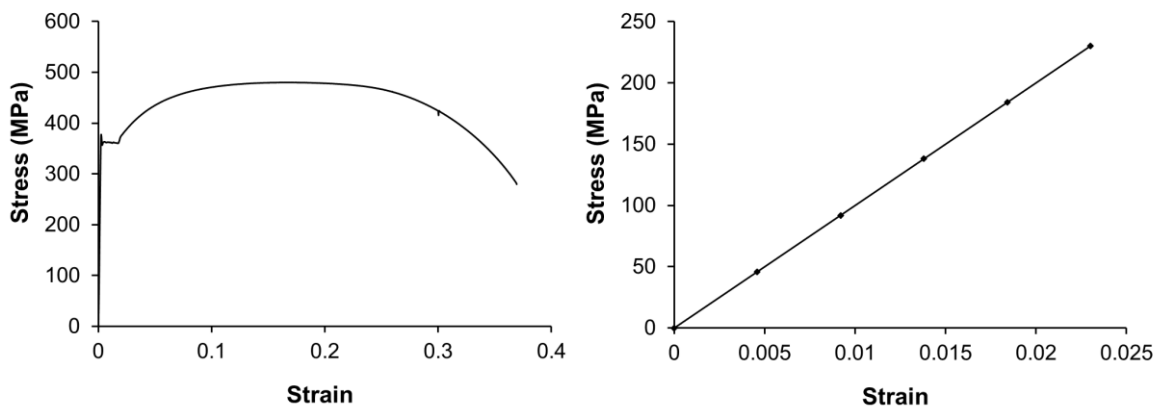


Figure 3.1a: Stress-strain behavior of steel     Figure 3.1b:  Stress-strain behavior of BFRP

Figure 3.1: Stress-strain behaviors

The corrosion defect was simulated in the beams by removing a circular-shaped area from top flange, as shown in Figure 3.2. The percentage of corrosion is the maximum depth of the portion removed from the top flange of the beam. For example, for 40% corrosion, the maximum depth (4.08 mm) of the steel removed from the beam was 40% of the top flange thickness. The flange thickness of the beam is 10.2 mm. Table 3.1 shows the test matrix used in the experimental study. Three of the specimens were control beam specimens and four were rehabilitated beam specimens. The control specimen which did not have any defect or thickness loss due to corrosion is referred to as uncorroded beam or "UB".  Remaining two control specimens had thickness loss due to corrosion of 20% (2.04 mm) and 40% (4.08 mm) of their flange thickness. These beams are referred to as control corroded beams and identified as "20CC" and "40CC", respectively. In the specimen ID of these beams, "40" and "20" are the maximum depth of corrosion in percentages of the flange thickness, and "CC" indicates control corrosion specimens which were not rehabilitated.

64

The beams rehabilitated with BFRP fabrics are identified as "R40-10L-3C", "R40-10L-6C", "R40-15L-3C", "R20-7L-3C". In the specimen ID of the rehabilitated beams, "R" indicates this beam is a rehabilitated specimen; the following number is either "40" or "20" which are the maximum loss of thickness in percentage of flange thickness; next number and letter combination such as "10L", "15L" and "7L" are the number of longitudinal BFRP fabric layers used for rehabilitation; and "3C" and "6C" represent that either 3 layers or 6 layers of BFRP cross fabrics used to avoid potential debonding failure.

Cross fabrics are layers of BFRP fabric that were attached perpendicularly on top of the main reinforcing layers of BFRP fabric and connected to the web of the beam up to the mid-height of the beam (Figure 3.3a). Cross-wrapping helps in holding the longitudinal layers of BFRP fabrics and prevents debonding of these fabrics. Jayasuriya el al. [19] and Bastani et al. [14] found that for the rehabilitation of steel beams with corrosion defect in the tension zone and shear zone, cross fabrics played an important role in the prevention of debonding failure. Hence, similar cross fabrics were used in the current study to prevent debonding failure.
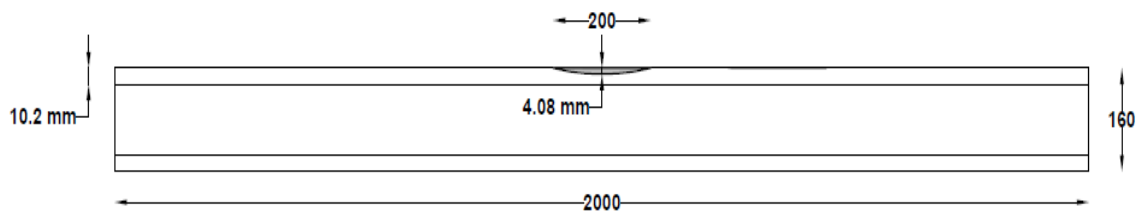


Figure 3.2: Corrosion profile of beam with 40% corrosion

Table 3.1: Test Matrix

| Specimen ID | Corrosion Percentage | Type of Beam | No. of longitudinal fabric layers | No. of cross fabric layers | Total Thickness of BFRP fabrics (mm) |
|---|---|---|---|---|---|
| UB | - | Control Virgin | - | - | - |
| 40CC | 40% | Control Corroded | - | - | - |
| 20CC | 20% | | - | - | - |
| R40-10L-3C | 40% | Rehabilitated Specimens | 10 | 3 | 4.5 |
| R40-10L-6C | 40% | | 10 | 6 | 4.5 |
| R40-15L-3C | 40% | | 15 | 3 | 6.75 |
| R20-7L-3C | 20% | | 7 | 3 | 3.15 |

### 3.3.1   Specimen Preparation and Test Setup

The first step of the rehabilitation process was to sandblast the beam specimens to get a clean and rough surface that facilitates a good bond between the steel and BFRP fabrics. Then the BFRP fabrics were cut to a length of 500 mm and a width of 100 mm. A layer of epoxy primer was first applied to the specimen on the area where rehabilitation was to be undertaken. Within 24 hours of applying the primer and after the area became tack free, the BFRP fabric layers were attached to the beam. First, the longitudinal layers were attached. Then the cross fabrics layers were attached as shown in Figures 3.3a and 3.33b using wet layup technique. In this technique, an epoxy resin was used for impregnation of the dry basalt fabrics and then the BFRP fabric were attached in layers. The rehabilitated specimens were cured for seven days before testing the specimens under bending load.
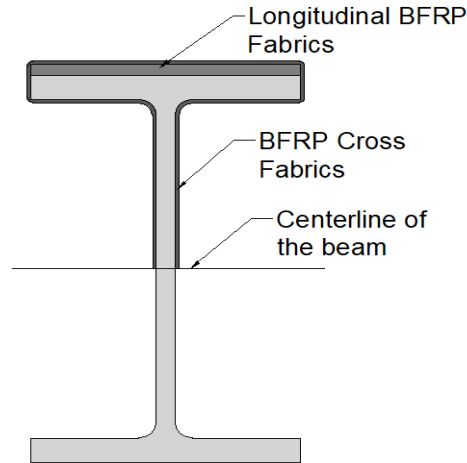
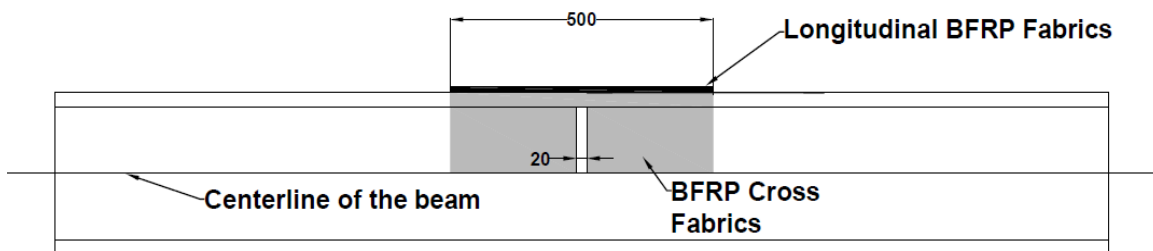Figure 3.3a: Cross sectional view of the rehabilitation scheme



Figure 3.3b: Side view of the rehabilitation scheme

Four-point bending load was applied in the experimental testing as shown in Figures 3.4 and 3.5. The load was applied to the beam specimen using a loading actuator, through a 1000 mm long spreader beam. Both the beam specimen and the spreader beam had a pin and roller boundary condition. The beam specimen had a span length of 1500 mm and the moment span of the setup was 750 mm. Five Linear Variable Differential Transformers (LVDTs) were used as shown in Figure 3.4 to measure deflections at those points. LVDT 2 was placed at the mid-span of the beam. LVDT 1 and LVDT 3 were placed at 375 mm from the mid-span of the beam. LVDT 4 was placed horizontally at mid-height to obtain the out of plane deflection, if any. LVDT 5 was part of the loading actuator and hence, it measured the deflection at the mid-span of the specimen. Symmetry of the specimen was checked during the test using slope values obtained from inclinometers placed at both ends of the beam. Loadcells were used to acquire the value of the applied load. Data from LVDT 2 and the loadcell attached to the loading actuator was used to plot the load-deflection curves. Data from

LVDTs 1, 2 and 3 along with the data from the loadcell attached to the loading actuator was used to plot the moment-curvature curves.
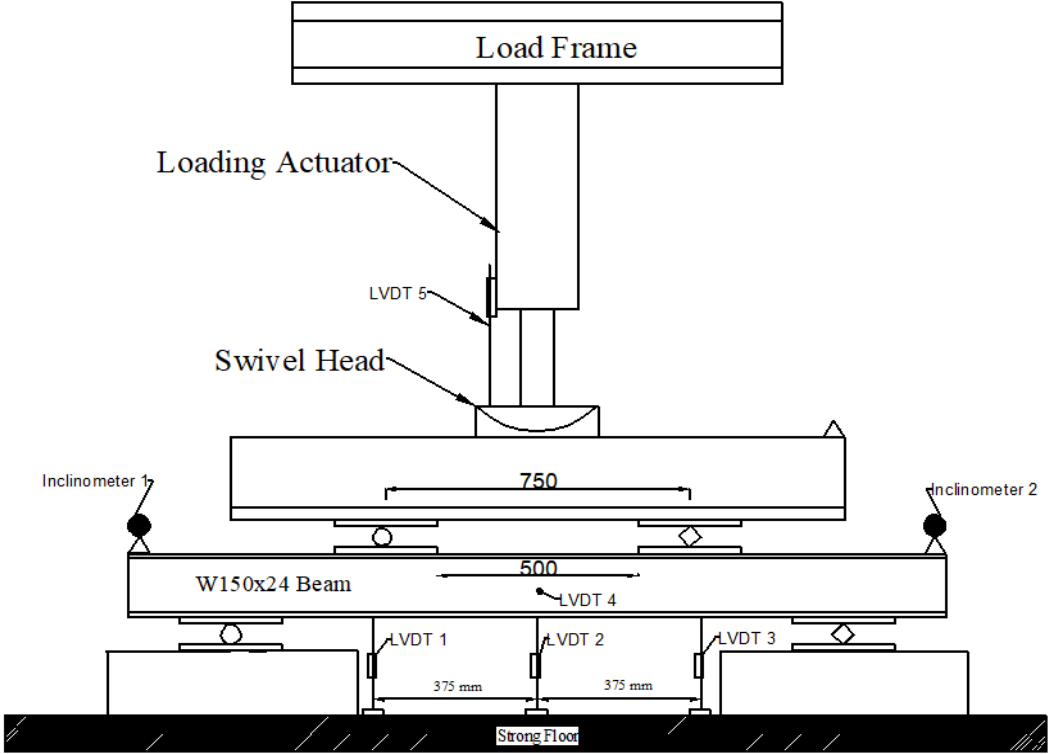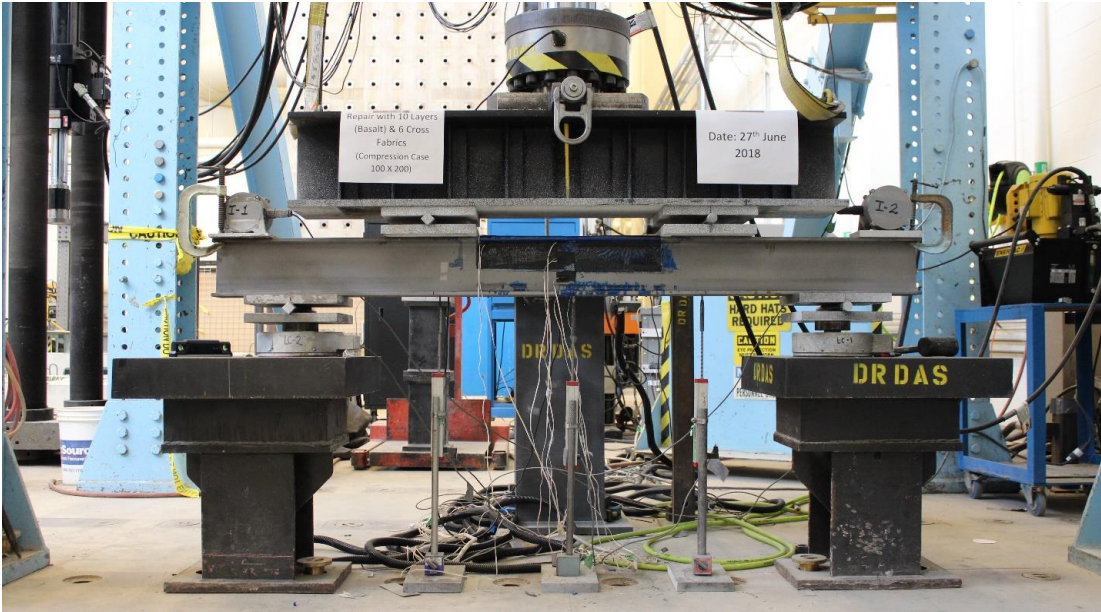


Figure 3.4: Schematic view of the test setup



Figure 3.5: Photo showing the test setup

Strain gauges were also installed at various locations of the beam to acquire the strain values at these locations. A total of nine strain gauges were installed on each specimen. Seven strain gauges (S1 to S7) were installed at the mid-span of the beam as shown in Figure 3.6. The strain data obtained from these strain gauges were used to obtain the neutral axis depth of the beam at various mid-span deflections (LVDT2). Two strain gauges (S8 and S9) were installed at 200 mm away from the mid-span. Strain gauge, S9 was attached to the BFRP fabric and strain gauge, S8 was installed on the steel surface as shown in Figure 3.7. Data from these two strain gauges was used to monitor any slippage or debonding between the steel substrate and the BFRP fabric layers as the testing continued.
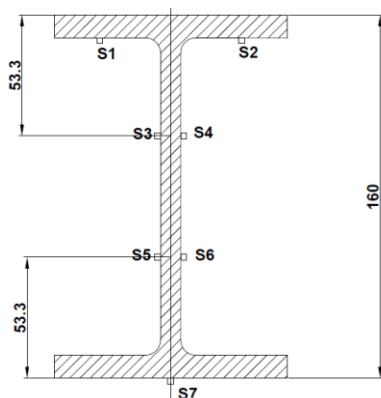


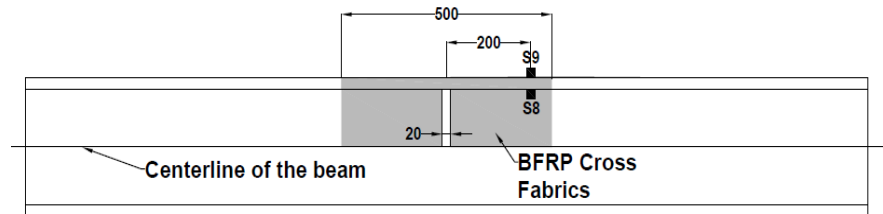Figure 3.6: Position of strain gauges at the mid-span of the beam

Figure 3.7: Position of strain gauges along the length of the BFRP fabric

## 3.4 Results and discussion

One objective of this research was to study the behavior of rehabilitated steel beams which have developed corrosion defect in the top (compression) flange. The effectiveness of the rehabilitation method was studied by comparing the load carrying capacities, load-deflection behaviors, moment-curvature relationships, and strain values of rehabilitated beams with those of the control specimens, (UB, 40CC, and 20CC). Ductilities of the beams were also determined and studied in this research. Finally, nonlinear finite element (FE) models were developed, and the FE models were validated with the test data. Then the validated FE models were used to undertake a parametric study.

### 3.4.1   Load-Deflection Behavior

The effect of cross fabrics in preventing debonding was investigated by rehabilitating two specimens with three layers (R40-10L-3C) and six layers (R40-10L-6C) of cross fabrics, respectively. However, the number of longitudinal fabrics layers used was same for both specimens (10). The load-deflection

behaviors of specimens R40-10L-3C and R40-10L-6C were obtained and compared with the control specimens (UB and 40CC) and shown in Figure 3.8. This figure shows that both rehabilitated beams exhibited very similar behavior and both beam specimens were successful in eliminating debonding failure. Hence, the remaining specimens were rehabilitated with three layers of cross fabrics. For the control corroded specimen 40CC, there was a substantial decrease in load resistance at a mid-span deflection of 50 mm and it was found unsafe to continue the test beyond this deflection. Hence, for all the specimens, the tests were terminated at a mid-span deflection of about 50 mm.
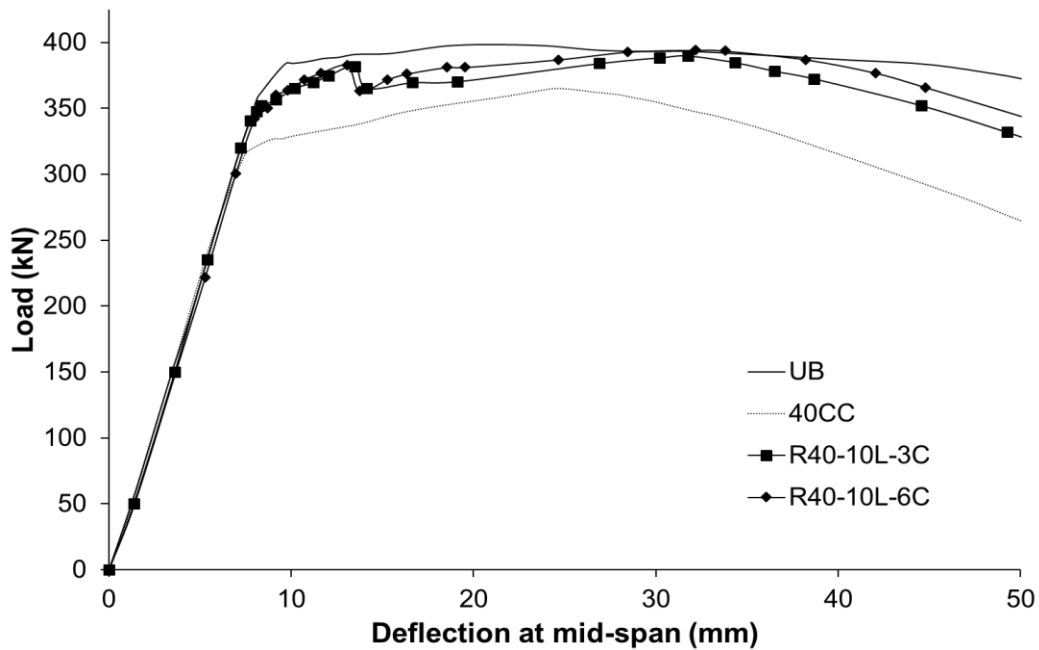


Figure 3.8: Load-defection curves for beams with 3 and 6 layers of cross fabrics

The load-deflection behaviors of rehabilitated specimen R20-7L-3C along with control specimens UB, 20CC are shown in Figure 3.9. The load-deflection behaviors for rehabilitated specimens R40-10L-3C, R40-15L-3C and the control specimens UB and 40CC are shown in Figure 3.10. It can be observed that for rehabilitated specimens with both 20% and 40% corrosion defects (specimens R20-7L-3C, R40-10L-3C, R40-10L-6C, and R40-15L-3C), there is an improvement in load carrying capacity of all the beams. Figure 3.10 shows that with the increase in the number of BFRP layers, the ultimate load of the rehabilitated beams improved.
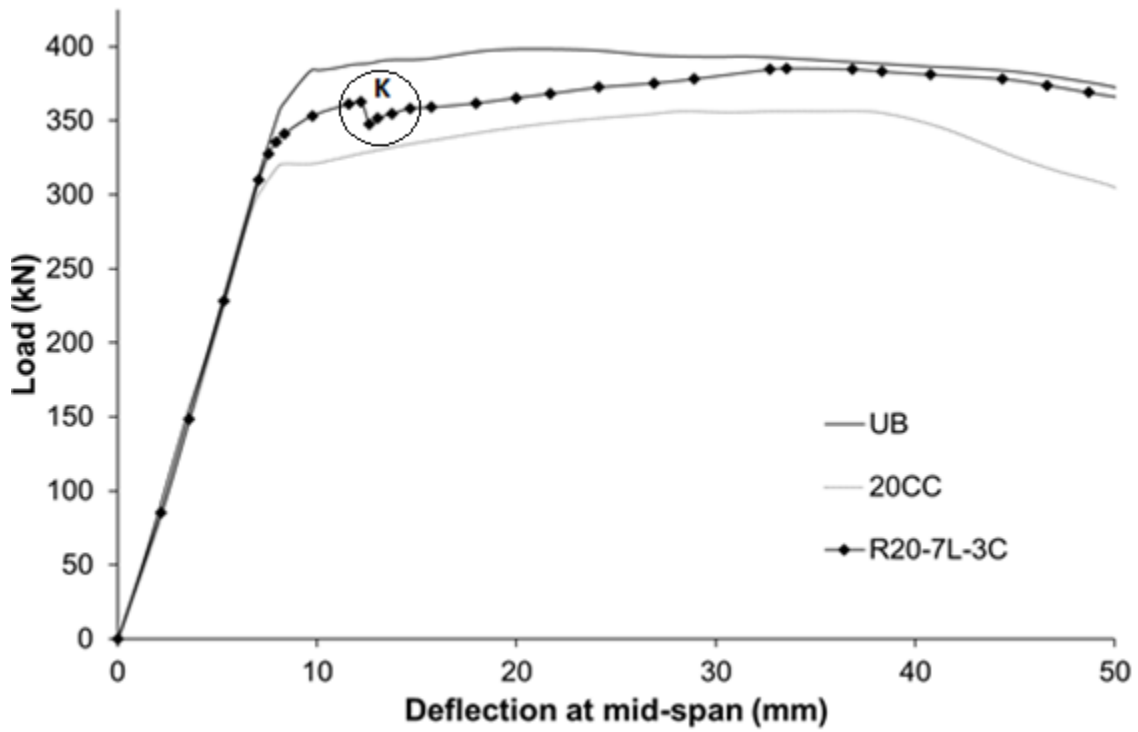
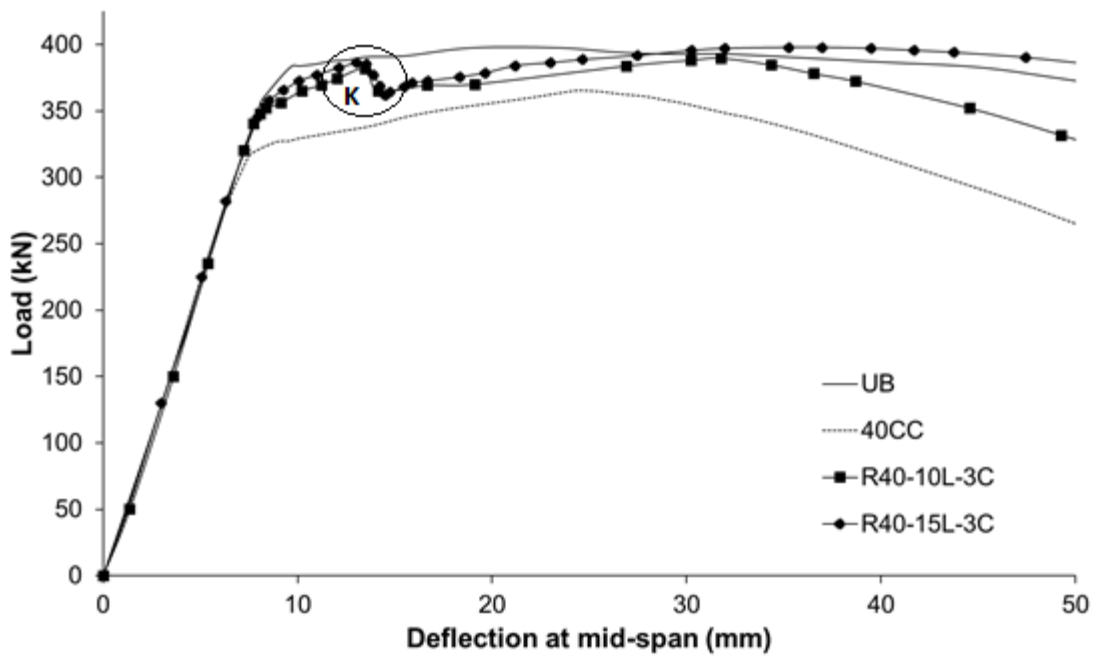Figure 3.9: Load-deflection curves of beams with 20% corrosion



Figure 3.10: Load-deflection curves of beams with 40% corrosion

The final failure mode observed in the rehabilitated beams was local buckling of the top flange and followed by a lateral torsional buckling of the beam. The first failure was observed in the attached BFRP fabrics due to kinking along the stress concentration line formed due to the corrosion defect (see Figure 3.11). It caused the first load drop in the experiment as indicated by K (see Figures 3.9 and 3.10).



Figure 3.11: Kinking along the stress concentration line

Literature review shows that the failure of the BFRP fabrics when subjected to axial compression can be either due to extensional microbuckling which is out of phase buckling of the fibers within the matrix (Figure 3.12a), shear microbuckling which is in phase buckling of the fibers within the matrix (Figure 3.12b), kinking which is highly localized fiber buckling occurring after the development of microbuckling (Figure 3.12c) or transverse tensile rupture due to Poisson stress [20].
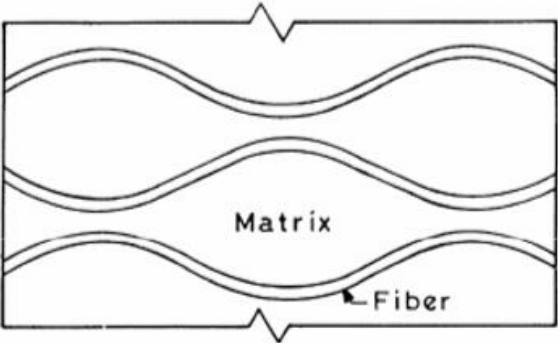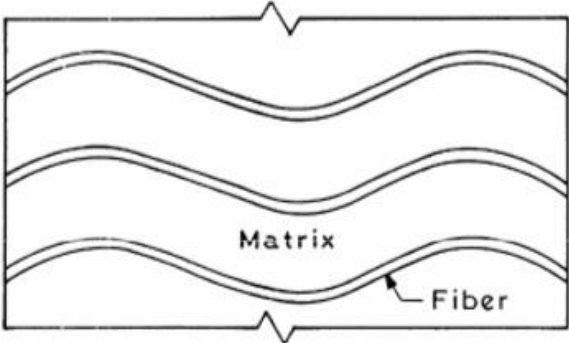


Figure 3.12a : Extensional microbuckling [20]     Figure 3.12b : Shear Microbuckling [20]
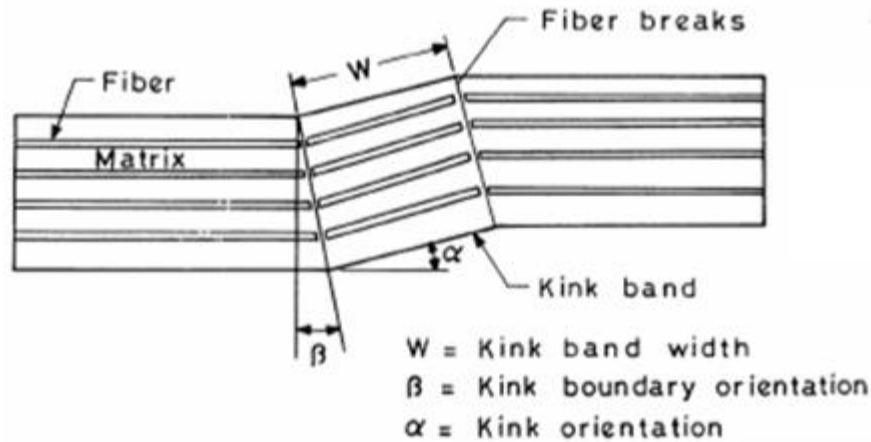
Figure 3.12c: Kinking [20]

Table 3.2 details the yield and ultimate load values for all the specimens. It was observed that for all the rehabilitated beams, there was a moderate increase in the yield load and a relatively large increase in the ultimate load as compared to the control corroded beams (20CC and 40CC). With the application of adequate number of layers of BFRP fabrics the ultimate strength of the rehabilitated beam was restored to that of the uncorroded virgin beam, UB. For specimen R40-15L-3C which was rehabilitated with 15 layers of BFRP fabric (total thickness of 6.75 mm), the yield load increased to 357 kN when compared with the yield load of control corroded specimen 40CC (319kN). The ultimate load increased from 365 kN for the specimen 40CC to 398 kN for specimen R40-15L-3C. Hence, increases in both yield load and ultimate load were observed in the rehabilitated specimen as compared to the control corroded specimens. The specimen R40-15L-3C was also able to restore the ultimate load to the level of uncorroded virgin (reference) specimen UB (398 kN). Hence, this study found that 15 layers of BFRP fabrics was adequate for restoring the ultimate strength of a beam with corrosion defect of 40% of the flange wall thickness. However, the yield strength could only be restored partially. For specimen R20-7L-3C, the yield load increased from 339 kN for specimen 20CC to 358 kN, and the ultimate load increased from 374 kN to 394 kN. Increases in yield and ultimate loads were observed in the rehabilitated specimen as compared to the control corroded specimens. The yield load and the ultimate loads values did not reach to that of the uncorroded beam, UB. However, the difference in ultimate load values obtained from specimens R20-7L-3C and UB was only about 1%. Figure 3.13 shows the final deflected shape of a typical rehabilitated beam.

Table 3.2: Comparison of yield and ultimate loads

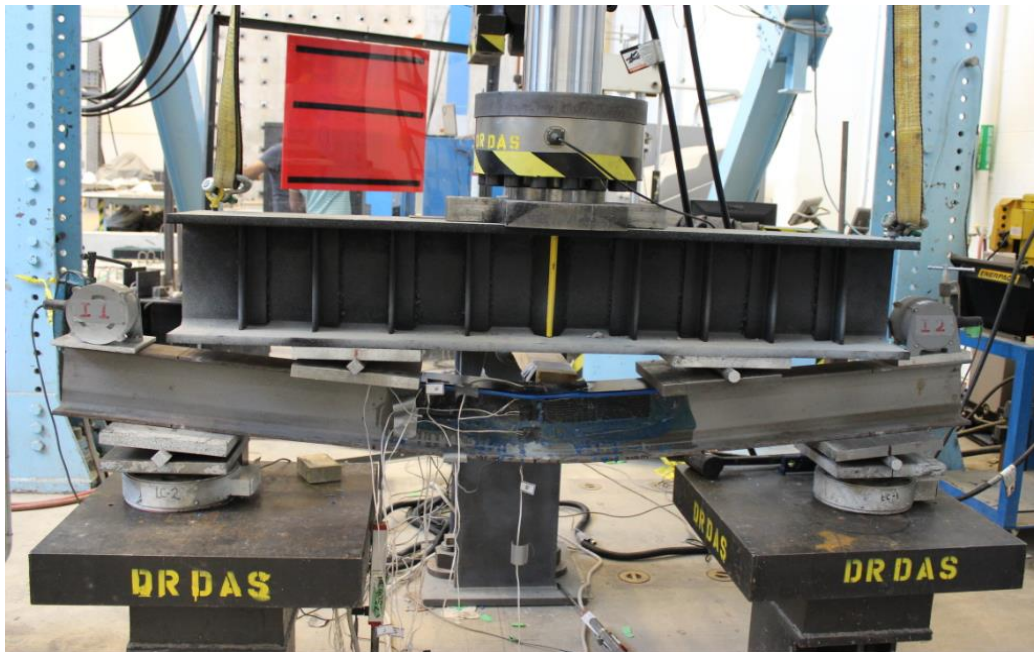| Specimen ID | Yield Load ($P_y$) | Ultimate Load ($P_u$) | % Change in $P_y$ compare to UB | % Change in $P_u$ compare to UB | % Change in $P_u$ compare to control |
|---|---|---|---|---|---|
| UB | 384 | 398 | Reference Beam | Reference Beam | - |
| 40CC | 319 | 365 | -16.8% | -8.2% | Reference Beam |
| R40-10L-3C | 341 | 390 | -11.3% | -2.0% | 6.7% |
| R40-10L-6C | 342 | 393 | -10.9% | -1.2% | 7.5% |
| R40-15L-3C | 357 | 398 | -7.0% | 0.0% | 8.9% |
| 20CC | 339 | 374 | -11.7% | -6.0% | Reference Beam |
| R20-7L-3C | 358 | 394 | -6.8% | -1.0% | 5.3% |



Figure 3.13: Final deflected shape of the rehabilitated beam

### 3.4.2 Moment-Curvature and Ductility

The moment-curvature relationships are shown in Figures 3.14 and 3.15. The curvature values were calculated using the deflection data obtained from LVDTs 1, 2, and 3 (Figure 3.4). The deflection data for each load point was fitted to a fourth order polynomial equation to obtain the equation for vertical displacement with is the displacement along the direction of application of load. The value of second derivate of the vertical displacement equation at the center of the beam was considered as the curvature. The moment was calculated by multiplying the reaction force at the support with the moment arm of the reaction force. The moment-curvature relationship provides a more general behavior of the steel section than the load-deflection relationship as it is not dependent on the loading and boundary conditions of the setup. Table 3.3 shows the yield moment, ultimate moment, and the respective curvatures for all the specimens tested. The ultimate moment-carrying capacity of the uncorroded control beam (UB) was found to be 74.0 kN-m. For the control corrosion specimens (40CC and 20CC), the moment-carrying capacities were 57.6 kN-m and 63.2 kN-m, respectively. However, when the beam 40CC which had 40% corrosion defect was rehabilitated with 15 layers of BFRP fabric (specimen R40-15L-3C), the ultimate moment capacity was 74 kN-m which is equal to that of uncorroded (virgin) specimen, UB.

Section ductility ($\mu$) was calculated for all the beams using the curvature values. Section ductility is defined as the ratio of curvature at the ultimate moment ($\emptyset_u$) to the curvature at yield moment ($\emptyset_y$), as shown in Equation 3.1.

$$\text{Section Ductility } ( \mu ) = \frac{\emptyset_u}{\emptyset_y} \tag{3.1}$$

Energy-based approach was also used to determine the ductility as explained and used by Naaman and Jeong [21]. Using this method, the energy dissipation ratio ($\mu_E$) is calculated as the ratio of total energy dissipated at ultimate load to the total energy dissipated at yield load as shown in Equation 3.2. In this equation, $\Delta U$ is the deflection at ultimate load, $\Delta Y$ is the deflection at yield load and P is the applied load on the beam. It was observed from both approaches that the ductility values of the rehabilitated specimens were higher than the ductility values of the control corroded specimens (specimens 20CC and 40CC). It should be noted that these ductility measures refer to the ductility ratio which compares two specific load points which are yield load point and ultimate load point.

$$\text{Energy dissipation ratio } ( \mu_E ) = \frac{\int_0^{\Delta U} P(\Delta)d\Delta}{\int_0^{\Delta Y} P(\Delta)d\Delta} \qquad\qquad (3.2)$$
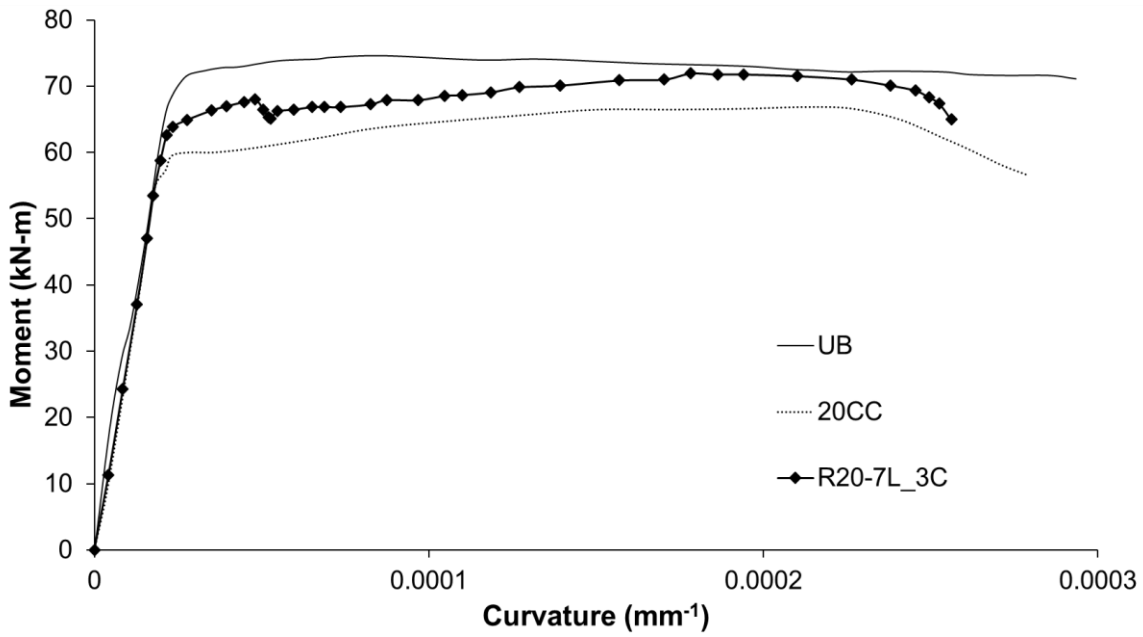


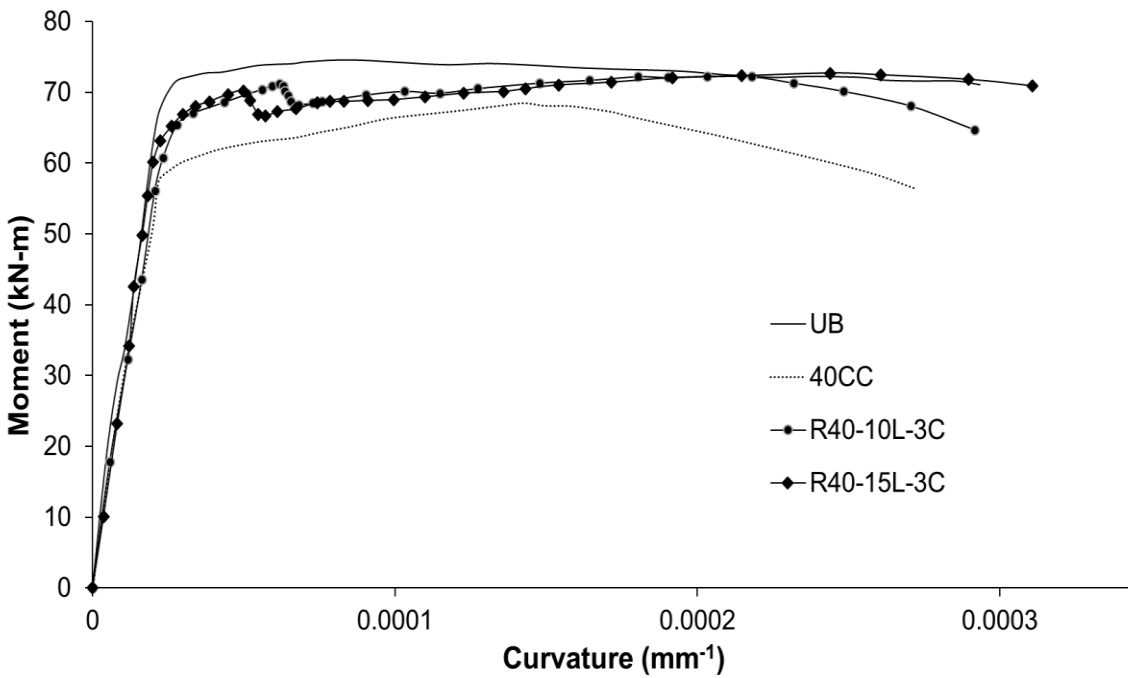Figure 3.14: Moment-curvature relationships for beams with 20% corrosion



Figure 3.15: Moment-curvature relationships for beams with 40% corrosion

Table 3.3: Comparison of yield, ultimate moment, and ductility of the beams

| Specimen | Yield Moment (N-mm) | Curvature at Yield moment ($\phi_y$) | Ultimate Moment (N-mm) | Curvature at Ultimate moment ($\phi_u$) | Section Ductility ($\phi_u/\phi_y$) | Relative Ductility | Energy Dissipation ratio | Relative Ductility |
|---|---|---|---|---|---|---|---|---|
| UB | 71.7 | $2.81 \times 10^{-5}$ | 74.0 | $1.3 \times 10^{-4}$ | 4.8 | 1.00 | 3.7 | 1.0 |
| 40CC | 57.6 | $2.19 \times 10^{-5}$ | 68.5 | $1.4 \times 10^{-4}$ | 6.5 | 1.37 | 5.3 | 1.5 |
| R40-10L-3C | 60.7 | $2.33 \times 10^{-5}$ | 71.3 | $1.5 \times 10^{-4}$ | 6.4 | 1.33 | 7.3 | 2.0 |
| R40-10L-6C | 65.2 | $2.62 \times 10^{-5}$ | 71.4 | $1.7 \times 10^{-4}$ | 6.5 | 1.38 | 6.8 | 1.8 |
| R40-15L-3C | 62.7 | $2.38 \times 10^{-5}$ | 74.0 | $1.7 \times 10^{-4}$ | 6.5 | 1.37 | 7.8 | 2.1 |
| 20CC | 63.2 | $2.31 \times 10^{-5}$ | 70.2 | $1.5 \times 10^{-4}$ | 6.5 | 1.36 | 7.3 | 2.0 |
| R20-7L-3C | 64.2 | $2.34 \times 10^{-5}$ | 72.7 | $1.6 \times 10^{-4}$ | 6.7 | 1.41 | 9.0 | 2.4 |

### 3.4.3   Strain Analysis

The layout of strain gauges is shown in Figures 3.6 and 3.7. Strain gauges 1 to 7 were attached to the mid-span of the beam at various depths. The data obtained from these strain gauges was used to determine the neutral axis depth of the beam as the loading process continued. Figure 3.16 shows the strain values of various strain gauges with respect to the mid-span deflection for specimen R40-15L-3C. It was observed that the magnitude of the strain in the compression zone (S2 and S4) was almost equal to the magnitude of the strain in the tension zone (S6 and S7). This indicated that the compression zone of the rehabilitated specimen had almost equal strength as the tension zone and thus, it can be concluded that the rehabilitation with 15 layers of BFRP fabric was effective. The distance of S2 and S7 from the mid-height of the beam section was 53.3 mm and distance of S4 and S6 was 26.7 mm. Hence, the magnitude of strain values at S2 and S7 were higher than the values of S4 and S6.
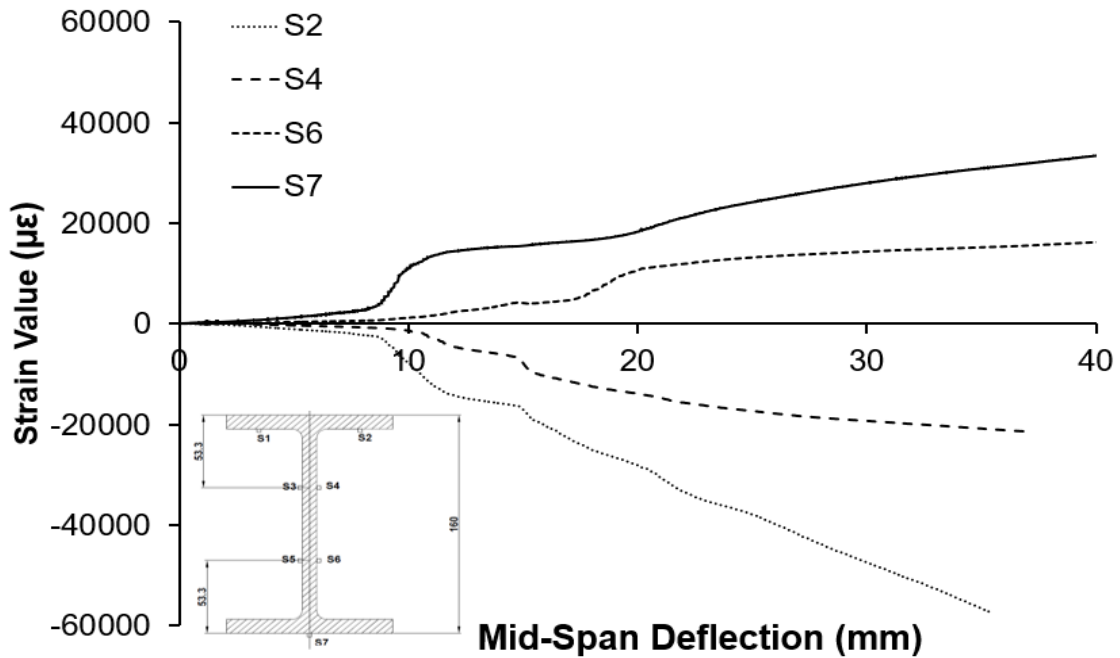
Figure 3.16: Strain vs. deflection at mid-span for R40-15L-3C

Figure 3.17 shows the strain values of the steel (S8 in Figure 3.7) and of the BFRP fabrics (S9 in Figure 3.7) at 200 mm from the mid-span of the beam for the same specimen, R40-15L-3C. It was observed that both strain values followed the same pattern, however, the strain value of the BFRP (S9) was found to be slightly higher than the strain value of steel substrate (S8). This is because the BFRP fabrics were located slightly away from the mid-height of the beam than the steel substrate. The distance of strain gauge S8 was 69.9 mm and distance of S9 was 86.75 mm from the mid-height of the beam. Hence, it can be concluded that there was no debonding between the steel and the BFRP fabrics.
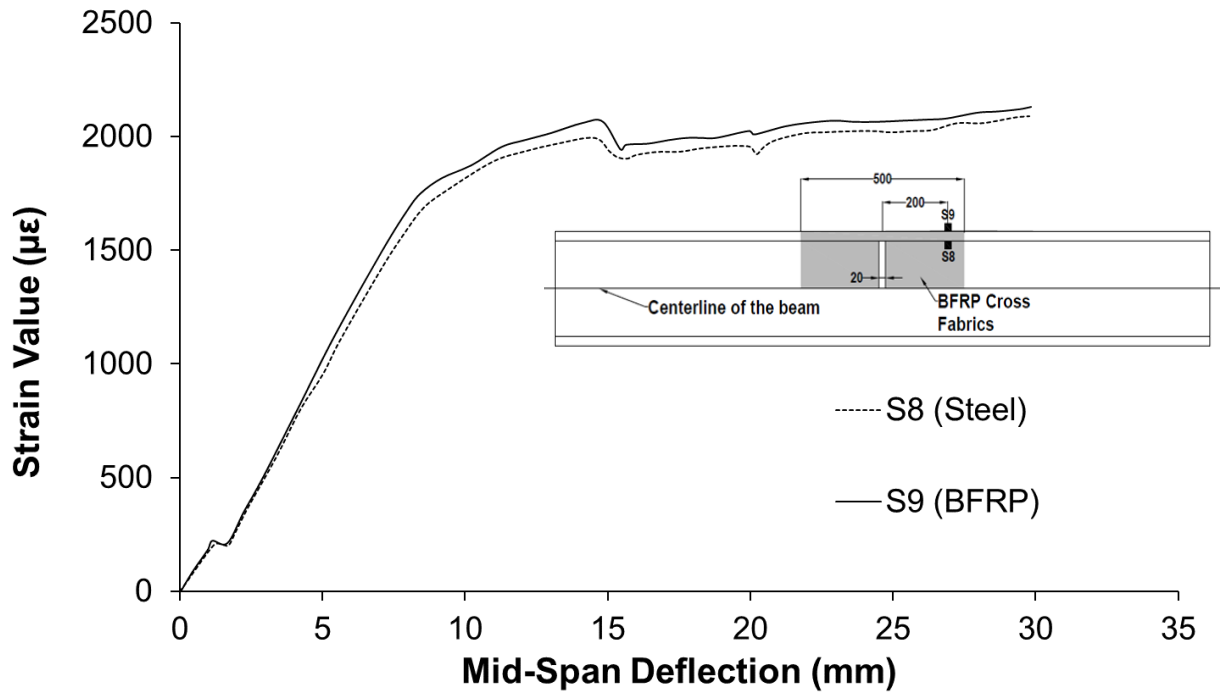
Figure 3.17: Comparison of strain value of steel and BFRP at 200 mm from center for R40-15L-3C

The location of the neutral axis (NA) was also used as an indicator for checking the improvement of the rehabilitated beams. The NA depth at any deflection value was determined by interpolation of the strain data obtained from the strain gauges attached at various locations of the mid-span section of the beam (Figure 3.7). The neutral axis depth at 20 mm mid-span deflection for all the specimens is shown in Table 3.4. Figures 3.18a and 3.18b show the change in neutral axis depth for the control corroded specimens with 40% (40CC) and 20% (20CC) corrosion depths, respectively. It was observed that the location of neutral axis moves downward for the control corrosion specimens 40CC and 20CC with respect to uncorroded control (virgin) specimen UB. However, with the application of BFRP fabrics, the location of the neutral axis moves upward. As the number of BFRP fabrics layers increases, the neutral axis of the rehabilitated beams moves back closer to that of specimen UB. Hence, it can be concluded that with rehabilitation of the corroded specimens with BFRP fabrics, the neutral axis depth of the corroded specimens (40CC and 20CC) can be restored to that of the uncorroded specimen (UB) if required number of BFRP fabric layers is added. For this study, 15 layers of BFRP fabric was sufficient for restoring the neutral axis depth of 40CC specimen.

Table 3.4: Neutral axis depth at 20 mm deflection

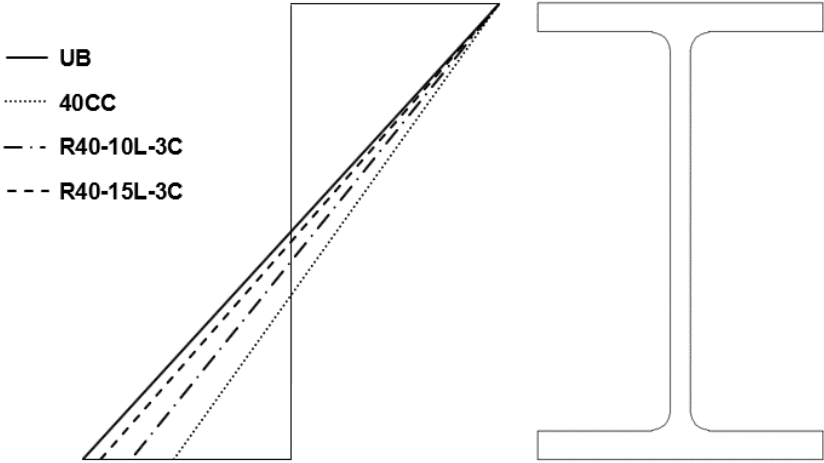| Specimen ID | NA Depth (mm) |
|---|---|
| UB | 80 |
| 40CC | 102.1 |
| R40-10L-3C | 90.2 |
| R40-15L-3C | 83.4 |
| 20CC | 88.4 |
| R20-7L-3C | 80.07 |



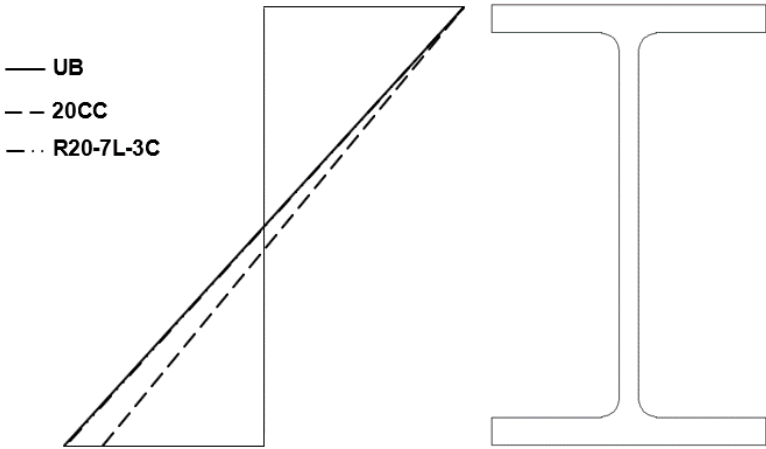Figure 3.18a: Neutral axis depth for beams with 40% depth of corrosion



Figure 3.18b: Neutral axis depth for beams with 20% depth of corrosion

## 3.5  Finite Element Simulation and Parametric Study

Experimental testing is the most reliable and accurate method for determining the behavior of a structure. However, due to time and costs involved in each experiment, it is difficult and may not be viable to conduct tests for each parameter and its range. Hence, in this study, numerical method was also used to supplement the experimental tests and perform a parametric study. Non-linear finite element software Abaqus/Standard [22] was used to the conduct the numerical study. FE models were developed to simulate the experimental behavior of the specimens. The models were validated with the test data and then these FE models were used to conduct a parametric study. The parameters considered in the parametric study are the number of BFRP layers and the depth of corrosion.

The steel beam was modelled using twenty-node quadratic brick (solid) element with reduced integration (C3D20R), and the BFRP fabrics was modelled using 8-node quadrilateral continuum shell element with reduced integration (SC8R). The shell element has the geometry of a brick element; however, the kinematic and constitutive behaviors are that of a conventional shell element. A mesh convergence study was conducted to determine the optimum mesh size for the models. The optimum mesh size for C3D20R elements was found to be 12 mm. The mesh convergence study for steel beam is shown in Figure 3.19. For the SC8R elements a mesh size of 10 mm was used. The material properties of steel used in the model are the modulus of elasticity, the Poisson's ratio, and the plastic stress-strain values obtained from the true stress-strain curve, as shown in Figure 3.1a.
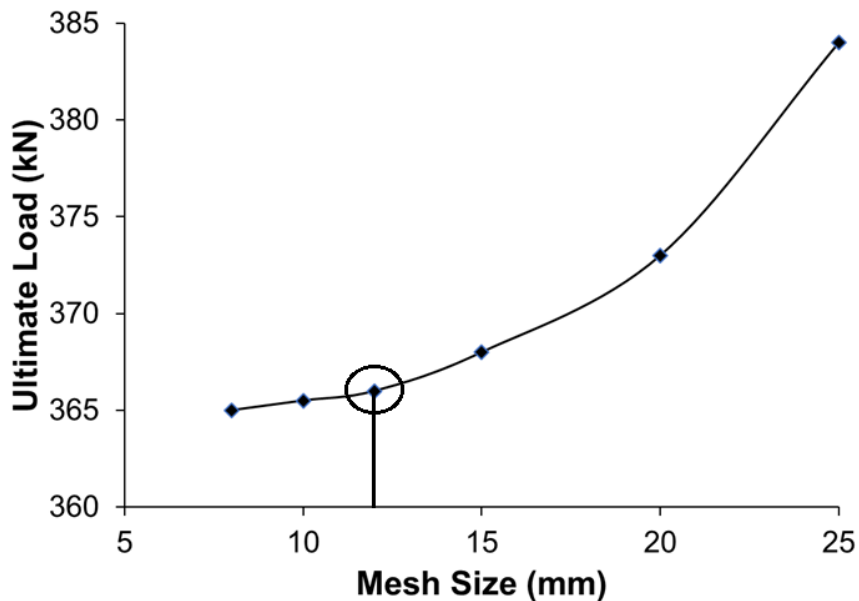


Figure 3.19: Mesh Convergence study for steel

The material properties of BFRP fabrics are shown in Table 3.5. These values were determined from the compression coupon test conducted on BFRP fabrics.

Table 3.5: Material properties of BFRP fabric

| E (GPa) | $\varepsilon_{y\ (\%)}$ |
|---------|---------|
| 10 | 2.2 |

Hashin criterion was used to simulate the damage of the BFRP fabrics by using the damage initiation criteria [23]. The four damage initiation criteria considered in Hashin criteria for simulating damage in the FRP material are tensile fiber failure, compressive fiber failure, tensile matrix failure, and compressive matrix failure. When any of these criteria is satisfied, the damage initiation occurs. The equations for these damage criteria are shown in Equation 3.3 to 3.6.

Tensile fibre failure:
$$\left(\frac{\sigma_{11}}{X_T}\right)^2 + \alpha\left(\frac{\sigma_{12}}{S_1}\right)^2 = \begin{cases} \text{no failure, } x < 1 \\ \text{failure, } x \geq 1 \end{cases} \tag{3.3}$$

Compressive fibre failure:
$$\left(\frac{\sigma_{11}}{X_C}\right)^2 = \begin{cases} \text{no failure, } x < 1 \\ \text{failure, } x \geq 1 \end{cases} \tag{3.4}$$

Tensile matrix failure:
$$\left(\frac{\sigma_{22}}{Y_T}\right)^2 + \left(\frac{\sigma_{12}}{S_1}\right)^2 = \begin{cases} \text{no failure, } x < 1 \\ \text{failure, } x \geq 1 \end{cases} \tag{3.5}$$

Compressive matrix failure:

$$\left(\frac{\sigma_{12}}{S_1}\right)^2 + \left(\frac{\sigma_{22}}{2S_2}\right)^2 + \left(\left(\frac{Y_C}{2S_2}\right)^2 - 1\right)\left(\frac{\sigma_{22}}{Y_C}\right) = \begin{cases} \text{no failure, } x < 1 \\ \text{failure, } x \geq 1 \end{cases} \tag{3.6}$$

In Equations 3.3 to 3.6, $X_T$ is the longitudinal tensile strength, $X_C$ is the longitudinal compressive strength, $Y_T$ is the transverse tensile strength, $Y_C$ is the transverse compressive strength, $S_1$ is the longitudinal shear strength, and $S_2$ is the transverse shear strength.

The damage initiation values of the BFRP fabrics used in the model are shown in Table 3.6. These values were determined from the coupon test results of the BFRP fabric.

Table 3.6: Damage initiation values for BFRP fabric

| $X_T$(MPa) | $X_C$ (MPa) | $Y_T$ (MPa) | $Y_C$ (MPa) | $S_1$ (MPa) | $S_2$ (MPa) |
|------------|-------------|-------------|-------------|-------------|-------------|
| 390 | 250 | 60 | 125 | 110 | 110 |

The amount of energy needed to cause complete failure or damage of the BFRP fabric was determined using the fracture energy parameter ($G_c$) as shown in Equation 3.7.

$$G_c = \frac{l^* * \sigma_u * \varepsilon_u}{2}$$ (3.7)

In Equation 3.7, $l^*$ is the characteristic length, $\sigma_u$, and $\varepsilon_u$, are the stress and strain values at the damage initiation point of the stress-strain curve, respectively. Characteristic length ($l^*$) is a function of the thickness of the BFRP fabric and the mesh size and was obtained using method proposed by Bažant and Oh [24].

In the FE models, the BFRP fabrics was modeled as a single layer of thickness equal to the total thickness of the BFRP fabrics used for the rehabilitation. A surface-to-surface tie constraint was used to attach the BFRP fabrics layer to the steel beam since no de-bonding or slippage was observed in the experimental study. As narrow strips of BFRP fabrics were used to fill up the void created by the corrosion, another layer of BFRP fabrics was created to simulate the small strips. This layer was also attached to the steel beam and the main BFRP fabrics using a surface-to-surface tie constraint. Figure 3.20 shows the comparison of the load-deflection data obtained from the test specimens and the FE models for the specimens UB and 40CC. A good correlation between test specimens and FE models is found.
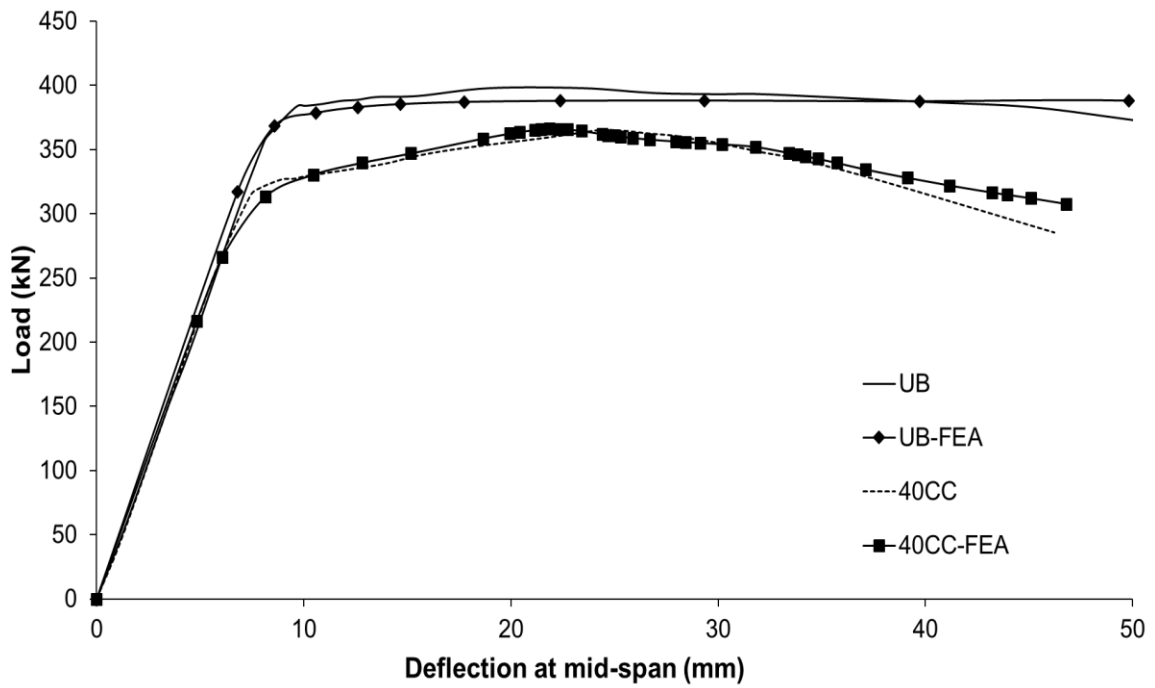
Figure 3.20: Validation of FEM models for the UB and 40CC beam

Figures 3.21 and 3.22 show the comparison of the load-deflection behaviors of the beam with 40% corrosion defect when rehabilitated with 10 layers and 15 layers of BFRP fabric, respectively obtained from the tests and the FE models. Again, a good correlation between the test specimens and FE models can be observed.
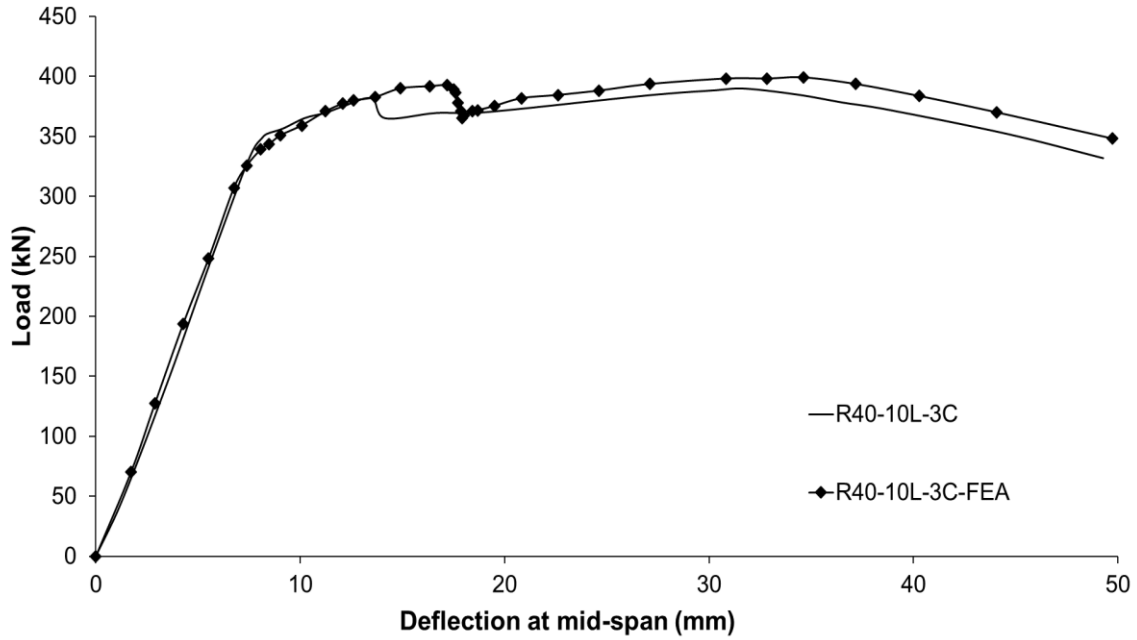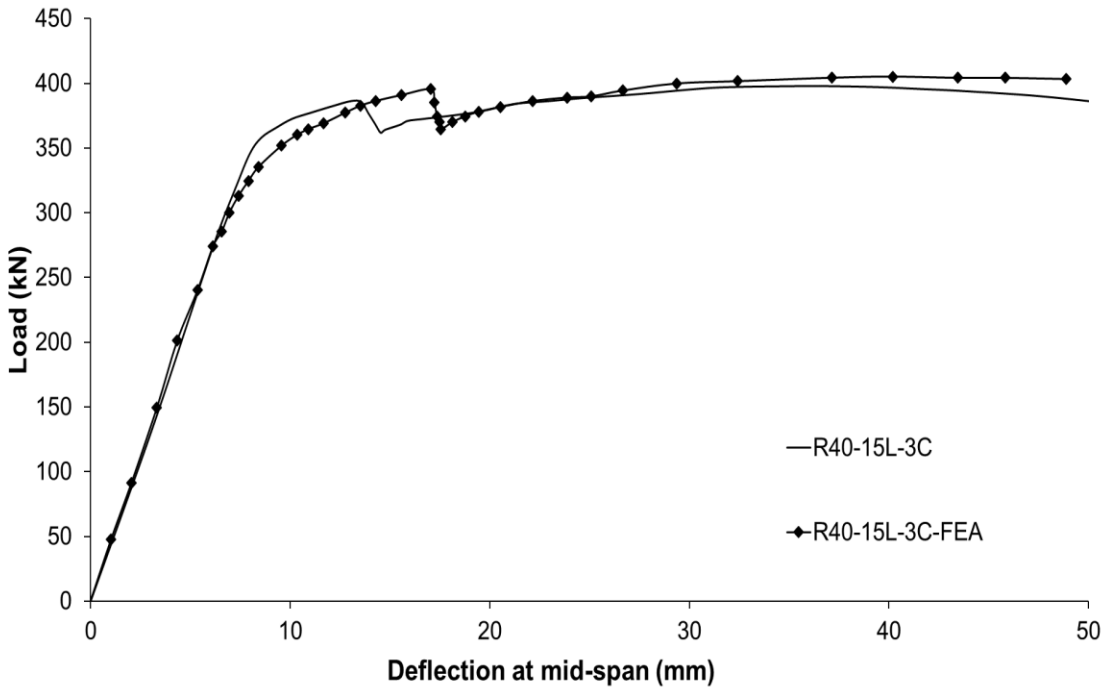
Figure 3.21: Validation of FEM models for R40-10L-3C beam



Figure 3.22: Validation of FEM models for R40-15L-3C beam

Figure 3.23 compares the load-deflection data of the steel beam with 20% corrosion defect and rehabilitated with 7 layers of BFRP fabric obtained from the test and FE model. A good agreement between the load-deflection data obtained from the test and the FEM model can be observed for this

rehabilitated beam as well. The comparison of the results obtained from all the beam specimens is presented in Table 3. 7.
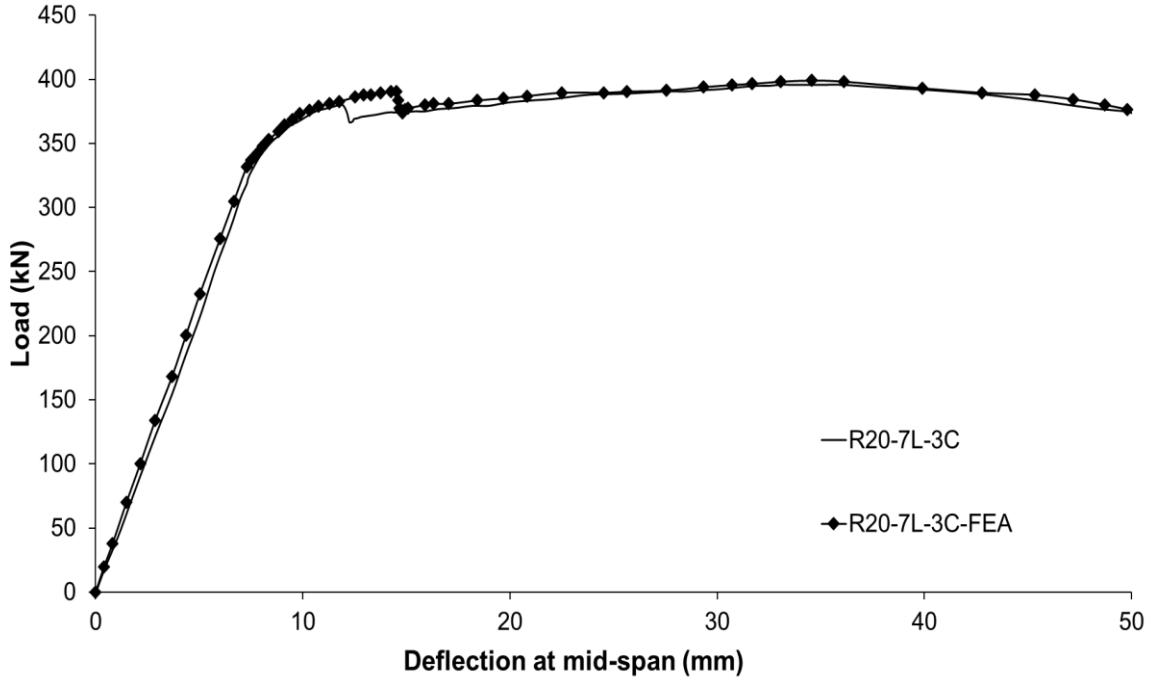


Figure 3.23: Validation of models for R20-7L-3C beam

Table 3.7: Comparison of experimental data and FEM model results

| Specimen ID | Experiment | FE Model | % Difference in Load | Experiment | FE Model | % Difference in Load |
|---|---|---|---|---|---|---|
| | Yield Load (kN) | Yield Load (kN) | | Ultimate Load (kN) | Ultimate Load (kN) | |
| UB | 384 | 375 | -2.34% | 398 | 387 | -2.69% |
| 40CC | 319 | 313 | -2.03% | 365 | 366 | 0.25% |
| R40-10L-3C | 340 | 343 | 0.71% | 390 | 399 | 2.35% |
| R40-15L-3C | 357 | 351 | -1.68% | 398 | 405 | 1.82% |
| 20CC | 338 | 340 | 0.30% | 374 | 378 | 1.09% |
| R20-7L-3C | 358 | 364 | 1.68% | 394 | 399 | 1.35% |

The failure mode obtained from FE model for specimen R40-10L-3C is shown in Figure 3.24. The damage of the composite fabric from the FE model beyond ultimate load and at 50 mm mid-span deflection for specimen R40-10L-3C is shown in Figure 3.25. The other FEM models for the rehabilitated specimens showed similar behavior (Appendix A Figures A.9 -A.14).
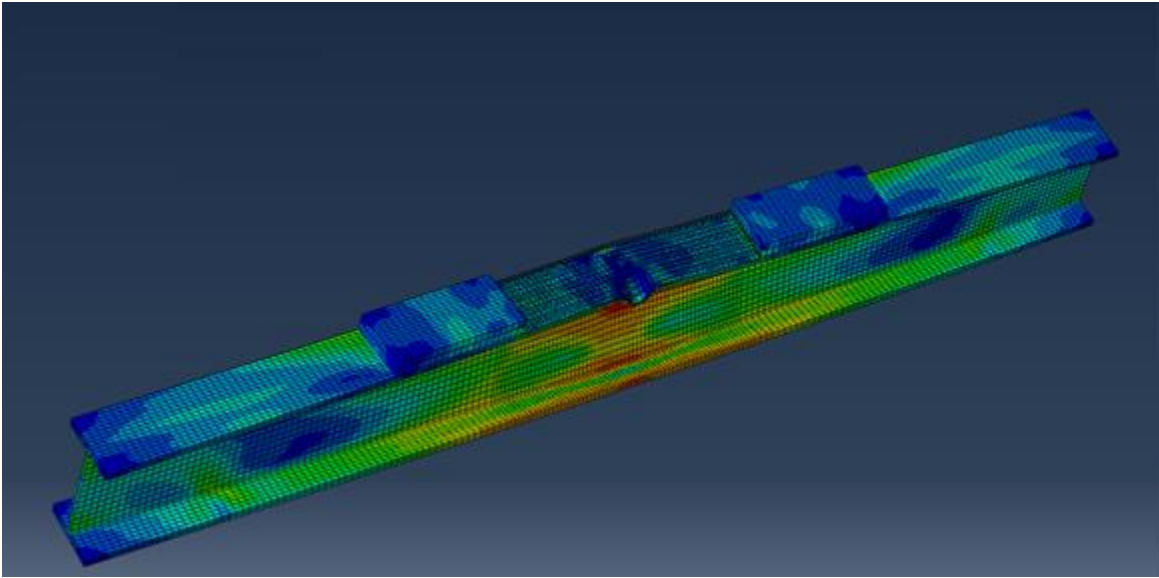


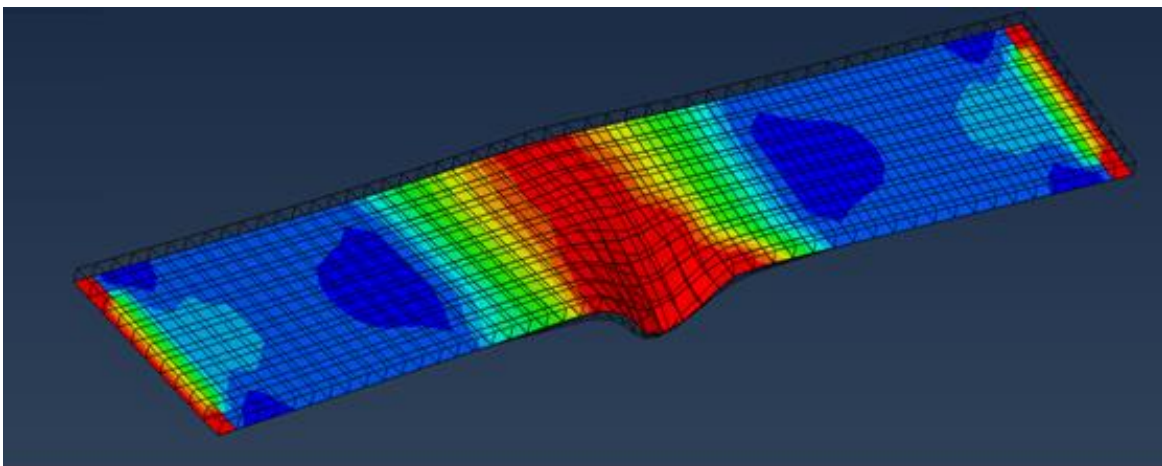Figure 3.24: Failure mode obtained in the FEA model for R40-10L-3C specimen



Figure 3.25: Damage in BFRP modelled using Hashin Criteria for R40-10L-3C specimen

The validated FE model was used for a parametric study. The parameters chosen are the percentage of corrosion depth in the top flange ranging from 10% to 50% of the flange thickness, while keeping the length of the corroded area unchanged at 200 mm. The number of layers of BFRP fabric was also

varied to determine the optimum number of BFRP fabric for each corrosion depth. Figure 3,26 shows the optimum number of BFRP fabric layers required to restore the ultimate strength of the corroded specimens to the level of uncorroded corrosion (virgin) specimen, UB for various corrosion depths. The optimum number of layers refers to the minimum number of BFRP fabrics layers required for restoring the ultimate load capacity of the rehabilitated specimens to level of the uncorroded control (virgin) specimen, UB.
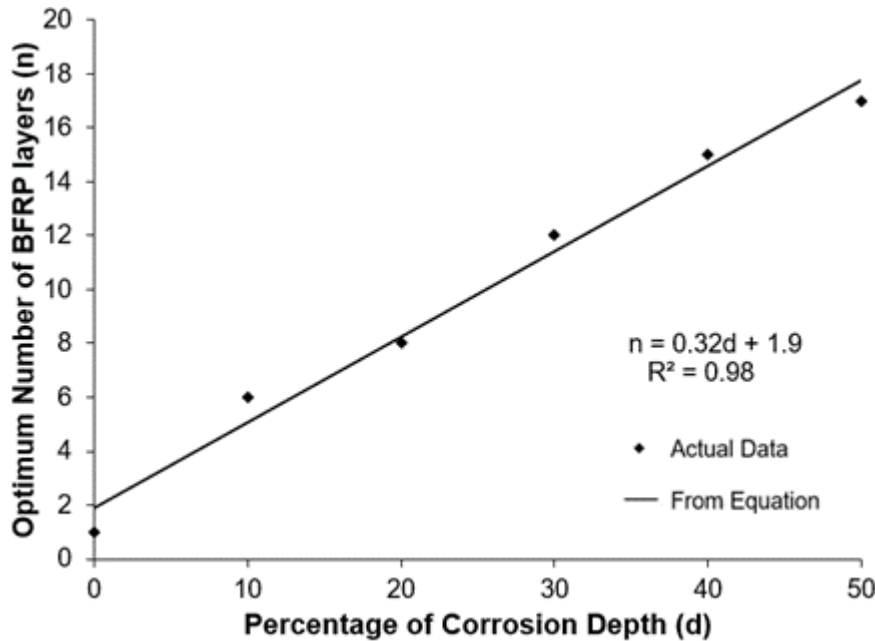


Figure 3.26: Relationship between percentage of corrosion and number of BFRP layers

Based on this data, Equation 3.8 is developed which can be used for determining the optimum numbers of BFRP fabrics layers required to rehabilitate a beam with corrosion defect in the compression flange.

$$n = 0.32d + 1.9 \tag{3.8}$$

In Equation 3.8, n is the optimum number of layers of BFRP fabric required for complete restoration of ultimate load to the level of specimen UB, and d is the percentage of corrosion depth in the compression flange. The $R^2$ value obtained for the fit is 0.98, which indicates a very good fit for the given data set. However, this equation is based on the data obtained from this study and the scope of this equation may be limited to this study. Further research is required to obtain a general equation which can be valid for all types of beams and different length of corrosion.

## 3.6  Conclusions

In this study, the feasibility of Basalt Fibre Reinforced Polymer (BFRP) composites in rehabilitating steel beams with corrosion in the compression flange is discussed using both experimental and finite element methods. It can be concluded that the BFRP fabrics can be effectively used for rehabilitating steel beams that have developed corrosion defect in the compression flange. The following can also be concluded from this study. However, these conclusions may be limited to the scope of this study.

1. The rehabilitation technique used in this study was effective in improving the load-carrying capacity of the rehabilitated beams. The technique was also effective in preventing the debonding of BFRP fabrics.

2. The ultimate strength of corroded steel beams with various depths of corrosion was fully restored to the value of the UB specimen. The yield strength of the rehabilitated specimens could also be restored partially.

3. The ductility of the rehabilitated beams was better than all control beams.

4. FE analysis presented in this study was able to predict the behavior of the rehabilitated steel beams since a good agreement between tests and the FE models was achieved.

5. Based on the parametric study a new semi-empirical equation is proposed which can be used for predicting the number of BFRP fabric layers required for successful rehabilitation when the steel beam had developed a corrosion defect in the compression flange.

## 3.7  Acknowledgments

## 3.8 Reference

[1]   Connecticut History.org, "Almost a Tragedy: The collapse of the Hartford Civic Center" https://connecticuthistory.org/almost-a-tragedy-the-collapse-of-the-hartford-civic-center/ viewed on October 13, 2018.

[2]   Davis, S.L. and Goldberg, D., 2013, "The fix we're in for the state of our nation's bridge", Transportation for America, Washington, D.C.

[3]   ASCE: American Society of Civil Engineers, "ASCE Infrastructure Report Card," 2017, ASCE, Virginia, USA, 1-6.
      <www.infrastructurereportcard.org/a/#p/bridges/overview>

[4]   FCM: "Informing the Future: The Canadian Infrastructure Report Card (CIRC-2016)", Federation of Canadian Municipalities, Ottawa, Ontario , Canada, 2016, 1-164.
      <http://canadianinfrastructure.ca/en/index.html>

[5]   N.H.A. Al-Salim, R.F. Hassan and M.H. Jaber. "Compression zone rehabilitation of damaged RC beams using polyester glue line", Journal of Engineering and Applied Science. 13 (5), 2018, 1195-2000. DOI: 10.3923/jeasci.2018.1195.1200

[6]   Sen R, Liby L and Mullins G., "Strengthening steel bridge sections using CFRP laminates", Composites Part B: Engineering, 32, 2001, 309–22. DOI: https://doi.org/10.1016/S1359-8368(01)00006-3

[7]   El Damatty AA, Abushagur M and Youssef MA., "Experimental and analytical investigation of steel beams rehabilitated using GFRP sheets", Steel and Composite Structures 3 (6), 2003, 421–438. DOI: http://dx.doi.org/10.12989/scs.2003.3.6.421

[8]   Green, M.F., Dent, A.J.S., and Bisby, L.A., "Effect of freeze-thaw cycling on the behavior of reinforced concrete beams strengthened in flexure with fibre reinforced polymer sheets", Canadian Journal of Civil Engineering, 30(6), 2003, 1081-1088. DOI: 10.1139/L03-059

[9]   Attari, N., Amziane, S., and Chemrouk, M., "Flexural strengthening of concrete beams using CFRP, GFRP and hybrid FRP sheets", Journal of Construction and Building Materials, 37, 2012, 746-757. DOI: https://doi.org/10.1016/j.conbuildmat.2012.07.052

[10]  Abdelrahman, K. and El-Hacha, R., "Behavior of large-scale concrete columns wrapped with CFRP and SFRP sheets", Journal of Composites for Construction. 16(4), 2012, 430-439. DOI: 10.1061/(ASCE)CC.1943-5614.0000278.

[11] Ilki, A., Peker, O., Karamuk, E., Demir, C., and Kumbasar, N., "FRP retrofit of low and medium strength circular and rectangular reinforced concrete columns", Journal of Materials in Civil Engineering, 20(2), 2008, 169–188. DOI: 10.1061/(ASCE)0899-1561(2008)20:2(169)

[12] X. Liu, A. Nanni, and P. F. Silva, "Rehabilitation of compression steel members using FRP pipes filled with non-expansive and expansive lightweight concrete", Advances in Structural Engineering, 8(2), 2005, 129-142. DOI: https://doi.org/10.1260/1369433054038029

[13] CISC: Canadian Institute of Steel Construction, "Handbook of Steel Construction", Markham, ON, Canada, 2017.

[14] P. Feng, S. Bekey, Y. Zhang, L. Ye and Y. Bai, "Experimental study on buckling resistance technique of steel members strengthened using FRP", International Journal of Structural Stability and Dynamics, 12(1), 2012, 153-178. DOI: https://doi.org/10.1142/S0219455412004604

[15] A. Bastani, S. Das and D. Lawn, "Rehabilitation of shear deficient steel beams using BFRP fabric", Structures, 19, 2019, 349-361, DOI: https://doi.org/10.1016/ j. istruc.2019.01.019

[16] Swentek I, Thompson J, Meirson G, Ugresic V and Henning F, "Comparison of basalt, glass, and carbon fiber composites using the high-pressure resin transfer molding process", Technical Report, Western University, London, ON, Canada, 2016, 1–25.

[17] ASTM. Standard Test Methods for Tension Testing of Metallic Materials. E8/E8M-15a. PA: ASTM International, West Conshohocken, Pennsylvania, USA ,2015.

[18] ASTM. Standard Test Method for Compressive Properties of Polymer Matrix Composite Materials with Unsupported Gage Section by Shear Loading D3410/D3410M-16. PA: ASTM International, West Conshohocken, Pennsylvania, USA, 2018.

[19] S. Jayasuriya, A. Bastani, S. Kenno, T. Bolisetti and S. Das, "Rehabilitation of corroded steel beams using BFRP fabric", Structures, 15, 2018, 152–161. DOI: https://doi.org/10.1016/j.istruc.2018.06.006

[20] N. K. Naik and R. S. Kumar, "Compressive strength of unidirectional composites: evaluation and comparison of prediction models", Composite Structures, 46, 1999, 299–308. DOI: https://doi.org/10.1016/S0263-8223(99)00098-7

[21] Tomlinson, D., and Fam, A., "Performance of concrete beams reinforced with basalt FRP for flexure and shear", Journal of Composites for Construction, 9 (2) ,2014, 1-10.

[22] SIMULIA. Analysis User's Manuals. Rising Sun Mills, Providence, RI, USA: Dassault Systèmes Simulia Corp, Rising Sun Mills, Providence, RI, USA, 2018.

[23] Hashin Z, Failure criteria for unidirectional fibre composites. Journal of Applied Mechanics, 47(2), 1980, 329–34. DOI:10.1115/1.3153664

[24] Bažant ZP, Oh B.H., Crack band theory for fracture of concrete, Materials and Construction, 16(3), 1983, 155–77. DOI: https://doi.org/10.1007/BF02486267

# Chapter 4: General Discussion and Conclusions

The objective of this research was to develop an effective rehabilitation technique for rehabilitation of steel beams which developed corrosion defect in the compression or tension flanges. BFRP fabrics were used as the rehabilitation material. The effectiveness of the rehabilitation technique was evaluated by comparing the ultimate load capacity, the yield load capacity, and the ductility of the rehabilitated specimens with the uncorroded control (virgin) and the control corrosion beam specimens. Lab-based experiments were completed. As well,  non-linear finite element models were developed and used in this research to undertake a parametric study. This chapter summarises the conclusions obtained from this study. However, these conclusions may be limited to the scope of the study.

## 4.1 Conclusions

The following conclusions are made based on the outcomes of this research.

1. The rehabilitation techniques used in this study were successful in eliminating debonding of BFRP fabrics. The study showed that the cross fabrics have a significant role in the prevention of debonding failure.

2. The ultimate strength of corroded steel beams subjected to corrosion damage in the bottom flange as well as corrosion defects of various depths in the top flange, were fully restored to that of the level of uncorroded control (virgin) beam, when the corroded beams were rehabilitated using BFRP fabric. Though the yield strength of the rehabilitated beams improved considerably, it never reached the yield strength of the uncorroded control (virgin) beam.

3. Ductility of the rehabilitated beams with corrosion defect in the tension (bottom) flange, was found to be less than that of the uncorroded control (virgin) beam and  control corroded beams. However, it was found that an increase in the number of layers of BFRP fabric resulted in moderate increase in the ductility of the beams. For rehabilitated beams with top flange corrosion, there was no reduction in the ductility values of the rehabilitated beams as compared to that of the uncorroded control (virgin) beams or control corroded beams.

4. There was an improvement in neutral axis depth for rehabilitated specimens of both corrosion in the bottom flange as well as corrosion in the top flange. It was found that after rehabilitation

with adequate layers of BFRP fabrics, the neutral axis depth can be restored to that of the uncorroded control (virgin) beam.

5. When corrosion defect occurs in the bottom (tension) flange, the beams with corrosion patch of lower aspect ratios experienced a higher increase in ultimate load as compared to beams with corrosion patch of higher aspect ratio, for the same thickness of BFRP applied. It was also observed that the ductility of the beams with lower corrosion aspect ratio was higher than the ductility of the beams with higher corrosion aspect ratios, for the same thickness of BFRP fabrics.

6. The study found that flexural rehabilitation, there is an optimum number of BFRP fabric layer that provides the best performance in terms of gain in ultimate strength. A higher number of layers of BFRP fabric may lead to a debonding failure.

7. Based on the parametric study conducted, new equations are proposed, and these equations can be used to determine the optimum number of BFRP fabric layers required to rehabilitate corroded steel beams with either top flange or bottom flange corrosion defects.


## 4.2 Recommendations

The following recommendations are made based on the current research study for future research works that can be taken up in this area:

1. It was observed for rehabilitating beams with corrosion defect in the bottom flange, with a rehabilitation with more than 15 layers of BFRP fabrics, debonding failure occurred. It is recommended to conduct more experiments to determine the maximum thickness of BFRP fabrics that can be successfully used following which debonding starts to take place, as well as to determine what factors affect the debonding.

2. The proposed equations in this study may only be applicable to the specific beam tested in this study. It is recommended to conduct more experiments with different cross section shapes and sizes so that a general equation can be proposed for determining the optimum number of BFRP layers required to restore the ultimate strength of the beams.

3. It is also recommended to conduct more experiments for rehabilitation of beams, with corrosion in the top flange of different shapes and compare the results with the rehabilitation of beams with corrosion in the bottom flange.

4. Rehabilitation of beams with corrosion in the top flange can be performed with other FRP like CFRP or GFRP and the results can be compared with this study.
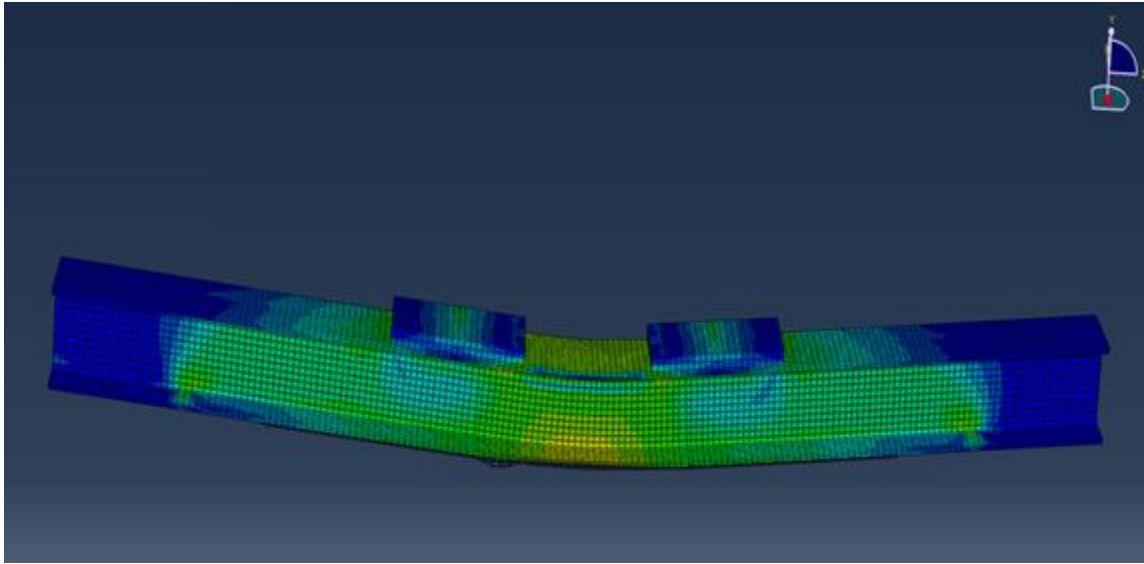
**Appendix A: FE Models for Rehabilitated Specimens**



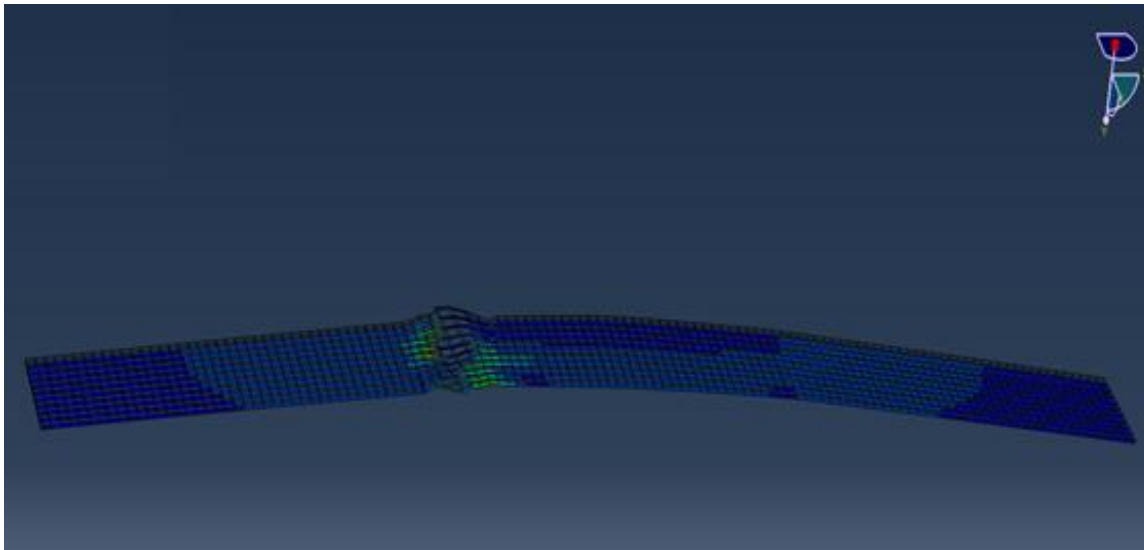Figure A.1: Final Deflected shape in the FEM model for specimen R400_7L



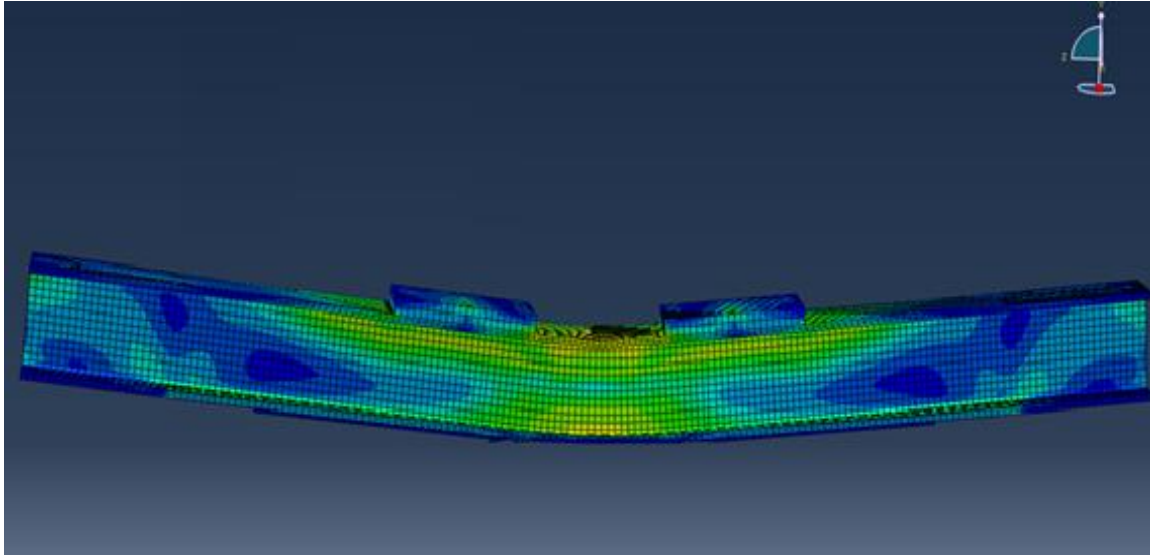Figure A.2: Shape of the BFRP laminate after rupture point for specimen R400_7L

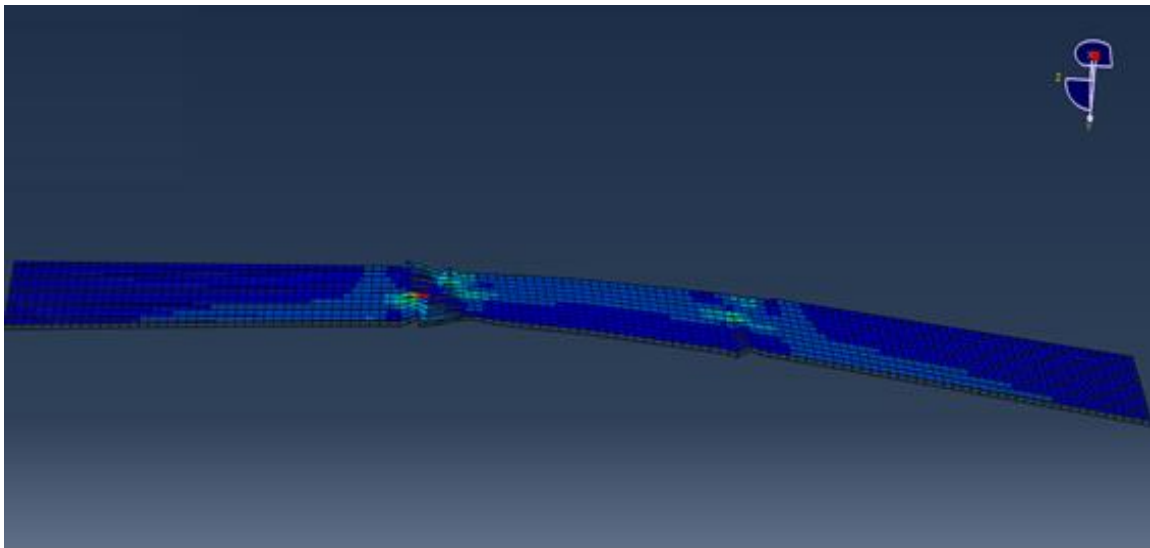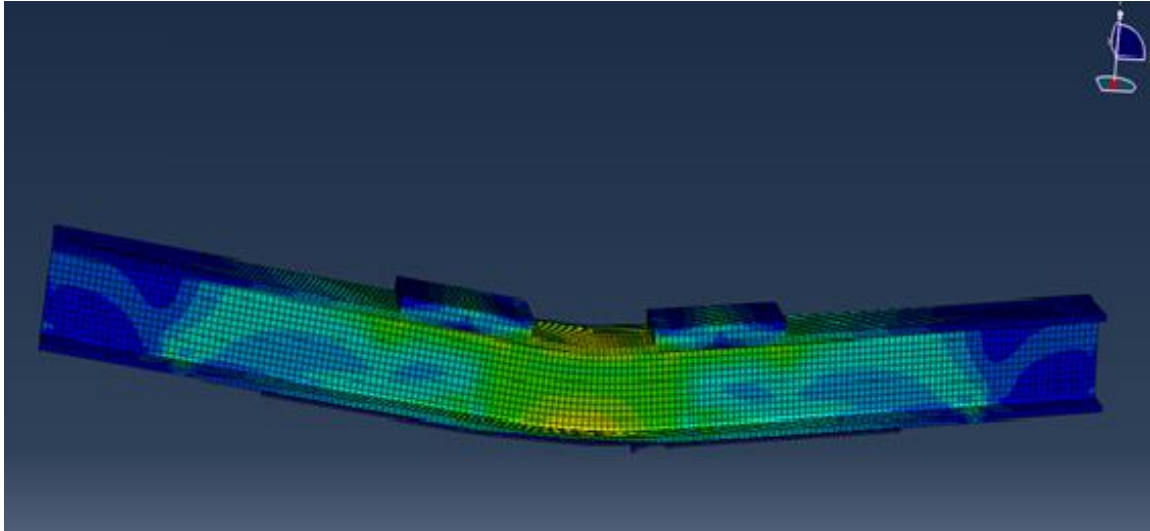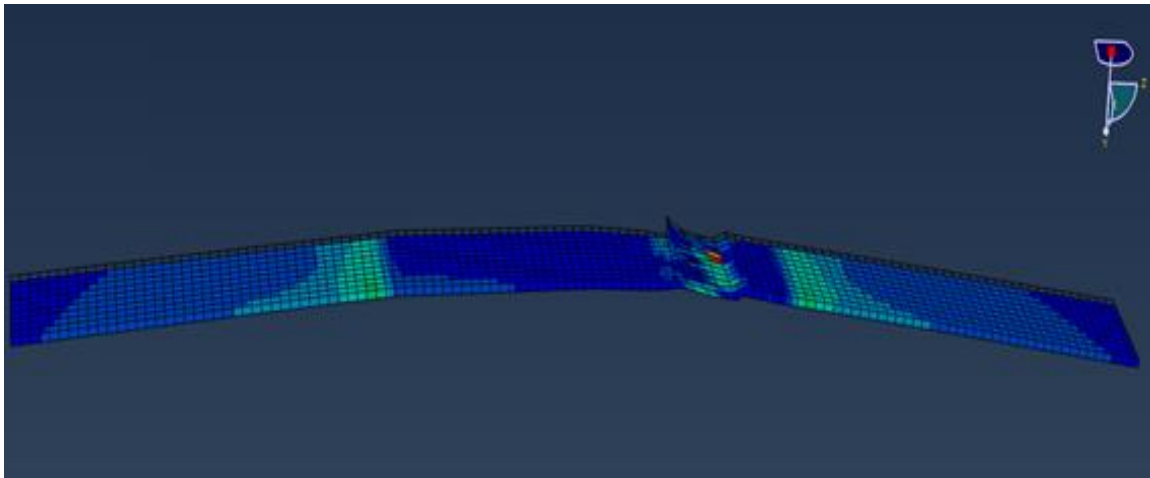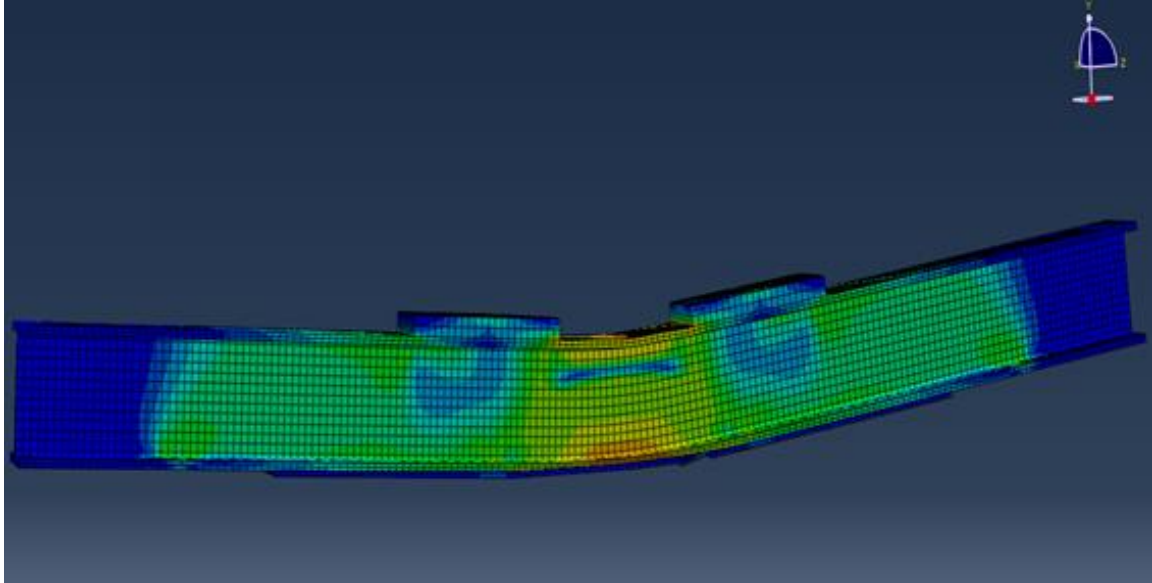Figure A.3: Final Deflected shape in the FEM model for specimen R400_10L



Figure A.4: Shape of the BFRP laminate after rupture point for specimen R400_10L

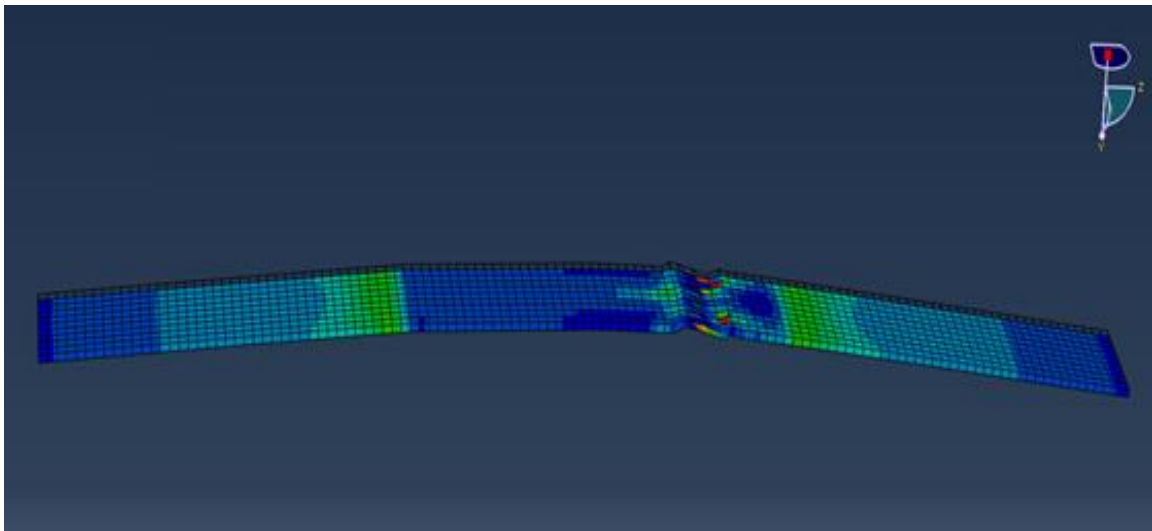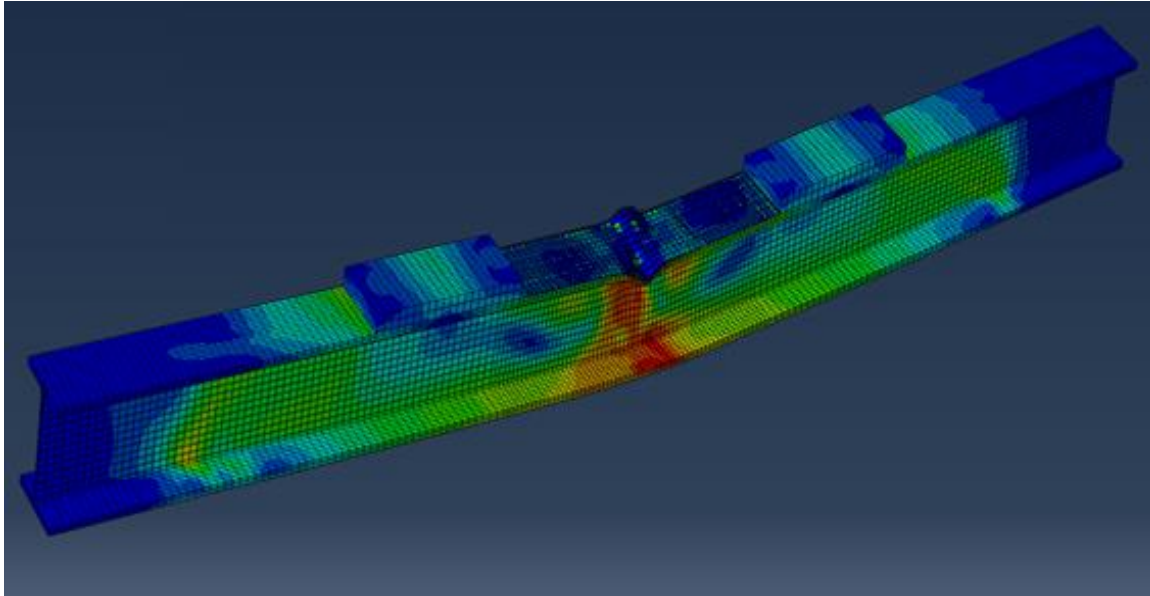Figure A.5: Final Deflected shape in the FEM model for specimen R400_15L



Figure A.6: Shape of the BFRP laminate after rupture point for specimen R400_15L

Figure A.7: Final Deflected shape in the FEM model for specimen R100_7L



Figure A.8: Shape of the BFRP laminate after rupture point for specimen R100_7L

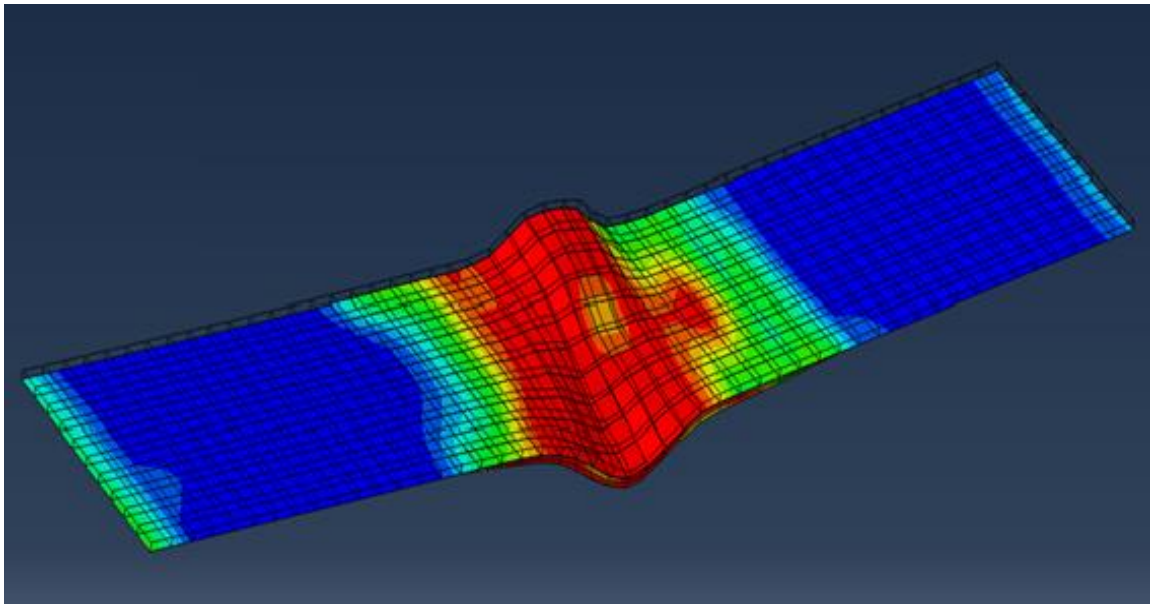Figure A.9: Failure mode obtained in the FEA model for R40-7L-3C specimen



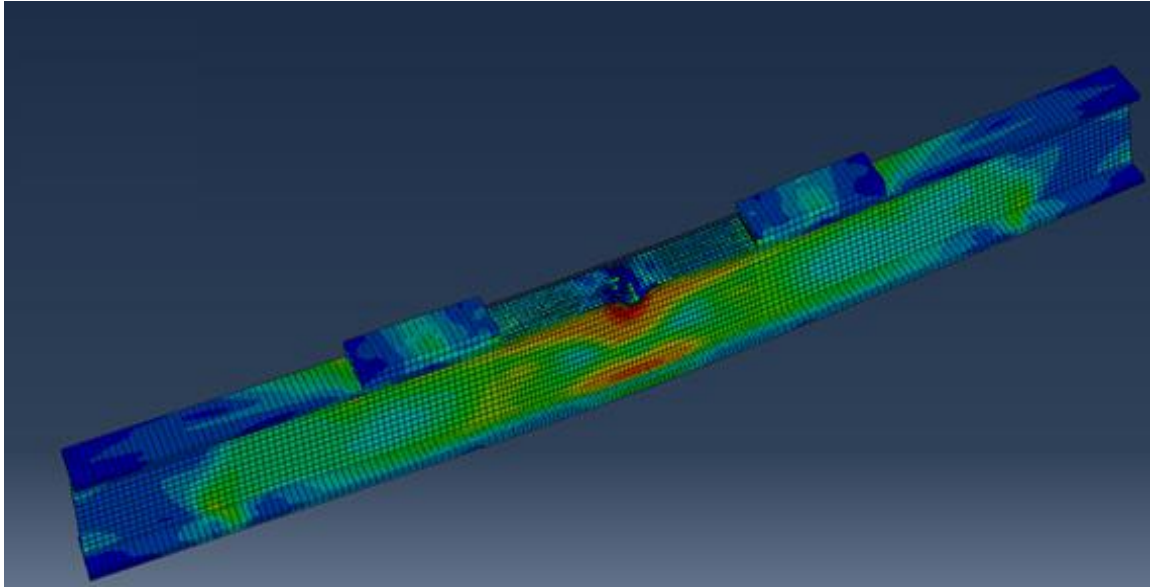Figure A.10: Damage in BFRP modelled using Hashin Criteria for R40-7L-3C

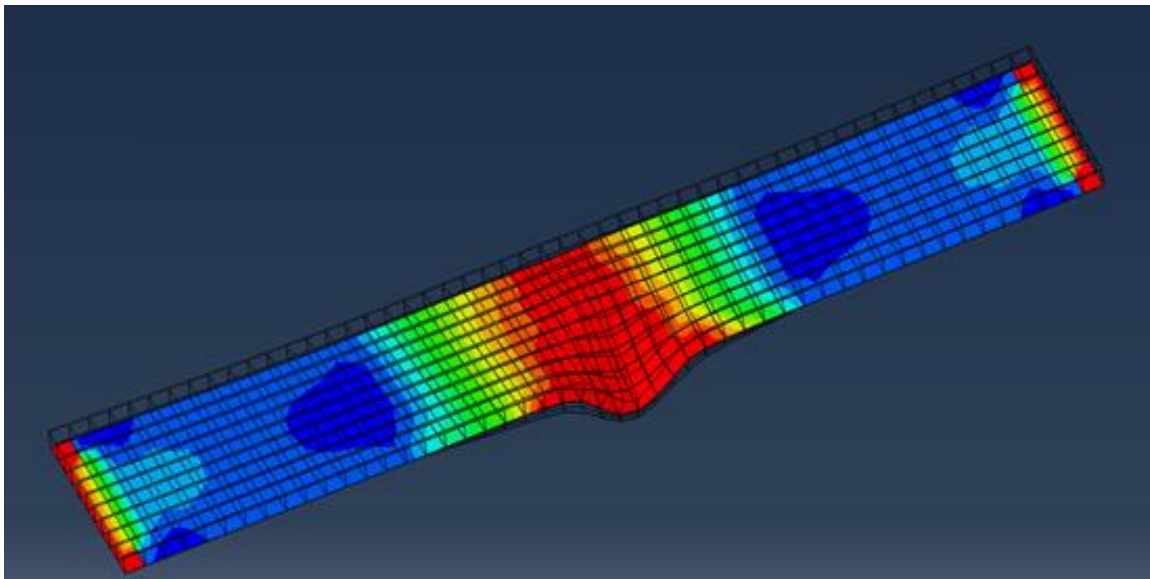Figure A.11: Failure mode obtained in the FEA model for R40-15L-3C specimen



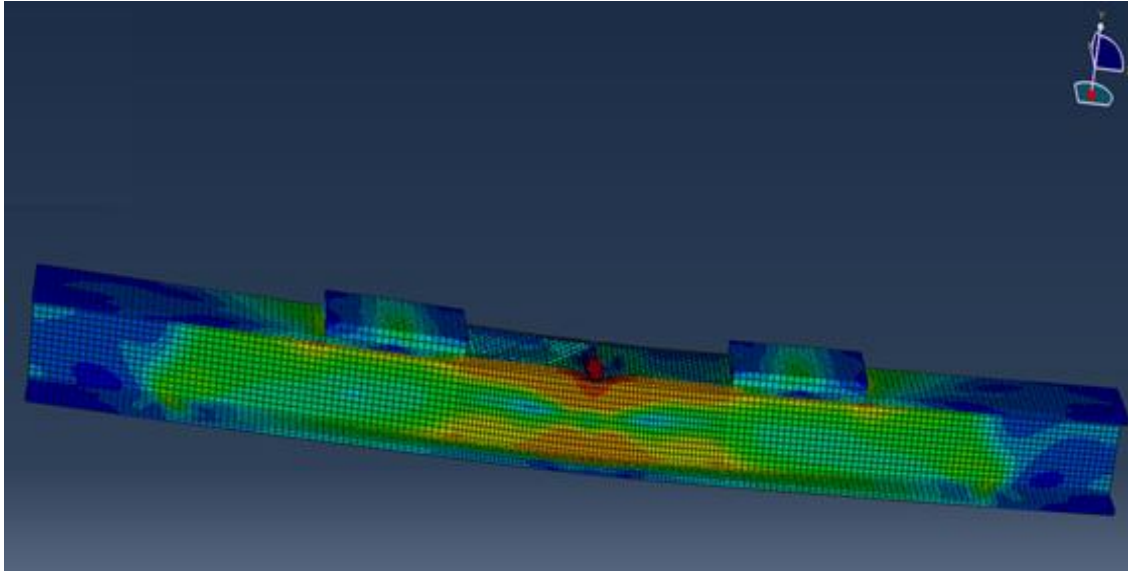Figure A.12: Damage in BFRP modelled using Hashin Criteria for R40-15L-3C

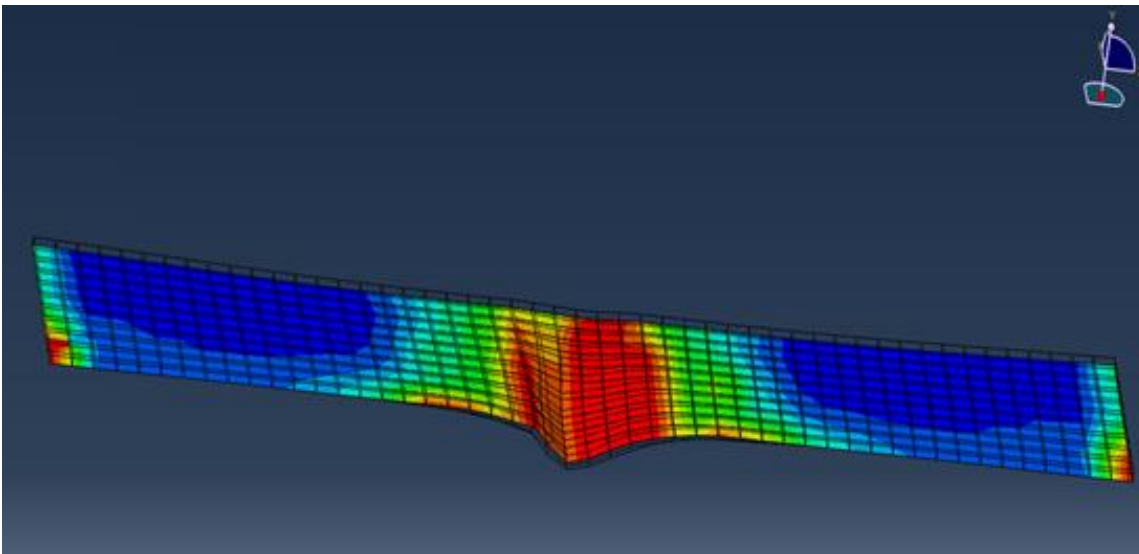Figure A.13: Failure mode obtained in the FEA model for R20-7L-3C specimen

`



Figure A.14: Damage in BFRP modelled using Hashin Criteria for R20-7L-3C

**Vita Auctoris**

NAME:                              *Soham Mitra*

PLACE OF BIRTH:          *Durgapur, West Bengal, India*

YEAR OF BIRTH:            *1992*

EDUCATION:                   *Indian Institute of Engineering Science and Technology, Shibpur,*

                                          *B.E.-Civil Engineering, West Bengal, India, 2015*

                                          *University of Windsor, M.A.Sc.-Civil Engineering, Windsor, ON,*

                                          *Canada, 2019*